AN INVESTIGATION INTO THE MATERIAL BEHAVIOUR OF REINFORCED CONCRETE BEAMS

by

Mogamat Faldi Samaai

A thesis submitted in partial fullfillment of the
requirements for the Degree of Master of Science
in Engineering

Department of Civil Engineering
University of Cape Town

January 1988

DECLARATION OF CANDIDATE

I hereby declare that this thesis is my own work and that it has not been submitted for a degree at any other University.

Signed by candidate

M.F. SAMAAI

JANUARY 1988

DEDICATION

I would like to dedicate this thesis
to the anonymous person who financed
my first-year of university studies.

ACKNOWLEDGEMENT

I would like to extend my sincere appreciation to the following:-

Prof J.B. Martin, under whose supervision this thesis was conducted.

Dr. H. Pearce for his assistance and guidance.

Renee de Beer for her patience and typing of this thesis.

The Council of Scientific and Industrial Research for their financial assistance.

ABSTRACT

An investigation into the material behaviour of reinforced concrete beams is presented. This investigation is divided into two parts. First, the experimental load-deflection tests on eleven under-reinforced two-span- and four slightly over-reinforced simply-supported beams are presented. The finite element simulation of these beams using the program, NLFRAM is then presented. This is followed by a material parameter study. In this study, the sensitivity and numerical efficiency of the material models in NLFRAM is assessed. This is done by systematically varying the parameters in the material models and comparing the load-deflection results.

The load-deflection results from these examples are compared with the experimental results. In this way, the accuracy of NLFRAM in simulating practical structures is examined. The results of these comparisons indicate that with the simple material models used in NLFRAM, numerical results which are cost effective and in good agreement with the experimental observations may be obtained.

CONTENTS

NOMENCLATURE

This is a list of symbols used in the main text of this thesis.

Special Symbols

-	a vector
T	the transpose of a vector or matrix
d	the differentiation with respect to
∂	the partial differentiation with respect to
$\underset{\sim}{u}$	transpose of a vector, $\underline{u}$
i (superscript)	ith iteration

Lower Case Characters

b	breadth
d	effective depth to reinforcement
e^+	eccentricity of top reinforcement from centre-line
e^-	eccentricity of bottom reinforcement from centre-line
$\underline{f}$	internal force
f_c	maximum compressive stress of concrete
f_{ck}	average compressive cube strength of concrete
f_{cl}	compressive stress limit
f'_{ct}	maximum tensile stress of concrete
f^1_y	first yield stress
f^2_y	second yield stress
k_E	elastic tangent stiffness matrix
k_G	geometric stiffness matrix
k_T	element tangent stiffness matrix
t	time
u	displacement in x-direction
v	displacement in y-direction
x;y	element co-ordinates system

Upper Case Characters

A	Area
DT	Displacement Transducer
E_C	Elastic Modulus of Concrete
E_S	Elastic Modulus of Steel
E_H	Hardening Modulus of steel
E_T	Transition Modulus of Steel
$\underline{F}_t$	internal nodal force
H_α	strain history parameters
K_T	tangent stiffness matrix
L	element length
LC	load cells
N	axial force
M	bending moment
P	point load
$\underline{P}_t$	nodal load vector
S	shear force

Greek Characters

α	tensile stress release factor
$\delta\underline{\tilde{u}}$	transpose of the virtual displacement vector
$\delta\epsilon$	virtual strain
Δ	increment in
ϵ	strain
ϵ_m^p	maximum tensile permanent strain
ϵ_{mc}	strain corresponding to maximum compressive stress
κ	curvature
θ	rotation or angle
σ	longitudinal stress
τ	shear stress in the element
ν	Poisson's ratio

CHAPTER 1

INTRODUCTION

1.1 General

The use of reinforced concrete as a structural building material has become an important feature of modern construction. This has been brought about as a result of extensive experimental investigations on large and small-scale models of reinforced concrete structures. The results of these investigations have been used in the formulation of design guidelines which generally result in safe designs. However, the analyses of new types of structures which fall outside the range of standard experiences cannot easily be performed using such guidelines.

The ever-increasing complexity of reinforced concrete structures, together with rises in cost, make it essential to seek less expensive alternative designs and construction methods without lowering the safety standards. Closely connected to this is the increase in the seriousness of the consequences of disaster, which makes detailed structural analysis more and more necessary. The central feature of such an analysis is an investigation of the loading and of the behaviour under overloading. Knowledge of the causes and effects of certain behaviour is important in order to predict the behaviour of other structures under similar loading conditions or similar structures under different loading conditions. In order to perform such an analysis, it is necessary that the structural response of the constituent materials, namely concrete and steel , is adequately understood.

Reinforced concrete, exhibits highly complex behavioural characteristics. These include phenomena such as a nonlinear stress-strain behaviour for concrete, concrete cracking, tension stiffening, shrinkage, creep and interaction effects between the concrete and the reinforcement. There exists a need for developing numerical methods to account for these complexities. The development of computers together with the use of numerical techniques such as the finite element method have greatly extended the possibilities of achieving this goal.

There are a number of factors that presently limit the wide acceptability of the finite element method in the analysis of reinforced concrete structures. The first important consideration is that the constitutive properties of concrete have not as yet been identified completely, and there is at present no generally accepted material law to model concrete behaviour. A second factor is that the finite element analysis of concrete structures is very costly and requires much user sophistication. This is largely due to the difficulties encountered in the stability and accuracy of the solutions.

These difficulties are, in general, a direct consequence of the specific numerical implementation of the concrete nonlinearities [1]. However, there is a wide range of material models and numerical solution techniques presently in use in the finite element analysis of reinforced concrete structures.

It is important to recognise that progress in practical nonlinear analysis procedures is largely based on the development of improved material models and kinematic descriptions and on the development of stable and effective computational procedures. In developing new material models, it is thus necessary to pay particular attention to their numerical implementations and also their practical application to real structues.

With these criteria in mind, an investigation into the material behaviour of reinforced concrete beams, subjected to monotonic loading is presented. This is achieved in two parts.

i) An experimental investigation of two-span and simply supported beams.

ii) A finite element analysis using the computer program, NLFRAM [2,3], simulating the behaviour of the beams tested in the laboratory.

In this thesis, a review of the constitutive models and solution techniques presently in use in the finite element analysis of reinforced concrete structures is first presented. The investigation of the beams tested in the laboratory is presented, followed by a description of the formulation of the finite element program, NLFRAM, the solution techniques, and the material models available in the program. Thereafter, a material parameter study, based on the beams tested in the laboratory, is presented. In this study, the sensitivity of the various material parameters used in the material models in NLFRAM is examined. Finally, the results of the experimental and finite element solution are compared in order to evaluate the stability and accuracy characteristics of the finite element representation.

1.2 Background to the Thesis

This thesis formed part of a research program into the material behaviour of reinforced concrete structures. This program was initiated by the UCT/CSIR Applied Mechanics Research Unit (AMRU) at the University of Cape Town. The objectives of this research programme were two-fold.

i) to create a data-base of experimental information relating to the behaviour of reinforced concrete elements and structures.

ii) to develop and improve the finite element program, NLFRAM, with regard to solution techniques and material modelling so as to reflect the findings of the experimental observations.

The finite element program, NLFRAM was developed by Hawla [2], for static and transient dynamic response analysis of beams and plane frames. The program is particularly applicable to reinforced concrete frames exhibiting geometric and/or material nonlinearities.

During the initial development of NLFRAM, an experimental investigation into the material behaviour of reinforced concrete was initiated. This took the form of a series of bending tests on simply-supported reinforced concrete beams (figure 1.1). The results of this investigation are presented by Lloyd [4].

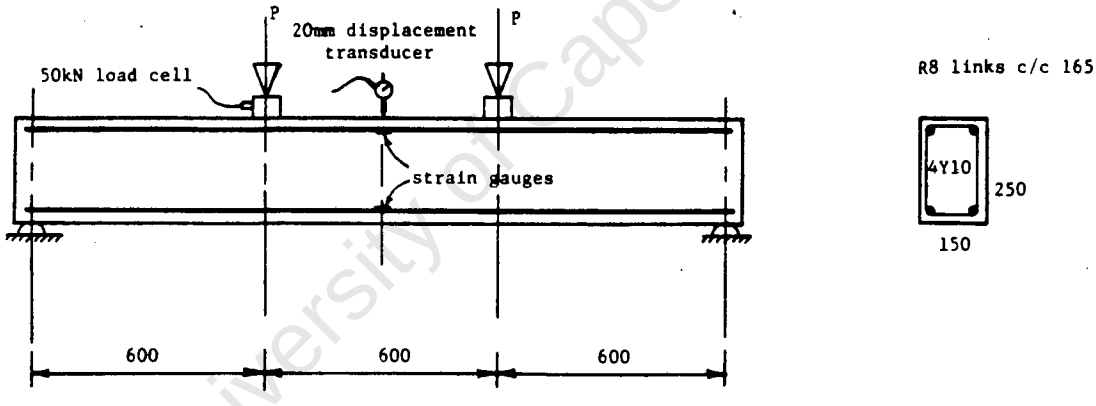

Figure 1.1: Simply-Supported Beam Tested by Lloyd

Lloyd and Hawla simulated the behaviour of these beams using NLFRAM and compared the load-deflection results [5]. From this comparison (figure 1.2), they concluded that the numerical solution obtained from NLFRAM agreed reasonably well with the load-deflection behaviour observed in the static load bending tests on a simply-supported reinforced concrete beam. However, there was a region of poor correlation between the actual and predicted response just prior to the yielding of the reinforcement. Also, sharp kinks occurred in the predicted response which were not observed in the experimental results. The former was ascribed to the simplified bilinear stress-strain curve used to model the reinforcement and the latter to the tensile modelling of the concrete. In order to produce a smoother response, Lloyd and Hawla recommended that a trilinear stress-strain curve be used to model the reinforcement and that the tensile stress of the concrete material model be gradually reduced after the tensile failure stress is reached [5].

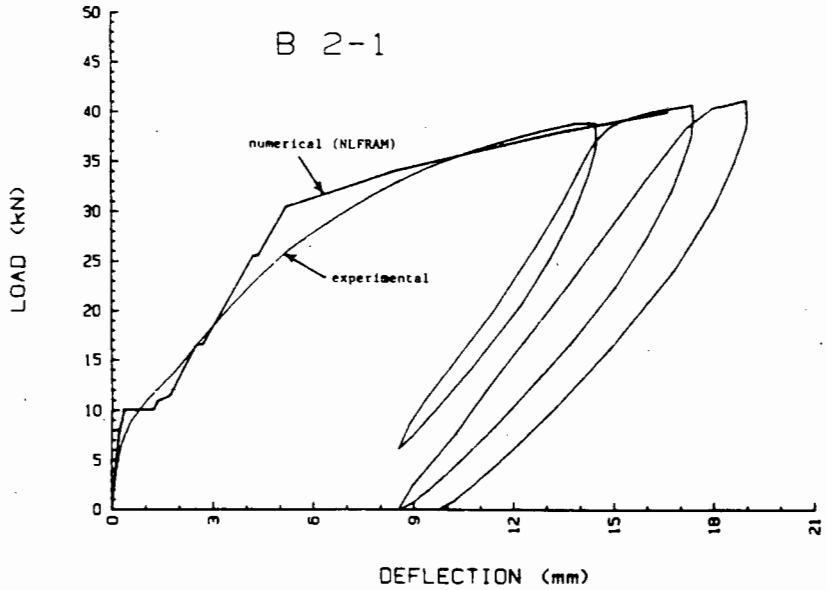

Figure 1.2: A First Numerical Approximation of the Beam Tested by Lloyd.

Hawla introduced these improvements into the material models in NLFRAM and again simulated the test beam shown in figure 1.1. The comparisons of these results are reported in [6]. From the load-deflection comparison of these results (shown in figure 1.3) Hawla concluded that by relatively simple refinements of the material models, the numerical solution can be greatly improved. Not only were all the major effects on the beam reproduced, but also the computational efficiency of the NLFRAM solution improved significantly. However, the results did require some explanation regarding the concrete behaviour. It was not clear why a maximum tensile stress of 1.5 MPa (used in the NLFRAM example shown in figure 1.3) produced far better results than the 3.0 MPa determined by Lloyd [4] from cylinder splitting tests for the beam shown in figure 1.1.

During the course of the investigation reported in this thesis, Hawla updated the program NLFRAM [3] and introduced new material models into the program. There are thus two versions of the program available [2,3]. Both of these are used in the present investigation. This investigation is an extension of the work performed by both Hawla and Lloyd.

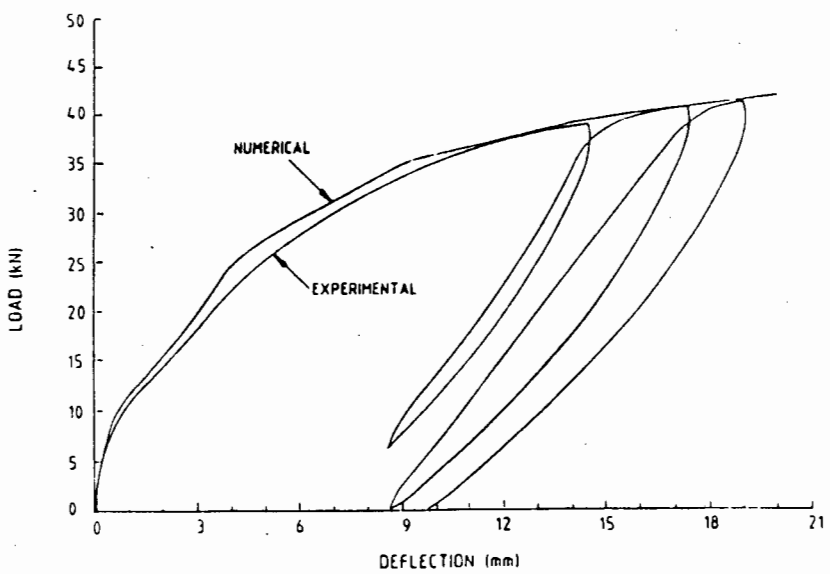

Figure 1.3: An Improved Numerical Approximation of the Beam Tested by Lloyd.

1.3 Objectives and Scope

The objectives and scope of this investigation are summarised below:

i) Set up an experimental procedure for the testing of reinforced concrete members. Document this procedure so that it could be of use to other investigators as well.

ii) Perform experimental load-deflection tests on two-span and simply-supported reinforced concrete beams. Observe and record the various effects of the beams under load. Also record the load-deflection data using a computerised data logging system and store the data for further use.

iii) Simulate the test beams numerically, using the two versions of NLFRAM [2,3].

iv) Using the test beams as a basis, do a parametric study of the material models available in NLFRAM. Investigate the sensitivity of the material models to variation of the material parameters and determine their numerical efficiency.

v) Compare the experimental and NLFRAM results. In so doing, test the validity of the various material models available in NLFRAM when compared to real-life situations.

CHAPTER 2

REVIEW OF THE LITERATURE

2.1 Introduction

The analysis and design of reinforced concrete structures are usually based on simple equilibrium conditions and empirical rules. These traditional methods generally result in safe designs, but they frequently contain inherent inconsistencies and often do not reflect a clear understanding of the actual composite action of the material. Present codes of practice continue, in many respects, to be based on empirical approaches and rely heavily on the results of a considerable amount of experimental data.

The situation is largely attributable to the complex behaviour of reinforced concrete. This includes phenomena like concrete cracking, tension stiffening, time dependency and interactive effects between concrete and reinforcement. The design of reinforced concrete structures which are likely to be subjected to extreme loading conditions at some stage during the life of the structure requires a detailed analysis of these phenomena. Numerical methods, and particularly the finite element technique have greatly extended the possibilities of mathematically simulating the behaviour of reinforced concrete.

The last decade has witnessed rapid advances in the use of the finite element method for the analysis of reinforced concrete structures. Accurate prediction of the structural response by a finite element analysis can however only be achieved if the non-linear characteristics of the material models used in the analysis reproduce the material behaviour.

Various material models are presently in use in the finite element analysis of reinforced concrete structures. In this review, these models are presented with the view of highlighting the advantages and disadvantages of their application to various types of structures. Furthermore, effects such as concrete cracking and crushing, tension stiffening, and the interaction between concrete and reinforcement are discussed since these are directly applicable to this investigation.

2.2 Constitutive Modelling of Reinforced Concrete

2.2.1 Continuum Models for Concrete

The material behaviour of concrete is highly complex and difficult to describe in a unified theory. There exists a large variety of material models, based on experimental data, which have been proposed in recent years to characterise the stress-strain and failure behaviour of concrete materials. Each of these models has certain inherent advantages and disadvantages which depend to a large degree on the particular application. The models may be categorised into the four following groups:

i) linear and nonlinear elastic models
ii) perfect and work-hardening plastic models
iii) models based on the endochronic theory of plasticity
iv) models based on the plastic-fracturing theory

The linear theory of elasticity is the most commonly used material law for concrete. The earliest finite element models for reinforced concrete used linear representation for the concrete [7,8,9,10]. In these linear elastic models, uncracked concrete is described as a material in which the state of stress depends only on the current state of strain. The basic stress-strain relationship is completely defined by two elastic constants, Poisson's ratio, ν, and Young's modulus, E. The concrete behaves elastically until the elastic limit stress is reached.

When the elastic limit stress is reached, the concrete will fail by fracturing. Concrete fracture occurs in two forms, cracking and crushing [11]. The cracking type of fracture is defined as the partial collapse of the material across the plane of cracking under tensile stress states. When the concrete cracks the material loses its tensile strength normal to the crack direction and the resistance of the material against further deformation in that direction is reduced to zero. The material parallel to the crack is assumed to retain its strength. The crushing type of fracture is defined as the disintegration of the material under compressive stress states. When crushing occurs, the current stresses drop abruptly to zero and the concrete is assumed to lose its strength completely.

For concrete experiencing tensile fracture (cracking), the stress-strain relations are also still modelled as linear elastic, but the material stiffness is modified to reflect the fact that the stresses in the direction normal to the crack are zero. However, concrete experiencing compressive fracture (crushing), exhibits strong nonlinearities which cannot be described by a linear elastic model. The linear elastic models for concrete are thus mainly applicable to structures in which the tensile behaviour of the concrete is the dominant factor.

The nonlinear elastic models provide a more realistic description of the nonlinear behaviour of concrete in compression. In general, there are two basic approaches: finite (or total) material characterisations in the form of secant formulations and incremental models in the form of tangential stress-strain relations [11].

The secant type of formulation has been extensively used in describing the nonlinear mechanical behaviour of concrete under biaxial and triaxial compressive stress states [12,13]. In general, most of the secant constitutive models for concrete have been formulated as an extension of the isotropic linear elastic stress-strain relationship. Their application is restricted primarily to monotonic or proportional loading regimes [11].

The incremental elasticity-based formulations belong to the class of constitutive relations called hypo-elastic. These models are used to describe the mechanical behaviour of a class of materials in which the state of stress depends on the current state of strain as well as on the stress path followed to reach that state. It has been observed that incremental models provide a more realistic description under non-monotonic and non-proportional loading regimes than the total-stress-strain models [14]. Examples of their application are given in [11].

Experimental evidence indicates that the deformation of concrete is basically inelastic [14]. The stress-strain behaviour can be separated into a recoverable and irrecoverable component. The recoverable component is treated within the classical theory of elasticity while the irrecoverable component is based on plasticity theories. Plasticity-based models have been used extensively in recent years to describe the behaviour of concrete [15,16,17,18,19,20].

The use of plasticity models for concrete behaviour has many advantages. It accounts, in principle, for the stress-history-dependent behaviour. Residual strain due to unloading can be evaluated. It allows unloading and reloading, thus providing for modelling of cyclic loading problems. However, studies have shown that some plasticity models predict an unreasonably high volume expansion, overestimate plastic deformation in tensile loadings, and underestimate that in confined compressive loadings [20]. Another statement concerning the limitation of the classical plasticity approach is that it is difficult to model softening behaviour. Han and Chen [20] assert that with certain modifications, most of the above problems can be solved within the framework of the plasticity theory. In general, plasticity based models may either describe concrete as an elastic-perfectly plastic material or as an elastic-plastic-hardening material.

The stress-strain relationships for the elastic-perfectly plastic model are developed in three parts:

i) Before yield;
ii) during plastic flow; and
iii) after fracture.

In order to describe the plastic stress-strain relationship during plastic flow, one must define the condition of yield and the strain criterion for fracture. Various yielding criteria for concrete under multiaxial states of stress are described in [14] and [15]. A considerable amount of numerical work has been done using the von Mises criterion, extended von Mises criterion (Drucker-Prager) and Coulomb or modified Coulomb criterion [15]. The elastic perfectly plastic model for concrete in biaxial stress states, using a von Mises failure surface in the compression zone, is shown in figure 2.1.

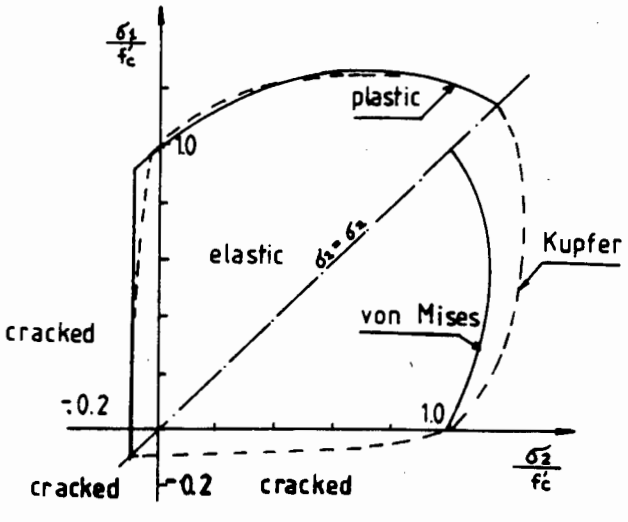

Figure 2.1: Biaxial Elastic Perfectly Plastic Model for Concrete.

To construct the stress-strain relation in the plastic range, the normality of the plastic deformation rate vector to the yield surface is commonly assumed. This associated flow rule is considered for concrete predominantly for practical reasons, since there is very little supportive experimental evidence available [15].

A generalization of the elastic perfectly plastic models can be achieved by the use of the strain-hardening theory of plasticity [15,16]. The constitutive relations for a strain-hardening plastic material are based on three fundamental assumptions:

i) the shape of the initial yield surface
ii) the evolution of subsequent loading surfaces (hardening rule)
iii) the formulation of an appropriate flow rule

According to this approach, the concrete behaves elastically only when the stresses are within the initial yield surface (figure 2.2). Microcracks are assumed to form continuously as the material is loaded. If the material is unloaded within the initial yield surface, the microcracks will close up again. However, under increasing load, the microcracks in the material grow in a stable manner. These cracks join together to form larger cracks and cause localised failure of the concrete. At this stage, the stress state is assumed to have reached the initial yield surface.

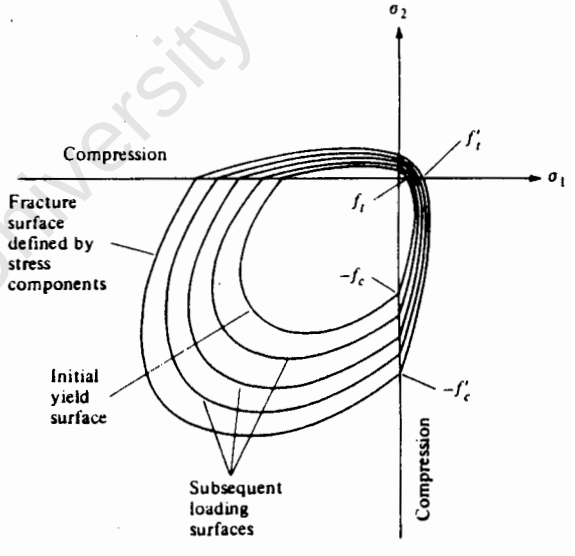

Figure 2.2: Loading Surfaces of Concrete in Biaxial Stress Plane for a Work-Hardening - Plasticity Model

When the material is stressed beyond the initial yield surface, a subsequent new surface called the loading surface is developed. This new surface replaces the initial yield surface (figure 2.2). If the material is unloaded and reloaded within this subsequent loading surface, no additional irrecoverable deformation will occur. If the stress point moves beyond this surface, additional irrecoverable deformation results. The associated flow rule is assumed to govern the post yielding stress-strain relations for concrete. Once the loading surface has been defined, the constitutive equations based on the concept of flow rule can be derived.

A surface defining the complete collapse of the yielded concrete is also postulated. This surface, called the strain fracture surface, is defined as the outermost extreme of the loading surface similar to that of perfectly-plastic yield surface. Once the stress fracture surface is reached, the concrete begins to flow under constant stresses. Finally, the concrete is assumed to crack or crush depending on the nature of the stress-states, when the strain fracture surface is reached. Formulations of the stress-strain relations in the plastic range for strain-hardening concrete material are given in [16,19,20,21,22]. The predictions based on these models have shown good agreement with experimental results. [18].

Recent developments in the modelling of concrete include the endochronic [23], and the plastic-fracturing theories [24]. The endochronic theory of plasticity is based on the concept of intrinsic time. This intrinsic time is used to measure the extent of damage of the internal structure of the concrete material when it is subjected to deformation histories. The theory appears to have the capability of characterizing the behaviour of concrete without recourse to yield conditions and hardening rules. Recent applications have demonstrated clearly the power of the endochronic approach [25]. However, further research in refining this theory is needed, particularly in order to simplify and reduce the number of material parameters used in the existing versions of the theory.

It has been suggested by Chen [9] that the plastic-fracturing theory [24] shows an even greater potential in developing a more unified and comprehensive material model for concrete. The basic idea in this theory is that the inelastic strain consists of one part due to plastic deformation, and one part which is connected to micro-cracking in the concrete. The theory is incrementally linear, which makes it very suitable for implementation in the finite element formulation.

2.2.2 Cracking of concrete

The tensile failure of concrete is characterised by a gradual growth of cracks which join together and eventually lead to localised failure of the material. It is a usual assumption that forming of cracks is a brittle process and that the strength in the tension loading direction abruptly goes to zero after such cracks have formed. However, experimental evidence on unreinforced concrete shows that cracks in large specimens tend to grow in a stable manner and that the tension strength decreases gradually [25] and [26].

In the finite element analysis of concrete structures, two principally different approaches have been employed for crack modelling. The discrete approach was introduced by Ngo and Scordelis [7]. Cracking of concrete was modelled by physically splitting a node and allowing a separation to develop along interelement boundaries. Cracks were therefore restricted to propagate along these boundaries. In this model geometrical restrictions imposed by the preselected finite element mesh cannot be avoided. Furthermore, the nodal splitting means a continual change in the topology of the problem. This results in computational inefficiencies in the finite element implementation of the procedure.

To overcome the need for automatic generation of cracks without redefinition of the element topology, and to allow for generality in possible crack direction, the smeared crack model was introduced by Rashid [27]. In this model, it is assumed that the concrete becomes orthotropic after the first cracking has occurred, one of the material axes being orientated along the direction of cracking. Such a formulation allows for a gradual decrease of strength in the direction of tension. Also, shear strength reserves due to aggregate interlocking can be accounted for by retaining a positive shear modulus. This shear capacity also has the effect that secondary cracking does not necessarily appear perpendicular to the first direction of cracks [25]. The smeared crack model is more popular and has been introduced in a number of finite element programs for concrete structures [14,28].

In spite of its simplicity of application, the smeared crack approach has nevertheless a drawback in the dependence of finite element mesh sizes, as pointed out by Bazant and Cedolin [29,30]. In their study, they investigated the effects of the finite-element mesh size on the smeared-crack model. From the analysis of a cracked panel using the fracture mechanics concept, it was found that the use of a strength criterion in the element analysis is dependent on element mesh size. This implies that the strength criterion in the element analysis is not objective and may lead to incorrect solutions. For the analysis of large-scale concrete structures such as nuclear containment vessels, the mesh size of the finite element model may become fairly large. Then, the objectivity requirement for the cracking criterion may have a serious effect on the analysis results. In this case, a modification of the cracking criterion is recommended [30] to account for the effect of element size.

2.2.3 Behaviour of the Steel reinforcement

The material properties of the steel reinforcing bars are easily established from uniaxial tests. The material properties are usually modelled using standard plasticity formulations. A bilinear or trilinear idealisation is adopted to model the elasto-plastic stress-strain relationships (figure 2.3).

To account for the effect of steel reinforcement in stiffness calculations, three alternative approaches can be used:

i) Smeared model,
ii) embedded model
iii) discrete model

In the smeared model, the reinforcement is assumed to be distributed uniformly over the element. Assuming perfect bonding between concrete and reinforcement, the constitutive relationships can be derived from the composite theory [19,28].

In the embedded model, the stiffness of reinforcement is evaluated individually in the element in conjunction with isoparametric shape functions [19]. Thus, the reinforcements need not be distributed uniformly and their locations and orientations can be arbitrary. In the discrete model, a one-dimensional bar element is superimposed on the two-dimensional elements [7]. In spite of its simplicity of concept, the discrete model has one disadvantage in that the finite element mesh patterns are restricted by the locations of reinforcement. Numerically, it is less effective than the embedded or smeared approach.

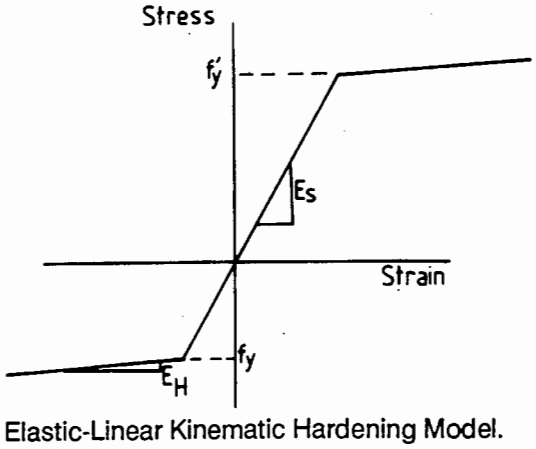

Figure 2.3: Elastic-Linear Kinematic Hardening Model.

2.2.4 Interaction between Concrete and Reinforcement.

In the finite element analysis of reinforced concrete structures, it is assumed that the two constituents, concrete and steel reinforcement contribute separately to the overall stiffness and strength using the principle of superposition. Full kinematic continuity between concrete and steel, at least at the nodal points on element boundaries is assumed. The two materials however have very different mechanical properties. This lack of material compatibility results in bond failure, slipping of the reinforcing bars, local deformations and cracking. A classification of the interaction of concrete and reinforcing steel and the finite element modelling thereof is given in references 14 and 25.

One of the most important of these interactive mechanisms occurs when both concrete and reinforcement are subjected to tension so that large cracks form (figure 2.4).

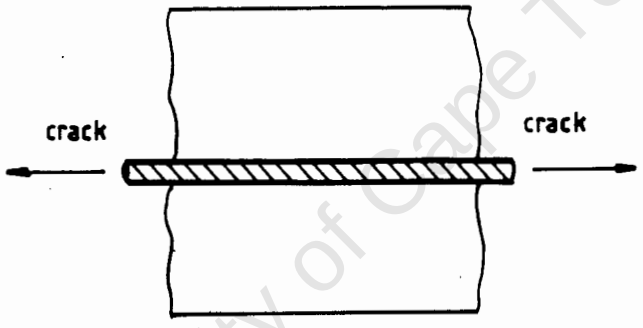

Figure 2.4: Tension-Cracking in Reinforced Concrete.

The figure shows the concrete between two such primary cracks. The opening of the cracks occurs at the same time as bond failure and relative movement between the bar and the concrete take place. The shear forces at the contact surface transfer tension stresses into the concrete between the cracks. This allows the concrete to offer some resistance to the relative movement between the bar and the concrete and thus contribute to the overall stiffness of the system. This stiffness effect, called tension-stiffening, may be significant for concrete beams under normal working loads.

The tension-stiffening effect is a property of the composite mixture of the concrete and reinforcement and can only be modelled realistically by using theories based on such considerations. However, such theories are complicated, and are not presently incorporated in the finite element analysis of reinforced concrete structures. This tension-stiffening effect can be accounted for in an indirect way by modelling the interaction as a material behaviour of one of the two components.

This may be done by assuming that the loss of tensile strength in the concrete occurs gradually during tensile failure (figure 2.5). This approach seems reasonable since the concrete adheres to the reinforcing bars and thus contribute to the overall stiffness of the structure. Several models, based either on experimental results or computational efficiency have been employed to simulate this gradual reduction in the concrete tensile strength [18,28,31,32].

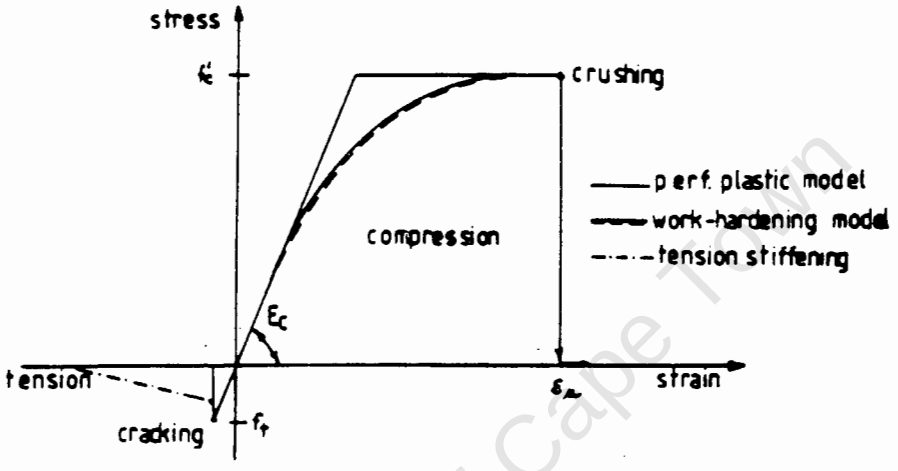

Figure 2.5: One-Dimensional Constitutive Model for Concrete with Tension Stiffening.

A second approach used to account for tension-stiffening effect is to increase the steel stiffness after concrete cracking takes place (figure 2.6). The additional stress in the steel represents the total tensile force carried by both the steel and concrete between cracks. The added stress is lumped at the level of the steel and orientated in the same directions. The relative effects of this approach have been studied by Gilbert and Warner [33]. Application of this approach is given in reference [34].

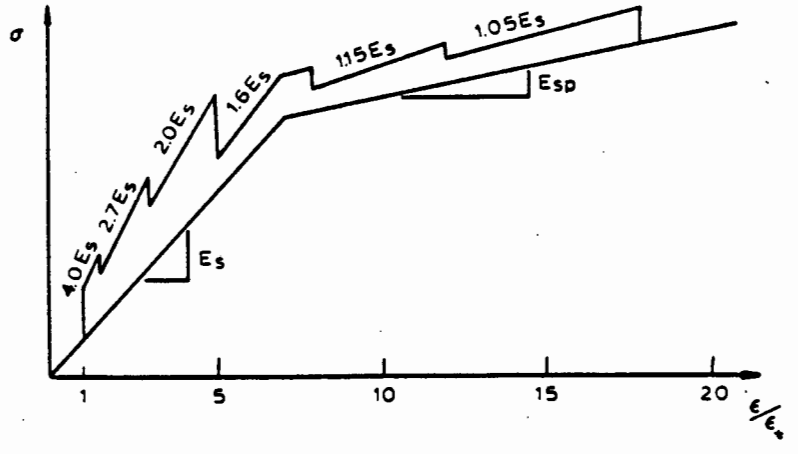

Figure 2.6: Reinforcement Tension Stiffening Model.

A brief review of the various modelling techniques used in the finite element analysis of reinforced concrete structures has been presented here. From the review, it is evident that some effects may be modelled in various ways without affecting the accuracy of the solution significantly. It is also evident that the modelling techniques are restricted since these are not applicable to all types of structures. Although a unified and comprehensive three-dimensional constitutive model still needs to be developed, the existing models have greatly increased our understanding of the behaviour of reinforced concrete structures.

CHAPTER 3

REINFORCED CONCRETE BEAM TESTS

3.1 Introduction

The series of bending tests on the reinforced concrete beams reported in this chapter is part of a research program into the material behaviour of reinforced concrete structures. This program has two main objectives:

i) to gather experimental information about reinforced concrete elements such as beams and frames.

ii) to develop and improve the material models and solution techniques in the finite element program NLFRAM [2,3] so as to simulate the experimental observations.

Prior to this investigation, Lloyd performed a series of bending tests on under-reinforced simply-supported beams [4]. The results of these tests are discussed in Chapter 1. The investigation reported herein is an extension of the work performed by Lloyd and involves load-deflection tests on a total of eighteen beams, of which fourteen are two-span and four simply-supported beams.

The two-span beams were designed as under-reinforced beams. Under these conditions, the tensile properties of the concrete were expected to dominate the beam behaviour. The first three of the two-span beams tested were used as trial beams. This was done in order to gain experience in setting up the system, controlling the load application and testing the accuracy of the measuring instruments. The load-deflection results of these beams are thus not reported. The rest of the two-span beams (a total of eleven) are divided into two sets, namely Set 1 and Set 2 (table 3.1). These beams differed only in that the designed compressive cube strength was 40 and 48 MPa for the beams in Set 1 and Set 2 respectively.

The four simply-supported beams formed a third set of tests, namely Set 3 (table 3.1). These beams were designed as slightly over-reinforced with a cube crushing strength of 30MPa. Under these conditions, the compressive properties of the constituent materials were expected to dominate the beam behaviour.

The beams in this investigation thus allow for a range of material effects under tensile and compressive conditions to be studied. It is therefore argued that the results of these tests are useful in the development of the material models in NLFRAM.

In this chapter, the constituent materials and the manufacture of the test beams are first described. This is followed by a description of the test beams and measuring devices, the setting-up of the beams in the test-bed and the testing procedure. Finally the observations made during the testing of the beams are discussed.

Table 3.1: Beam Identification

Beam	Set	Beam	Set
FS 1	trial	FS 10	Set 2
FS 2	trial	FS 11	Set 1
FS 3	trial	FS 12	Set 1
FS 4	Set 1	FS 13	Set 1
FS 5	Set 1	FS 14	Set 1
FS 6	Set 1	SS 1	Set 3
FS 7	Set 2	SS 2	Set 3
FS 8	Set 2	SS 3	Set 3
FS 9	Set 2	SS 4	Set 3

3.2 Materials and Specimen Manufacture

This section describes the material constituents, concrete and steel reinforcing bars as well as the preparation of the test specimens.

3.2.1 Materials

The concrete was prepared using Ordinary Portland cement, 13mm stone, dry sand and water in the mix proportions shown in Table 3.2. The mix design for the beams in Set 1 was the same as that used by Lloyd for the simply-supported beams in reference [4]. The mix designs for the beams in Set 2 and Set 3 were based on the design curves given in reference [35]. From each batch of concrete prepared, three standard concrete cubes (100 x 100 x 100mm) were made. These were used to determine the compressive strength of the concrete.

The main reinforcement for the beams in Set 1 and Set 2 consisted of Y10 bars while Y16 bars were used in Set 3. Uniaxial tensile tests were performed on a representative sample from each batch of steel reinforcing bars to determine a generalised stress-strain relationship for the steel. The results of these tests are presented in Chapter 4. Shear Reinforcement in the form of R8 mild steel stirrups was used in all the beams. Cement spacer blocks of nominal thickness 15mm were tied to the stirrups to ensure a minimum of 15mm cover to the stirrup reinforcement throughout.

Table 3.2: Mix proportions of the constituents of the concrete.

	Cement (kg)	Sand (kg)	Stone (kg)	Water (kg)	Designed Strength MPa
Set 1	37,1	88,3	75,9	19,2	40
Set 2	45,1	55,0	71,0	19,0	48
Set 3	25,0	60,0	71,0	15,0	30

3.2.2 Manufacture of the Specimens

The formwork in which the beams were cast was made up of steel plates (figure 3.1). The advantage of this being that the form was re-usable.

The steel cages for the two beams (figure 3.1) were prepared and placed in the form. The constituents of the concrete were weighed and mixed according to the mix proportions specified in Table 3.2, poured into the form and vibrated using a needle vibrator. The exposed surface of the beams was then smoothed with a steel trowel (figure 3.2). From each batch of concrete prepared, three test cubes were also made. After the excess surface water had evaporated, the beams and cubes were covered with black plastic sheeting. These remained in place for a period of three days after which the forms were stripped and the specimens placed on the laboratory floor for the remainder of the curing period. The beams and test-cubes were at all times exposed to the same environmental conditions.

Figure 3.1: The Steel Formwork with Reinforcing Frames prior to Casting of the Concrete.

Figure 3.2: The exposed surface of the beams smoothed with a steel trowel

3.3 Description of the Test Beams

3.3.1 The Two-Span Beams - Set 1 and Set 2

All the beams in Set 1 and Set 2 had the same dimensions. These beams had an overall length of 4,0 metres and were tested as continuous beams on three supports, the spans being each 1,8 metres in length. The cross-sectional dimensions were b = 152mm and h = 250mm (figure3.3). The effective depth for both the top and bottom reinforcement was d = 222mm.

In all the beams the longitudinal reinforcement consisted of Y10 high yield reinforcing bars. In the cross-section of each beam there were always three longitudinal bars as top steel and two as bottom steel. The longitudinal reinforcement remained constant over the entire length of the beam. Transverse reinforcement was provided in the form of R8 mild steel stirrups. The stirrups served as shear reinforcing links and also for fixing the longitudinal bars into position (figure 3.3). The stirrups were spaced along the length of the beam as shown in (figure 3.4).

3.3.2 The Simply-Supported beams in Set 3

The beams investigated in Set 3 had an overall length of 3,1 metres. These beams were tested over a simply-supported span of 3,0 metres (figure 3.5). The cross-sectional dimensions were the same as for the beams in Set 1 and Set 2 (250 x 152mm) (figure 3.5). The effective depth to the tensile reinforcement was d=220mm. Three Y16 bars which remained constant throughout the length of the beam, were used as tensile (bottom) reinforcement. No compressive (top) steel was provided. Shear reinforcement provided was of the R8 mild steel type. These stirrups were spaced at 90mm centres throughout the beam (figure 3.6). Since no top reinforcement was provided, binding wire was used to hold the stirrups in position.

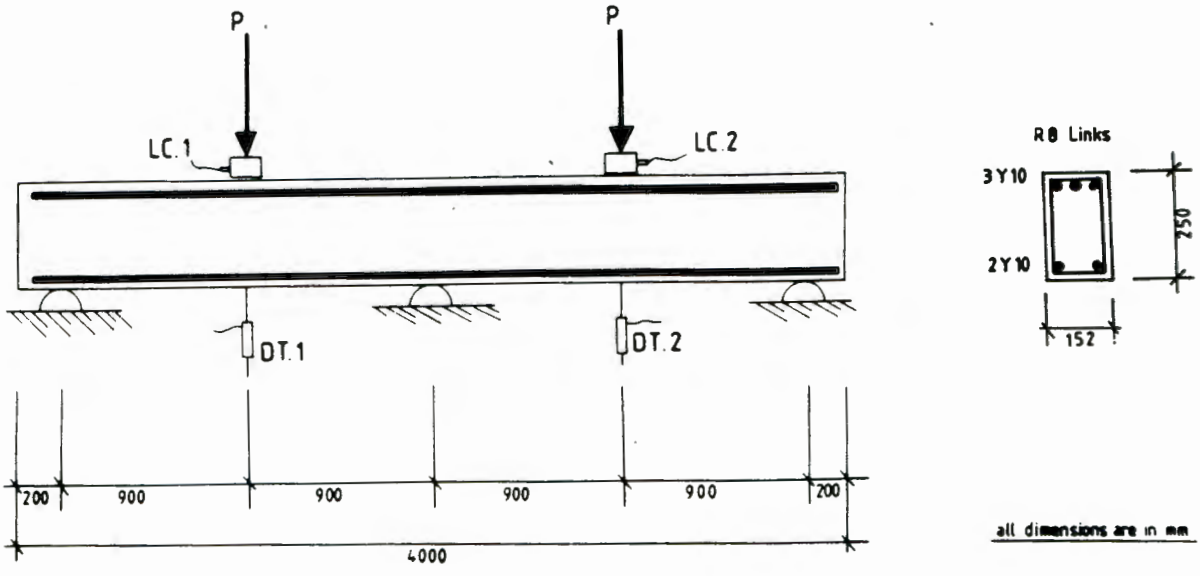

Figure 3.3: Two-Span Beam of Set 1 and Set 2.

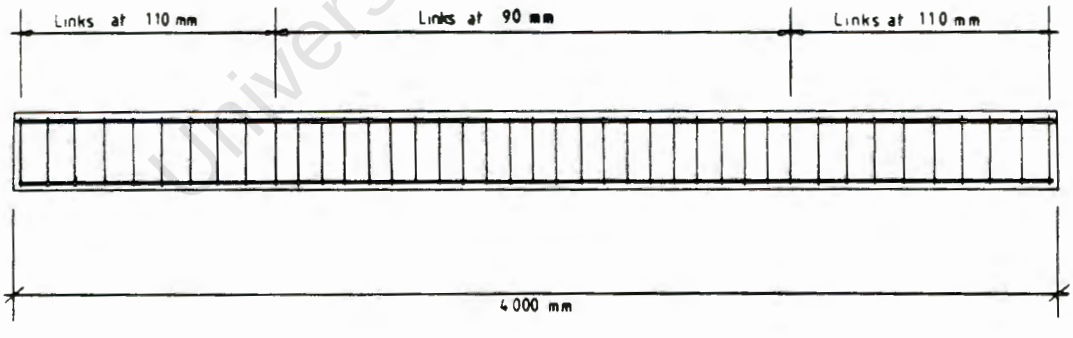

Figure 3.4: Stirrup spacing for the Two-Span Beams.

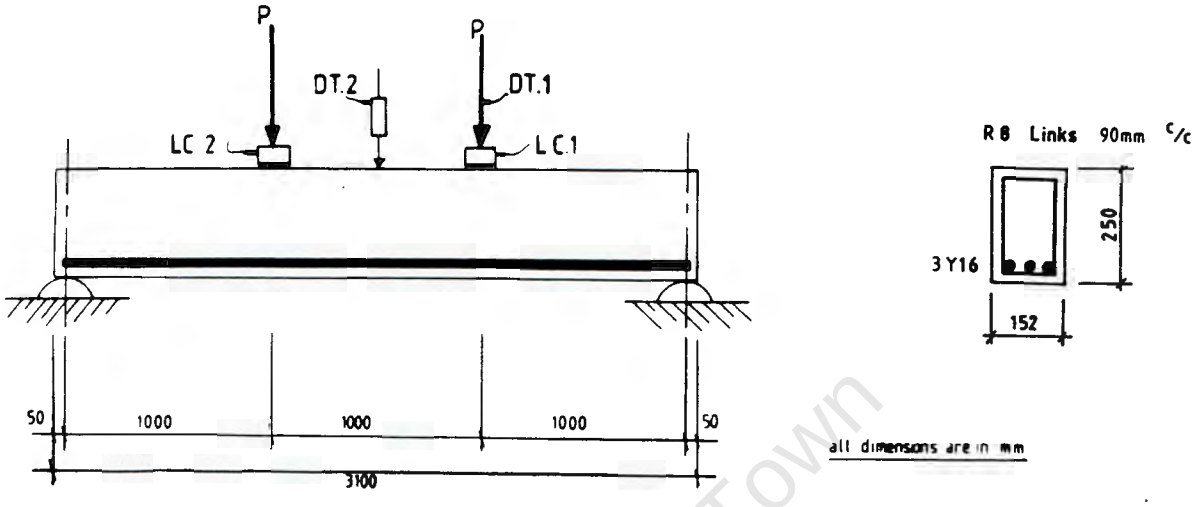

Figure 3.5: Simply-Supported Beam of Set 3.

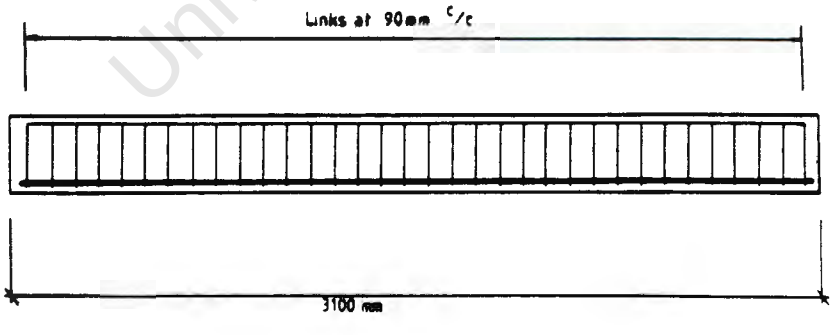

Figure 3.6: Stirrup Spacing for the Simply Supported Beams.

3.4 Instrumentation and Measurement

3.4.1 Instrumentation

In each test, monitoring of the applied loads and resulting deflections was accomplished using the instrumentation described below:

Applied loads: Two Kyowa-BL-20TB load cells were used to monitor the applied loads (figure 3.7). These load cells are the centre-hole type and detected the applied loads through an internal "strain-tube" on which four different strain gauges are mounted in a full Wheatstone bridge circuit arrangement. Applied loads of up to 200kN could be measured using these load cells (See Appendix A for specifications).

Displacements: Two Kyowa DT-100A displacement transducers, with a measuring range of 100mm, were used for the deflection measurement (figure 3.8). These transducers are also of the strain gauge type (See Appendix A for specifications).

The load cells and displacement transducers were recalibrated from time to time to test their consistency and accuracy (Appendix A).

Since these instruments are voltage measurement devices, additional read-out instruments were required for recording the relevant data and for converting this data into equivalent load or displacement readings. For this purpose, an HP 3054 DL data logging system, consisting of an HP 3497 A data acquisition control unit, a DC power supply bench (HP 6214 A model) and an HP 87 micro-computer with dual disc drive, printer and plotter, was used (figure 3.9). The data acquisition control unit is equipped with 20 Channel Guarded Input Relay assembley for DC voltage measurement.

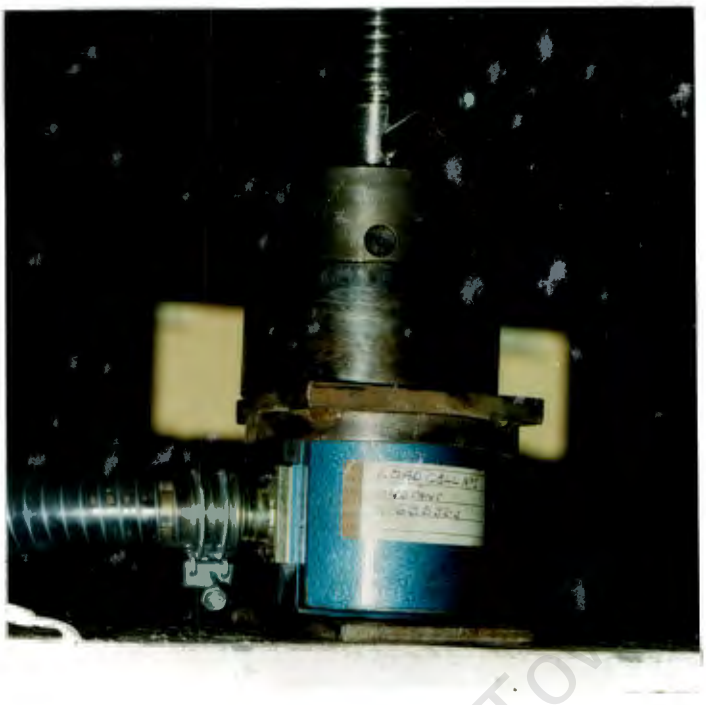

Figure 3.7: Kyowa-BL-20TB Load Cell.

Figure 3.8: Kyowa-DT-100A Displacement Transducer.

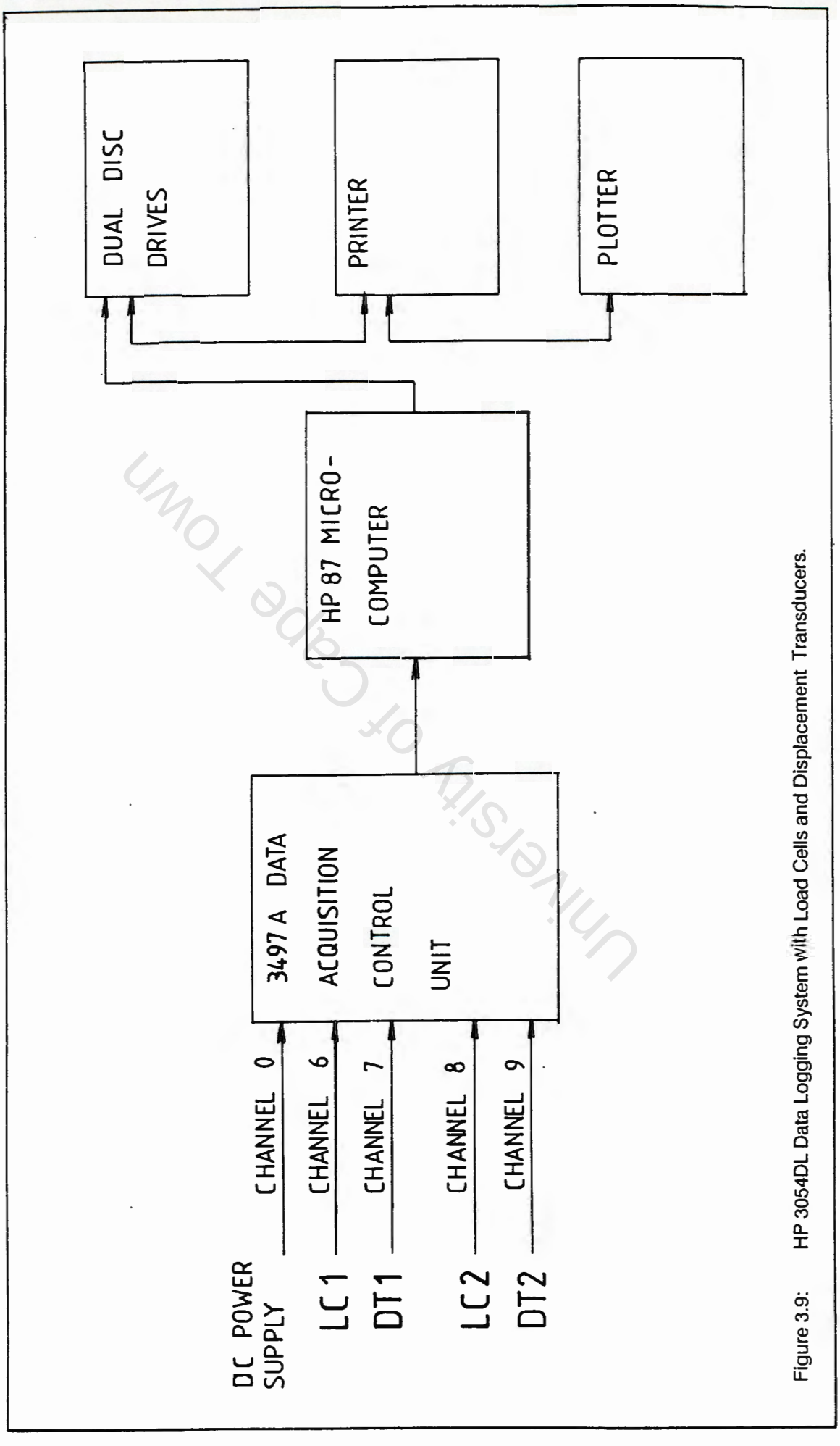

Figure 3.9: HP 3054DL Data Logging System with Load Cells and Displacement Transducers.

3.4.2 Measurements

The load cells, displacement transducers and the DC power supply bench were connected to the following channels on the 20 channel Guarded Input Relay assembly.

Channel 0: power source - DC power supply bench
Channel 6: load cell 1 (LC1)
Channel 7: displacement transducer 1 (DT1)
Channel 8: load cell 2 (LC2)
Channel 9: displacement transducer 2 (DT2)

As the loads were applied, the change in voltage in the load cells and displacement transducers were relayed to the relevant channels in the Gaurded Input Relay assembly. These voltages were then displayed on the digital counter of the data acquisition unit. At intervals of approximately 18 seconds, the program FSTEST (written for the HP 87 micro-computer) scanned the reading reflected on the counter. The program FSTEST converted these readings into equivalent loads and displacements (measured in kN and mm respectively). During each scan a burst of readings was taken, the results were printed and the data was written to a data file previously created on a data disc. A maximum of 400 scans was permitted.

The program FSTEST is a modified version of BTEST, written by Lloyd [36] for logging the experimental readings (see Appendix B). The program BTEST allowed for only one load cell and displacement transducer to be connected to the system. FSTEST allowed for an additional load cell and displacement transducer to be added to the system.

3.5 Testing Procedure

The experimental tests were performed in an Amsler test-bed in the laboratory. The beams in Set 1 and Set 2 described earlier, were tested as two-span continuous beams on three supports, the spans being each 1,8 metres in length. Each support consisted of a concrete block, roughly 400 x 400mm in area and 600mm in height. A metal half cylinder was placed on top of each concrete block. The test-beam was lowered onto these half-cylinders and the spans adjusted until they were as shown in figure 3.3. Final adjustments to the height of the supports were made by wedging in thin plates (about 0,5 mm thick) between the concrete blocks and the half cylinders until the beam was completely level. The applied loading consisted of a point load at the centre of each span. The loads were thus symmetrically arranged with respect to the interior support. A load cell and a displacement transducer was placed at the positions where the loads were applied (figure 3.3).

The beams in Set 3 were set-up over two supports, the span between supports being 3,0 metres. Each support consisted of the concrete block on which a metal half cylinder was placed (these were described earlier). The loading consisted of identical point loads applied at the third-points of the beam (figure 3.5). A load cell was placed at each position of load application while a displacement transducer was placed at midspan and at one of the points of load application (figure 3.5).

The load cells and displacement transducers were connected to the data control unit. This in turn was linked to the micro-computer system. At the start of the test, a data-file was created and the program FSTEST was loaded. The program then performed various checks on the measuring devices connected to the HP87 and printed the findings. If these checks were passed, zero readings were taken and the scanning commenced.

At this stage the loads were applied to the beam. Application of the loads was controlled manually via the Amsler control unit. For Set 1 and Set 2, the loads were gradually applied at an initial rate of about 1kN per minute. When the loads reached about 70kN, the rate of loading was decreased to about 1kN every 2 minutes. For Set 3, the loads were applied at a rate of about 1kN per minute for the full duration of the test.

The beams FS4 to FS6 of Set 1 and all the beams in Set 3 (refer to table 3.1) were loaded monotonically to failure. Beams FS7 to FS10 of Set 2 and FS11 to FS14 of Set 1 were loaded until some yield of the tension reinforcement had occurred. Subsequent unloading and reloading cycles were arbitrarily applied until the beam failed in flexure.

At this stage the beam was unloaded and the test terminated by pressing the function key, K1 on the keyboard of the HP87 (See Appendix B). The stored results were subsequently plotted using the plotting program, FSPLOT (See Appendix B).

3.6 Observations made during Testing of the Two-span Beams.

The observed behaviour of the two-span beams during the load-deflection tests are discussed in this section. The discussions for the beams in Set 1 and Set 2 are combined since no difference in behaviour was visually observed.

The beams FS4 to FS6 of Set 1 were loaded monotonically to failure. In these beams, the first visible cracks appeared when the applied loads reached about 24kN. These fine vertical cracks occurred in the tension regions at the midspans (directly under the loads) and over the interior support. As the applied loads were increased, these cracks multiplied and grew larger. When the loads reached about 70kN (just prior to the yielding of the steels), the cracks had opened to between 1 and 2mm. (figures 3.10 and 3.11). After the tension steel had yielded, the cracks opened even wider, especially over the interior support and at midspan of one of the two spans. Failure of a beam generally occurred after the tension steel in one of the spans and over the interior support had yielded so much and the concrete was so severely cracked that its resistance to loading was negligible (figures 3.12; 3.13; 3.14 and 3.15). At this stage, the displacements at the centre of the span in which failure occurred was far higher than in the opposite span (see displaced shape of beam at failure in figure 3.15).

In one span in beam FS6, the major crack formed directly above one of the displacement transducers. As the applied loads increased and the steel began yielding, the crack opened wider and the movable probe of the transducer moved up into the crack (figures 3.16 and 3.17). The results obtained after the loads reached 90kN should thus be disregarded since they do not reflect the true load-deflection behaviour of the beam.

The beams FS11 to FS14 of Set 1 and FS7 to FS10 of Set 2 were loaded monotonically only until some yield of the tension steel had occurred. Thereafter, the beams were subjected to repeated unloading and reloading cycles. During the first loading cycle up to the yielding of the steel, these beams behaved similarly to the beams discussed earlier. During the first unloading cycle, the tension cracks almost closed up. These opened up again, (this time even wider) during the first reloading cycle. These unloading and reloading cycles were repeated until the cracks were so wide that the beam could not sustain any more load. Failure occurred in a similar way as for the beams FS4 to FS6 (figure 3.18).

The span which experienced the higher displacements at failure occurred arbitrarily, i.e. in beam FS11 the greater displacements were experienced in span 1 while in beam FS12 the greater displacement occurred in span 2 (compare figures 3.18 and 3.19). This behaviour was not unexpected since reinforced concrete is not a homogeneous material.

All the beams in Set 1 and Set 2, with the exception of beam FS10, failed in bending. The beam FS10 failed in shear mainly as a result of the rate of loading being too high. In beam FS9, the displacement transducer also moved up a major crack (as happened in beam FS6). The results obtained after the first unloading - reloading cycle should therefore also be disregarded.

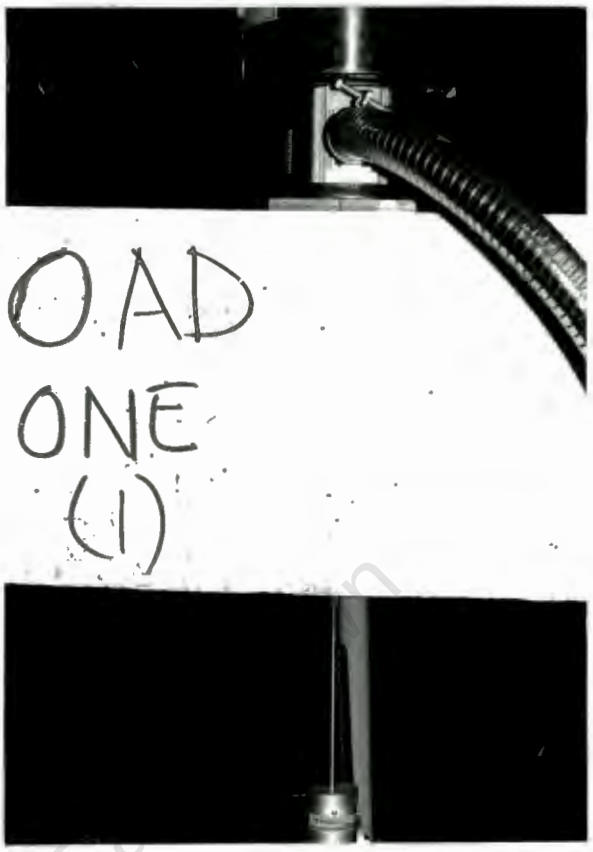

Figure 3.10: Cracking under LC1 in test-beam FS6 when the applied loads reached 76kN.

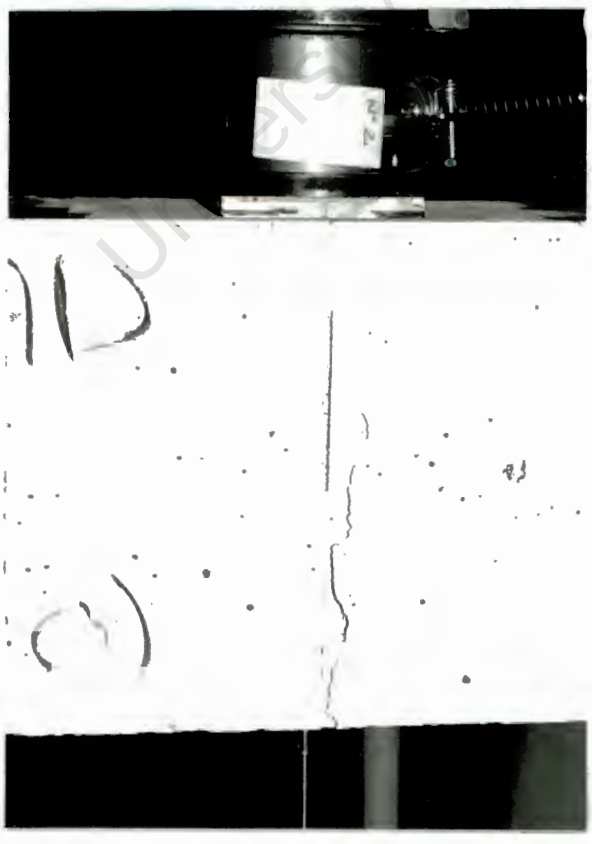

Figure 3.11: Cracking under LC2 in test-beam FS6 when the applied loads reached 76kN.

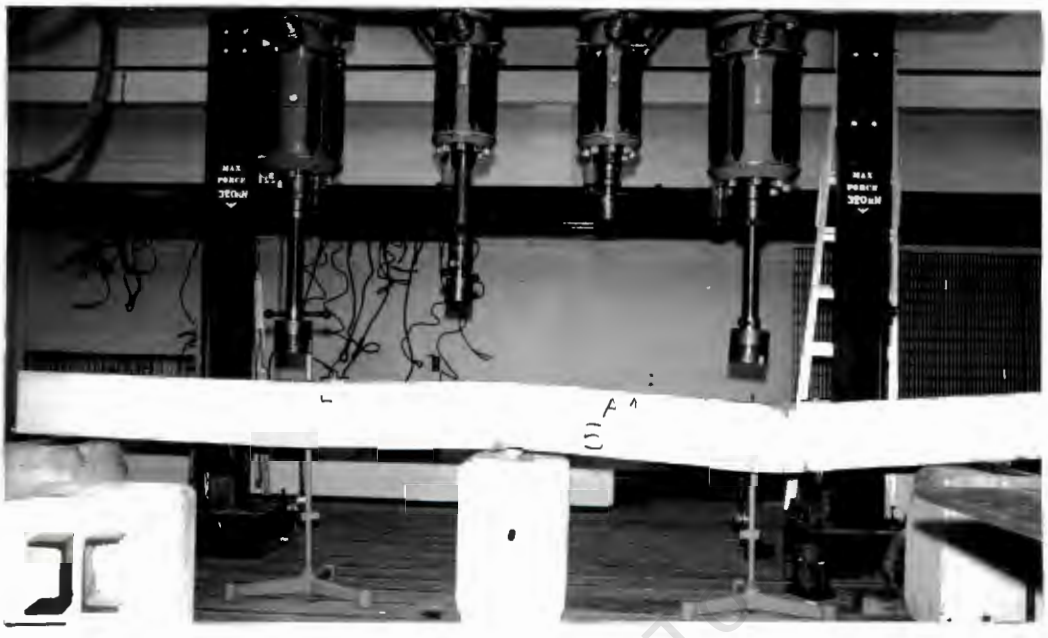

Figure 3.12: Profile of test-beam FS5 at failure

Figure 3.13: Tensile cracking over the interior support of beam FS5 at failure

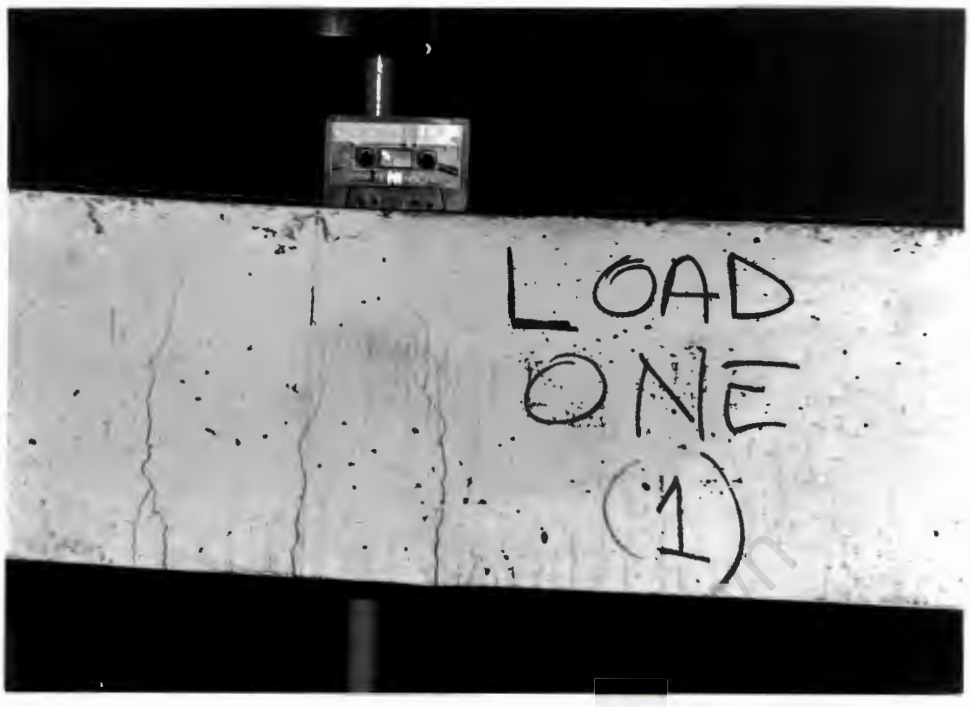

Figure 3.14: Tensile cracking under Load One - beam FS5 at failure.

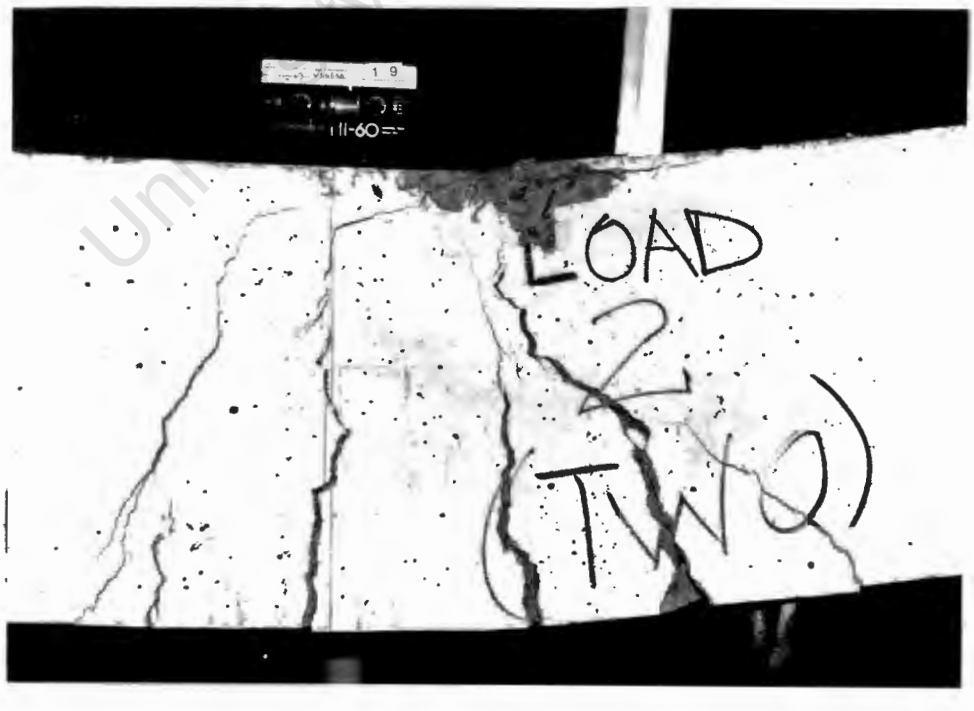

Figure 3.15: Tensile cracking under Load Two - beam FS5 at failure.

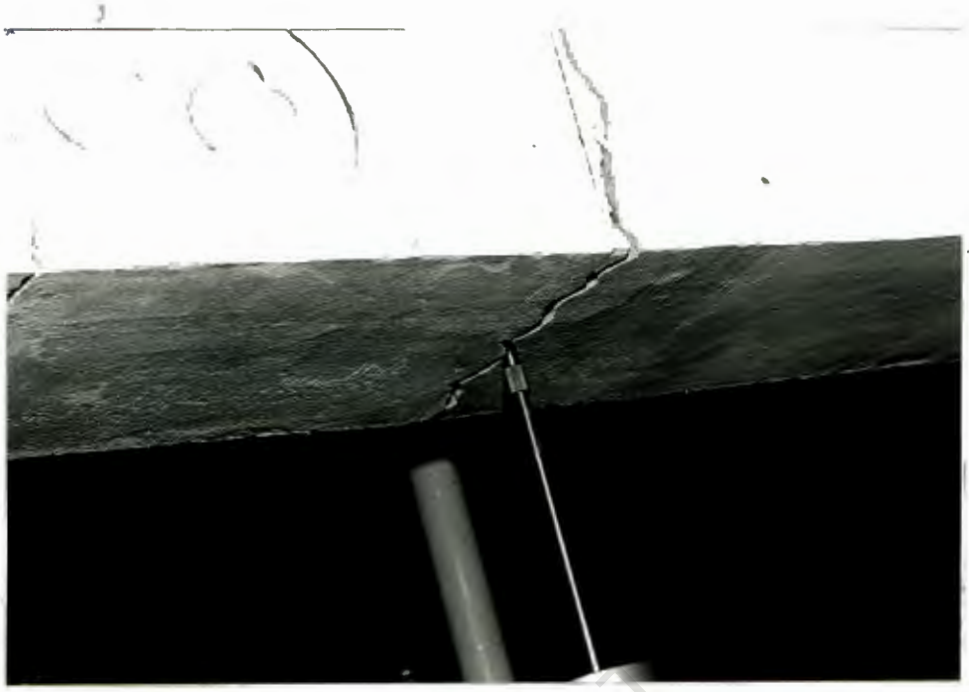

Figure 3.16: Displacement transducer starts to move up into crack directly under Load two in beam FS6.

Figure 3.17: Position of displacement transducer under load two at failure of beam FS6.

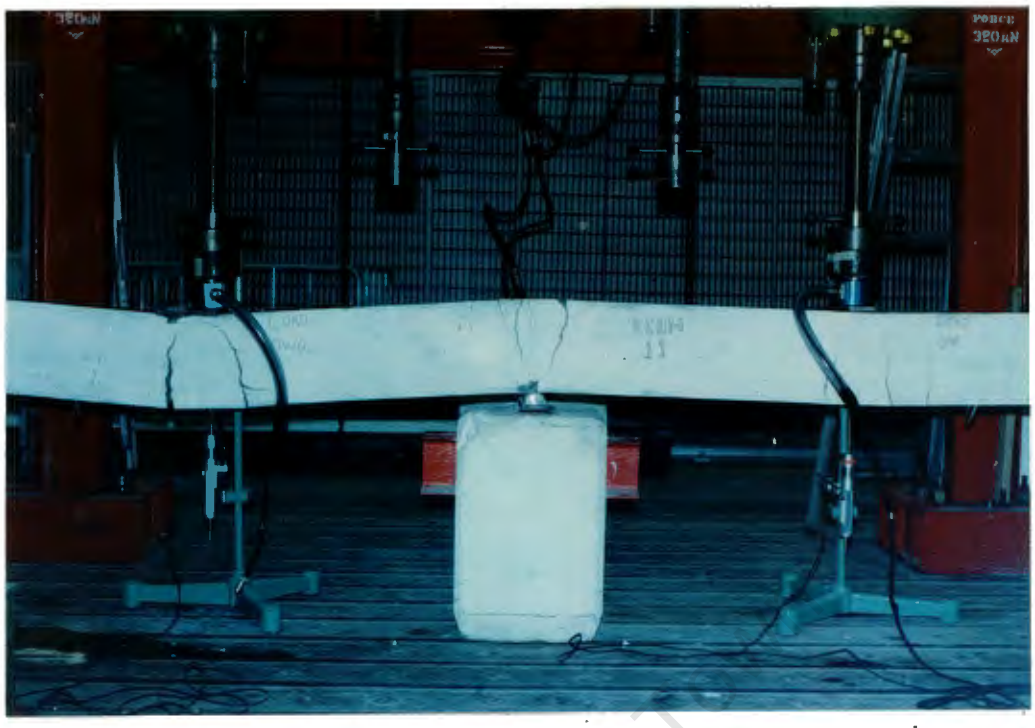

Figure 3.18: Beam FSII at failure. The beam failed in the left span and over the interior support.

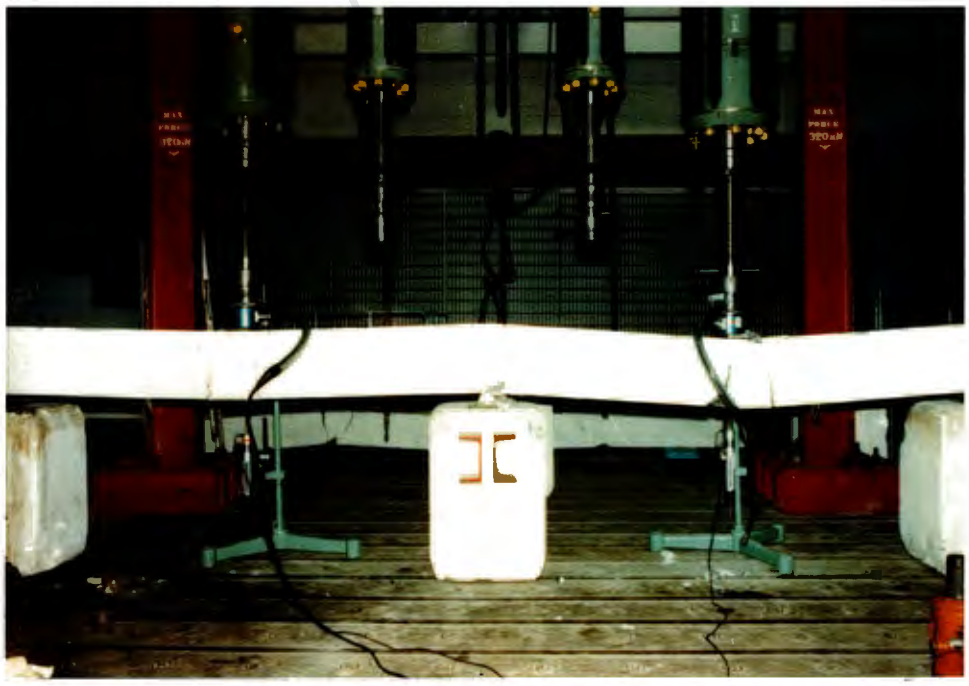

Figure 3.19: Beam FS12 at failure: Beam failure in the right span and over the interior support.

3.7 Observations made during Testing of the Simply Supported Beams.

The observations made during the testing of the simply-supported beams in Set 3 are discussed here. In all, four simply-supported beams were tested. These all behaved in a similar way during the testing process.

The over-reinforced beams in Set 3, beams SS1 to SS4 were subjected to increasing point loads at the third points until failure occurred. Considering beam SS2 as an example, the first visible cracks occurred when the loads reached 15kN. These were visible in the tension zone and were well spread between the points of load application (figure 3.20).

When the applied loads reached about 28kN, a major crack began opening up in the tension zone at the midspan of the beam (figure 3.21). At the same time fine horizontal cracks began developing in the compression zone directly above this major tension crack (figures 3.21 and 3.22). As the loads increased, the concrete began to crush in the compression zone while the major tension crack opened wider (figures 3.22 and 3.23). With further applied load (at about 50kN), the tension crack seemed to have opened to a maximum width and the crushing of the compression concrete intensified. The beam began failing in compression when the loads reached 56kN. At this stage, the concrete was so severely crushed in the compression zone at midspan that the beam could not sustain any further applied loads (figure 3.24, and 3.25). The loads in the structure were then gradually released. The beams SS1, SS3 and SS4 were tested in the same way and similar behaviour observed.

Figure 3.20: Cracking in the tension zone of beam SS2 when the loads reached 19kN.

Figure 3.21: A major vertical crack begins to develop in the tension zone (bottom) close to the midspan in beam SS2 when the loads reached 28kN. Also, the concrete begins to crush in the compression zone (top).

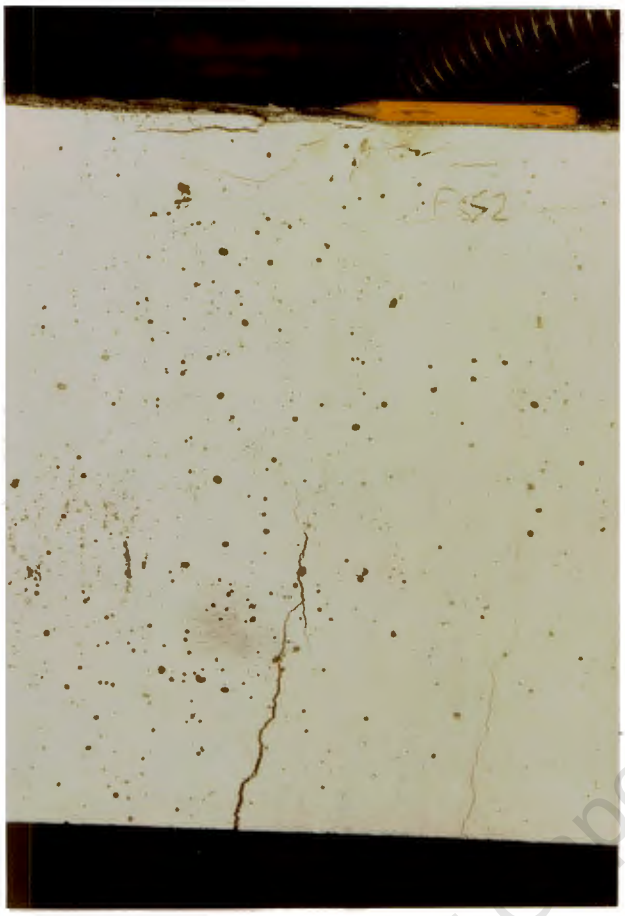

Figure 3.22:
The crushing of the concrete in the compressive zone continues while the major tension crack open even wider when the loads reached 40kN.

Figure 3.23:
The crushing of the compression concrete intensifies while the tension crack appeared to have reached a maximum width when the loads reached 50kN.

Figure 3.24:
The crushing of the compressive concrete intensified further when the loads reached 55kN.

Figure 3.25: When the loads reached 56kN, the concrete was so severely crushed in the compressive zone that the beam, SS2, could not sustain any further applied load.

CHAPTER 4

TEST RESULTS FOR THE EXPERIMENTAL BEAMS

4.1 Introduction

The results obtained in the experimental investigation are presented and discussed in this chapter. These results are divided into two catagories:

i) test results on samples of the constituent materials, concrete and steel, used to determine the material properties.

ii) load-deflection plots for the two-span beams in Set 1 and Set 2 and for the simply-supported beams in Set 3.

4.2 Concrete Cube Tests

Prior to the load-deflection test of a beam, the six concrete cubes cast at the time of manufacture of the beam were crushed in the Amsler compression testing machine in the laboratory. The averaged cube strength obtained from these tests was used to calculate the general compressive strength of the beam. The results from these tests are presented in Table 4.1.

4.3 Reinforcement Uniaxial Tests

Uniaxial stress-strain tests were performed on four samples of Y10 and three samples of Y16 reinforcing bars. These samples were randomly selected from the batches of Y10 and Y16 bars used in the manufacture of the two-span and simply supported beams respectively. The strains were measured using a mechanical dial gauge extensometer clamped onto the bar over a fixed gauge length of 8 inches (203 mm). The results of these tests are graphically presented in figure 4.1 and 4.2. These results were used to determine the material properties of the steel such as the Elastic modulus, hardening modulus and the yield stress.

Table 4.1 Average Concrete Compressive Cube Strengths

Set No	Beam	Age at Test (days)	Average Cube Strength (MPa)
trial	FS1	34	40,5
trial	FS2	37	40,2
trial	FS3	31	40,9
Set1	FS4	29	40,5
Set1	FS5	28	41,5
Set1	FS6	30	41,4
Set1	FS11	29	42,0
Set1	FS12	31	41,5
Set1	FS13	28	37,4
Set1	FS14	30	39,8
Set2	FS7	29	48,2
Set2	FS8	31	49,6
Set2	FS9	29	47,3
Set2	FS10	31	47,0
Set3	SS1	28	29,8
Set3	SS2	30	29,9
Set3	SS3	28	29,9
Set3	SS4	30	30,1

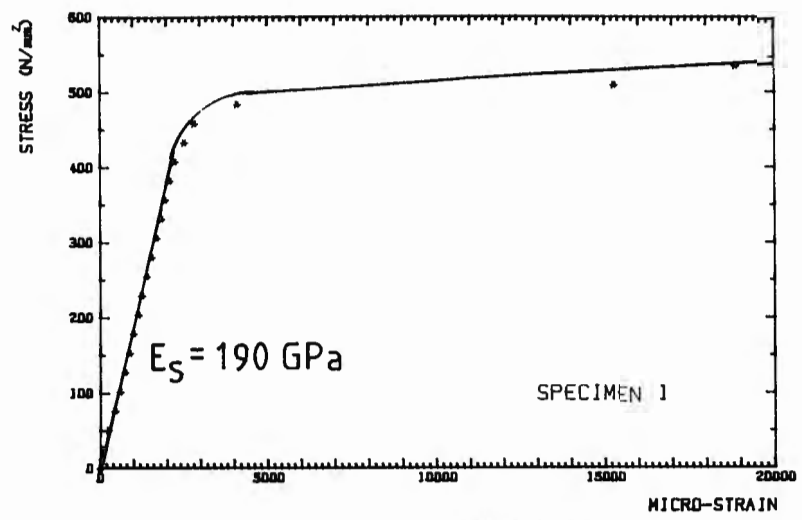

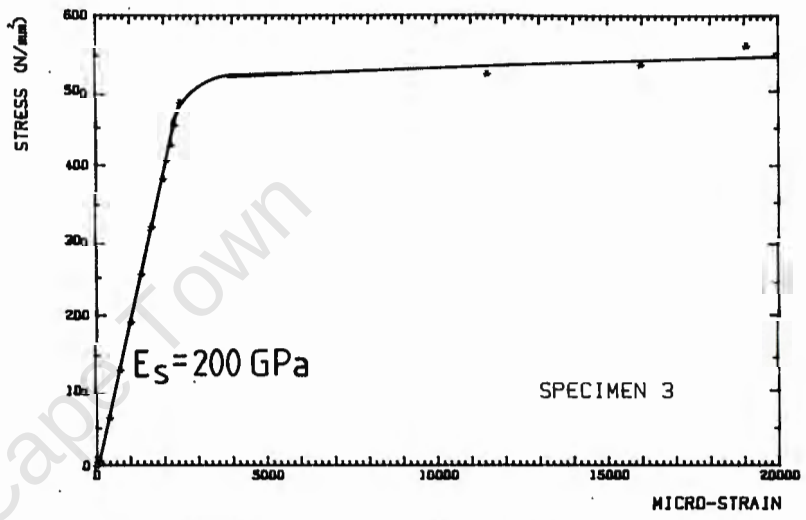

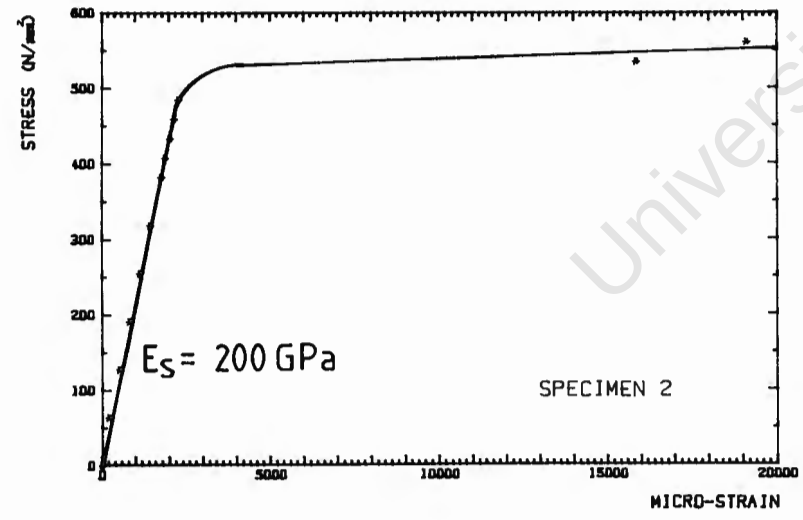

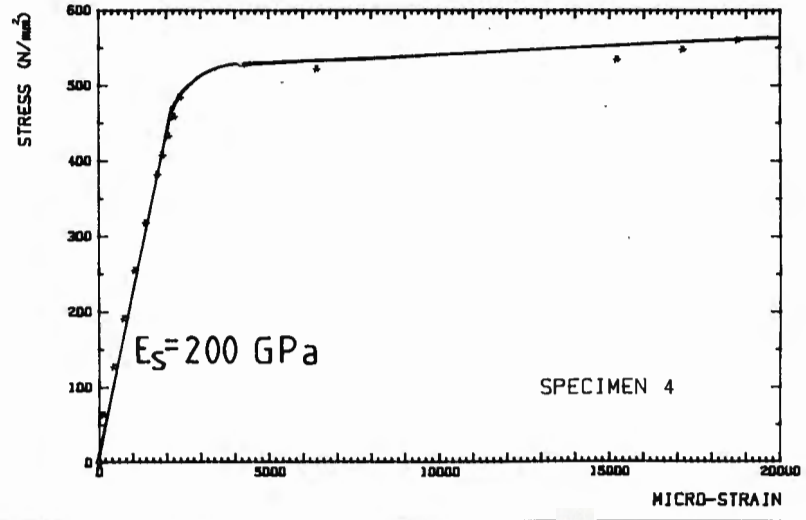

Figure 4.1 STRESS-STRAIN PLOTS FOR SAMPLE OF Y10mm BARS

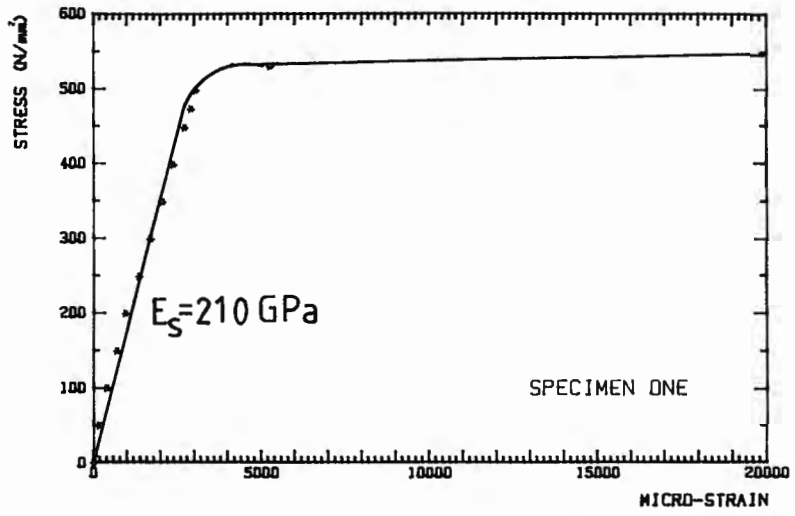

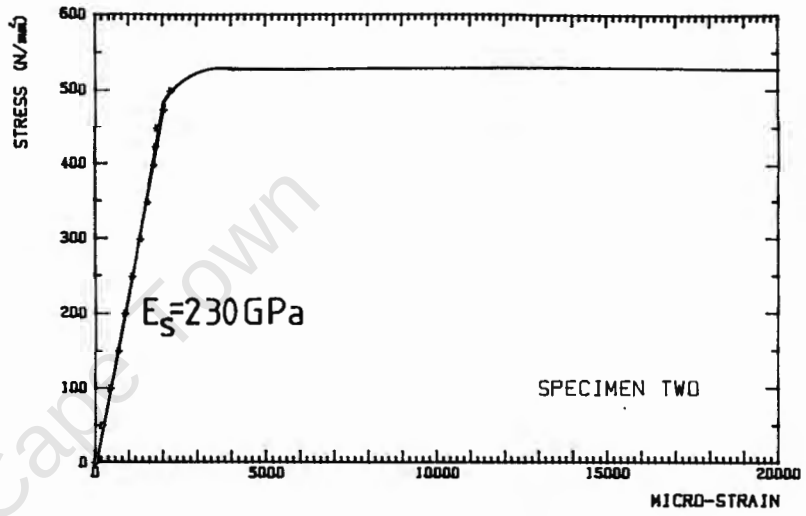

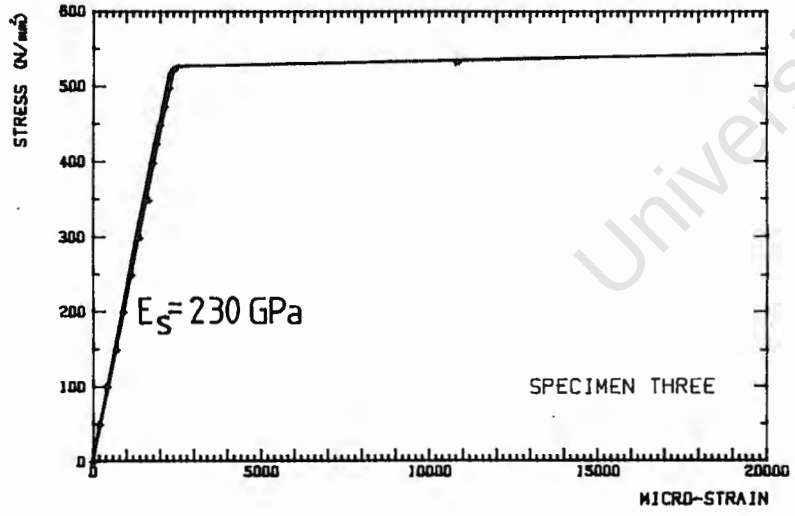

Figure 4.2 STRESS-STRAIN PLOTS FOR SAMPLE OF Y16mm BARS

4.4 Reinforced Concrete Beam Test Results

The computer plots, representing the load-deflection results of the beams tested in the laboratory are presented and discussed in this section. These plots are obtained using the plotting program FSPLOT (refer to Appendix B). The plots in figures 4.3 to 4.9 and figures 4.10 to 4.13 represents the midspan load-deflection behaviour of the two-span beams in Set 1 and Set 2 respectively. In these plots, the label "LOAD ONE" represents the load-deflection data measured by LC1 and DT1 while the label "LOAD TWO" represents the load-deflection data measured by LC2 and DT2. The plots in figures 4.14 to 4.17 represent the load-deflection behaviour of the beams in Set 3. In these plots, the "LOAD vs 1/3rd PT. DEFLECTION" represents the load-deflection data measured by a load cell and displacement transducer placed at a third point of the beam. The label "LOAD vs MIDSPAN DEFLECTION" represents the load deflection data measured by a load cell placed at the other third span and a displacement transducer placed at midspan.

The beams FS4 to FS6 of Set 1 (figures 4.3 to 4.5) were loaded monotonically until failure occurred. The general shapes of the plots are similar in each case. The first kink in the load-deflection curve occurs at about 24kN. This represents the initial cracking of the concrete in tension. The second kink occurs when the loads had reached about 76kN. This kink represents the initial yielding of the steel. Thereafter, the displacements increase rapidly with very little increase in applied loads. Also note that in the one span the increase in displacements is far greater than in the other span. This is due to the steel yielding more rapidly in the one span than in the other; eventually resulting in failure of the beam in the span with the larger displacements and over the interior support (as observed in Section 3.6). This phenomenon is mainly due to the non-homogeneous nature of the concrete material.

The rest of the beams in Set 1 and Set 2 (figures 4.6 to 4.13) were loaded monotonically only until some yield of the steel had occurred. Up to this stage, the midspan load-deflection behaviour of these beams is similar to the beams FS4 to FS6 discussed earlier. Thereafter, the beams were subjected to repeated unloading and reloading cycles until failure occurred. The hysteresis loop during unloading and subsequent reloading is evident in the load-deflection plots for these beams in figures 4.6 to 4.13. The reloading curve is virtually linear-elastic up to the load prior to unloading, since the concrete was fully cracked with negligible stiffness, so that the reinforcement provided most of the stiffness. Note that the displacements begin to increase more rapidly in the one span than in the other with each reloading cycle; eventually leading to failure in the span with the larger displacements and over the interior support as observed in Section 3.6.

As mentioned in Section 3.6, the results for beam FS6 (figure 4.5), after the loads reached 90kN, should be ignored since the movable probe of the displacement transducer moved up into a crack. Similarly, the results for beam FS9 (figure 4.12), should also be ignored after the second reloading cycle.

The simply-supported beams in Set 3, figures 4.14 to 4.17, were loaded monotonically until the concrete at midspan crushed so much in the compression zone that the beams could not sustain any more load. The beams were then unloaded. In these plots, the first kink in the load-deflection curves occur when the loads reached about 8kN. This represents the initial tensile cracking of the concrete. When the loads reached about 56kN, a second kink in the curves occur. This kink represents the ultimate crushing of the concrete in compression at the midspan of the beam.

In general, the load-deflection results for the two-span beams showed little variations from test to test. A similar observation can be made for the simply supported beams. In Chapter 6, finite element models of these beams are implemented in NLFRAM. In Chapter 7, the load-deflection results of the experimental beams are directly compared with the results from the finite element analysis.

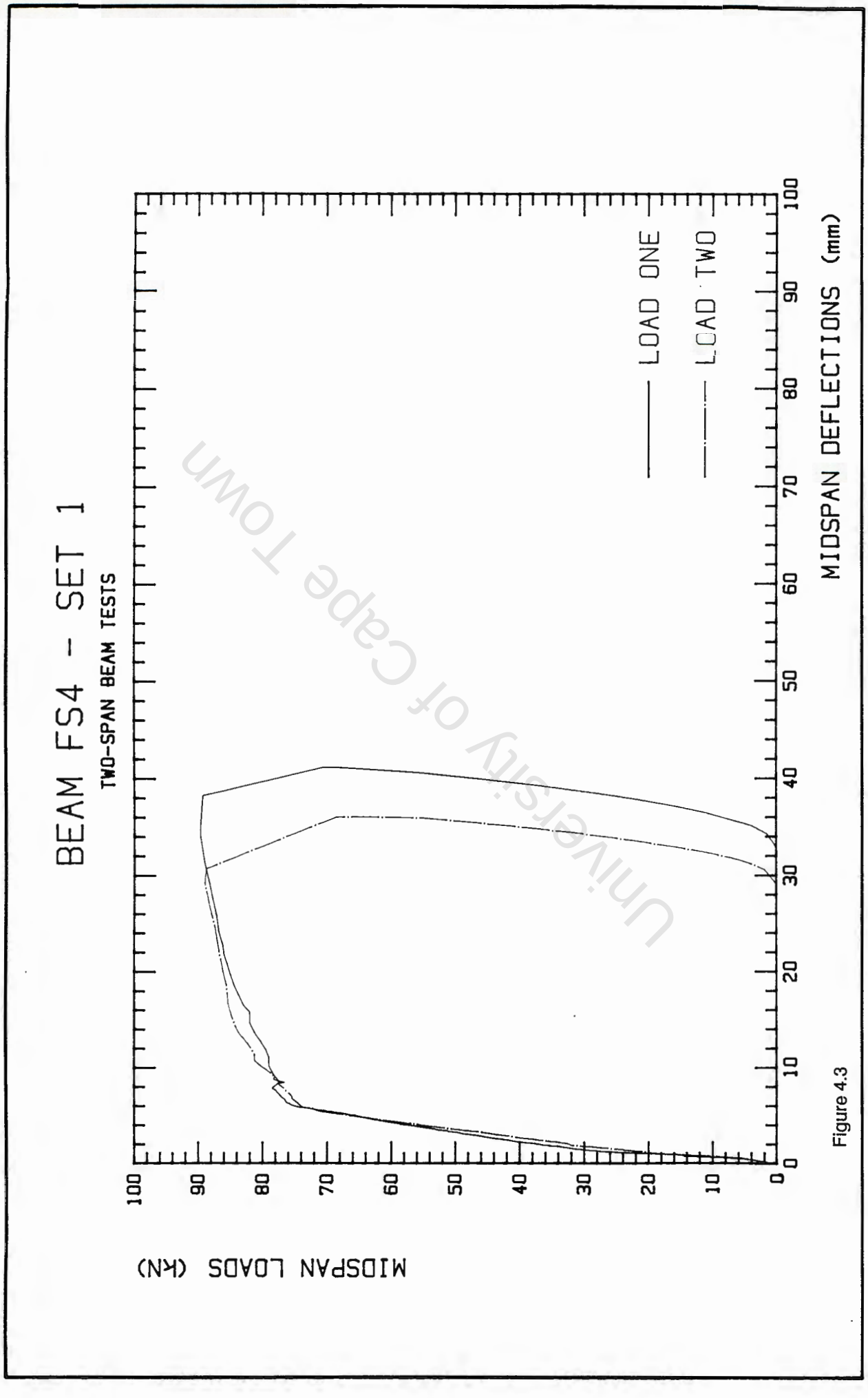

Figure 4.3

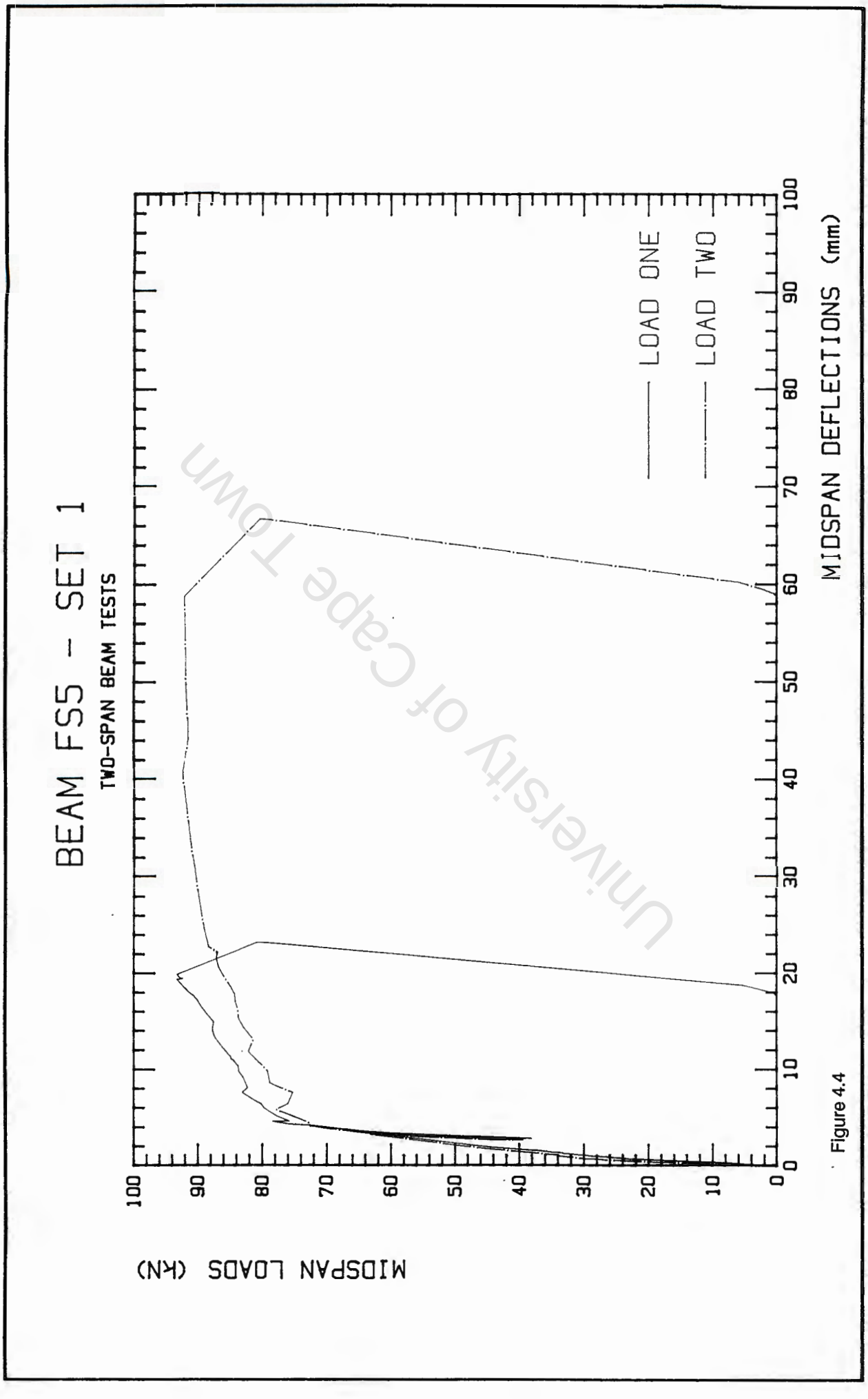

Figure 4.4

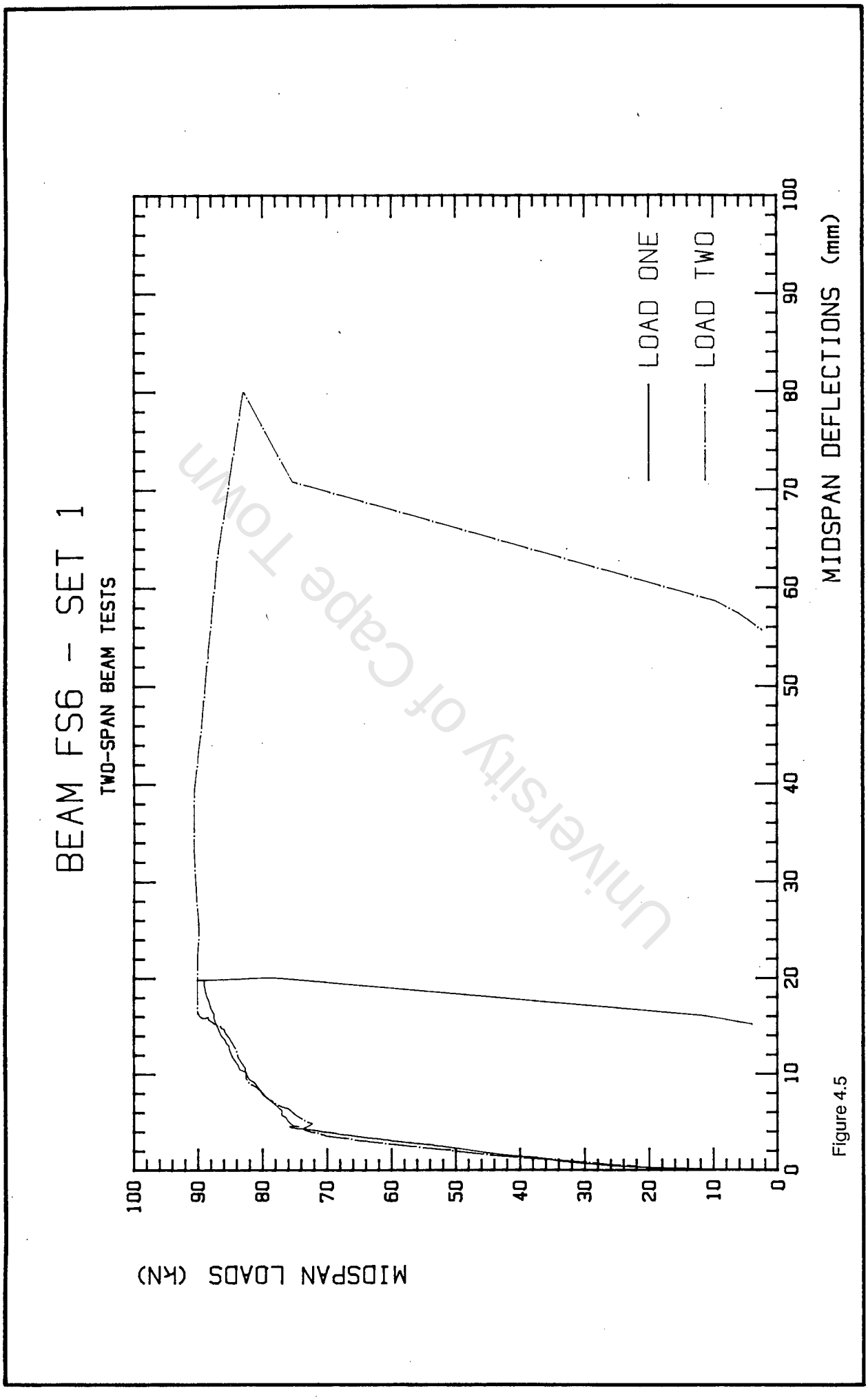

Figure 4.5

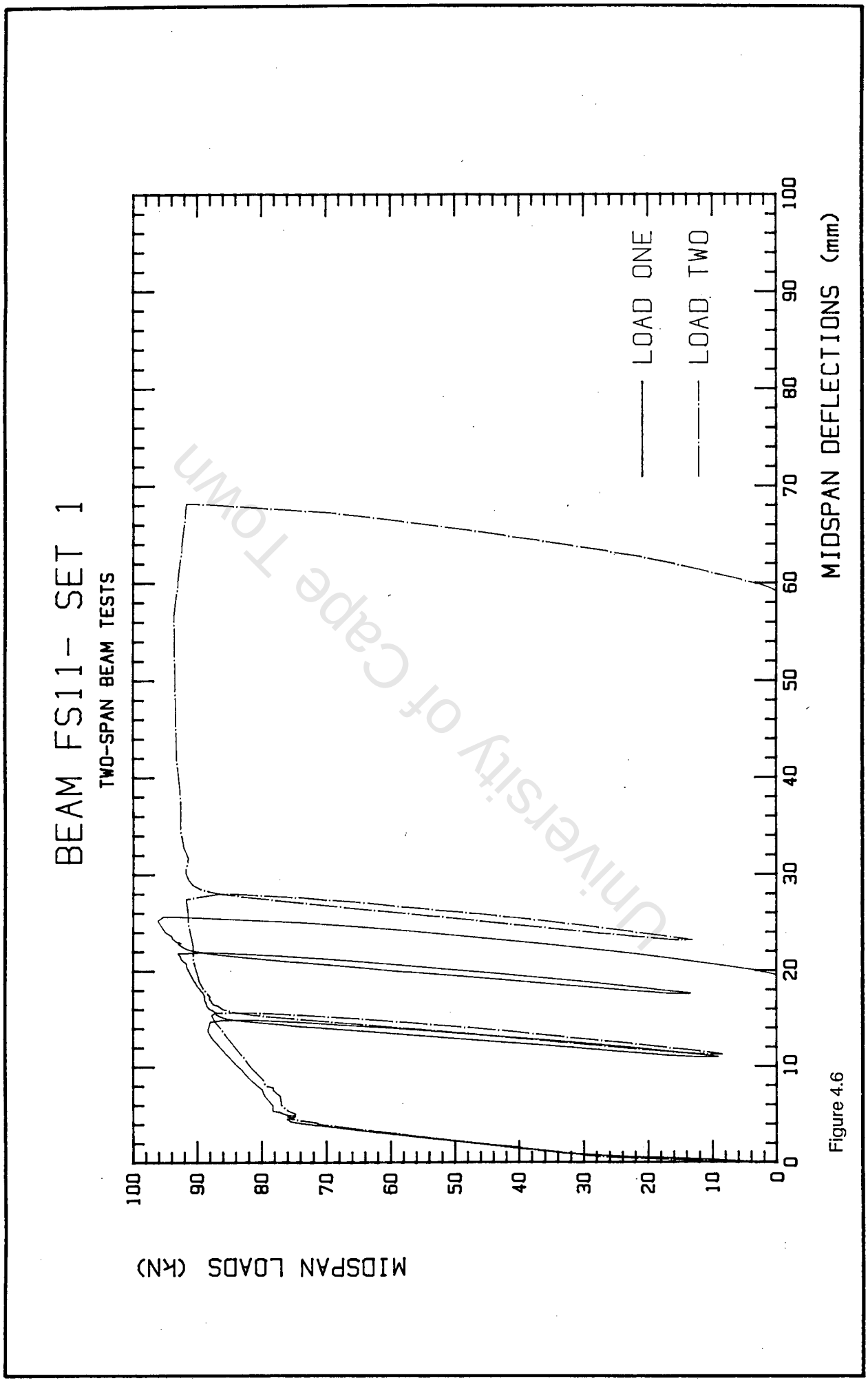

Figure 4.6

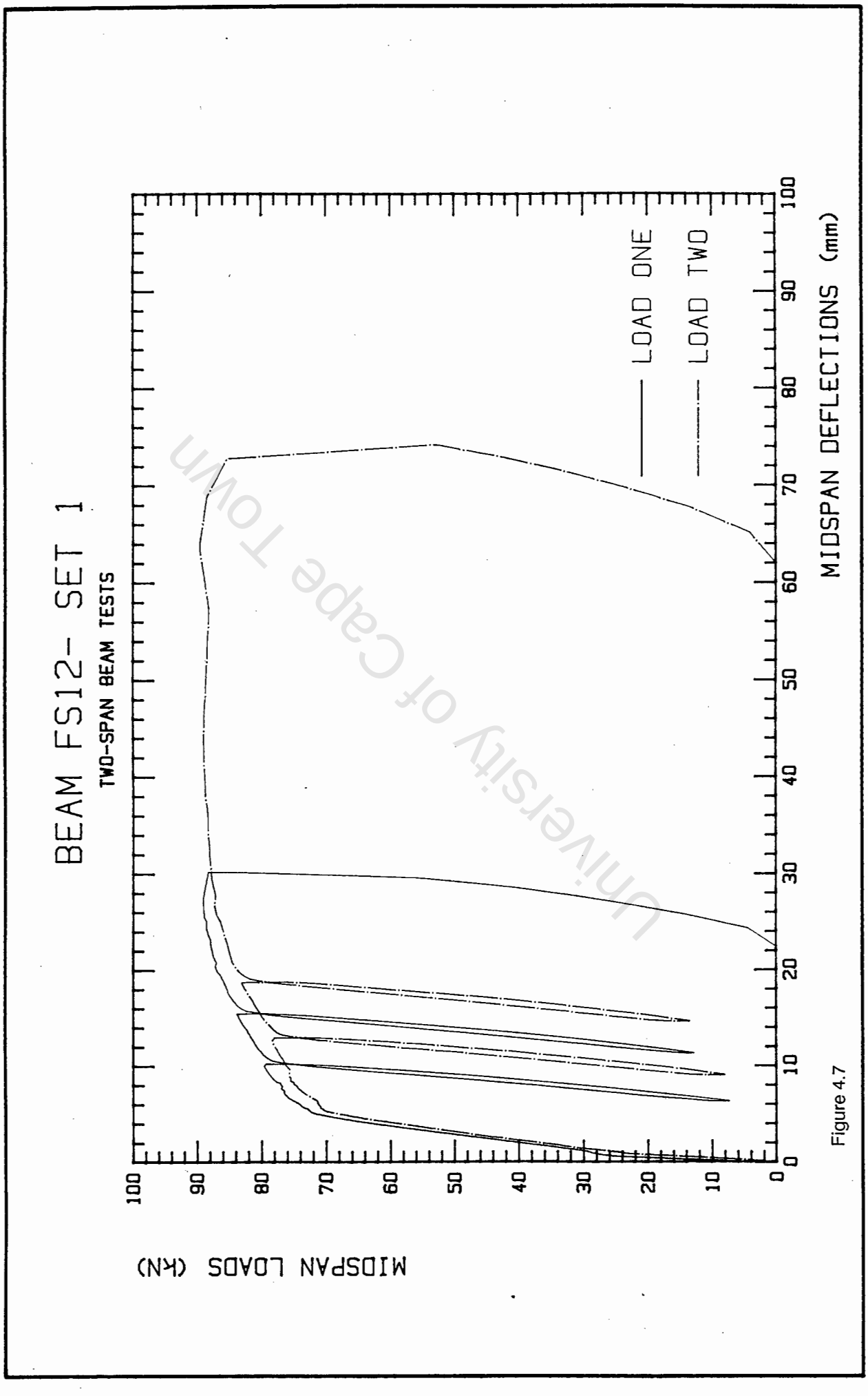

Figure 4.7

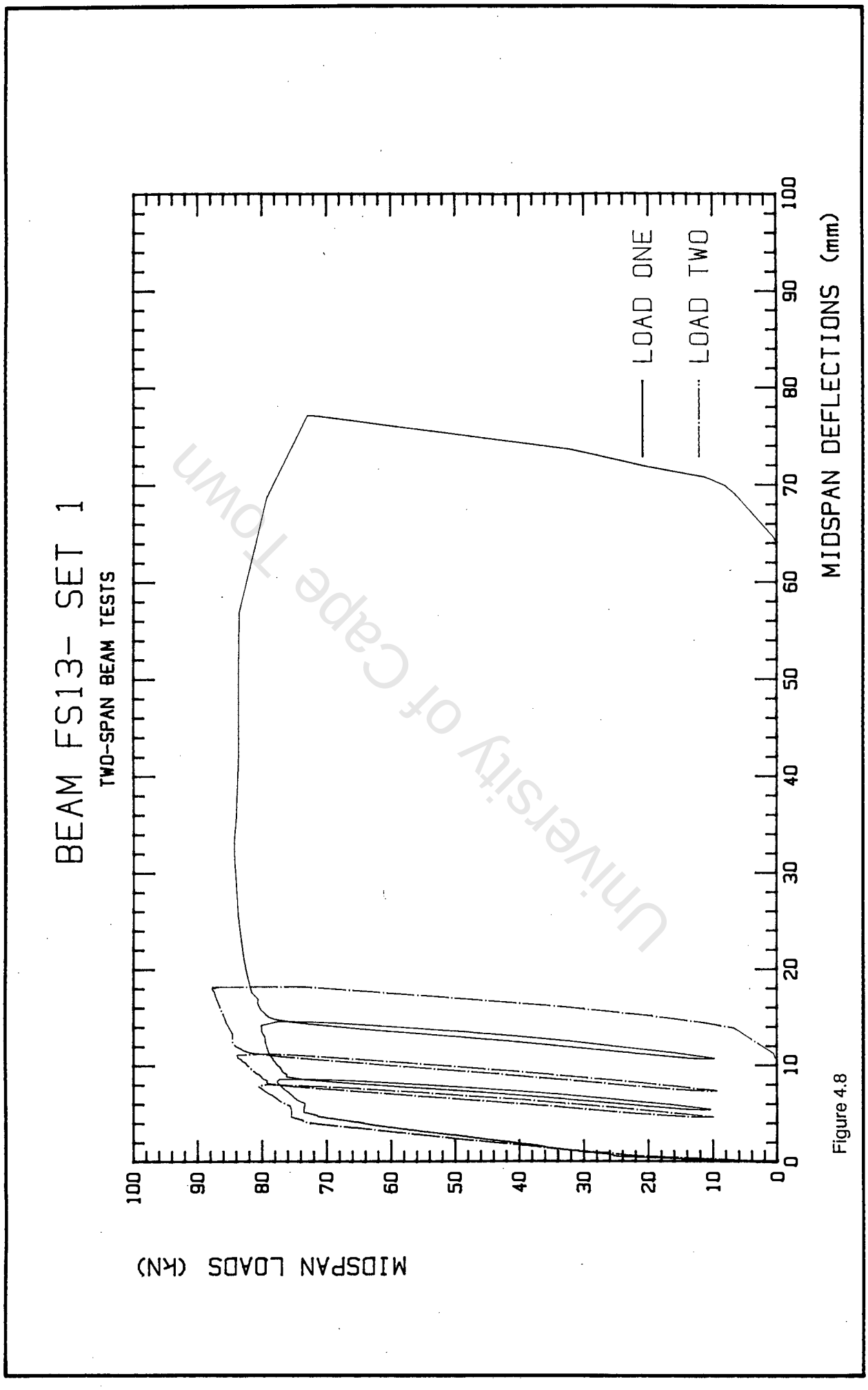

Figure 4.8

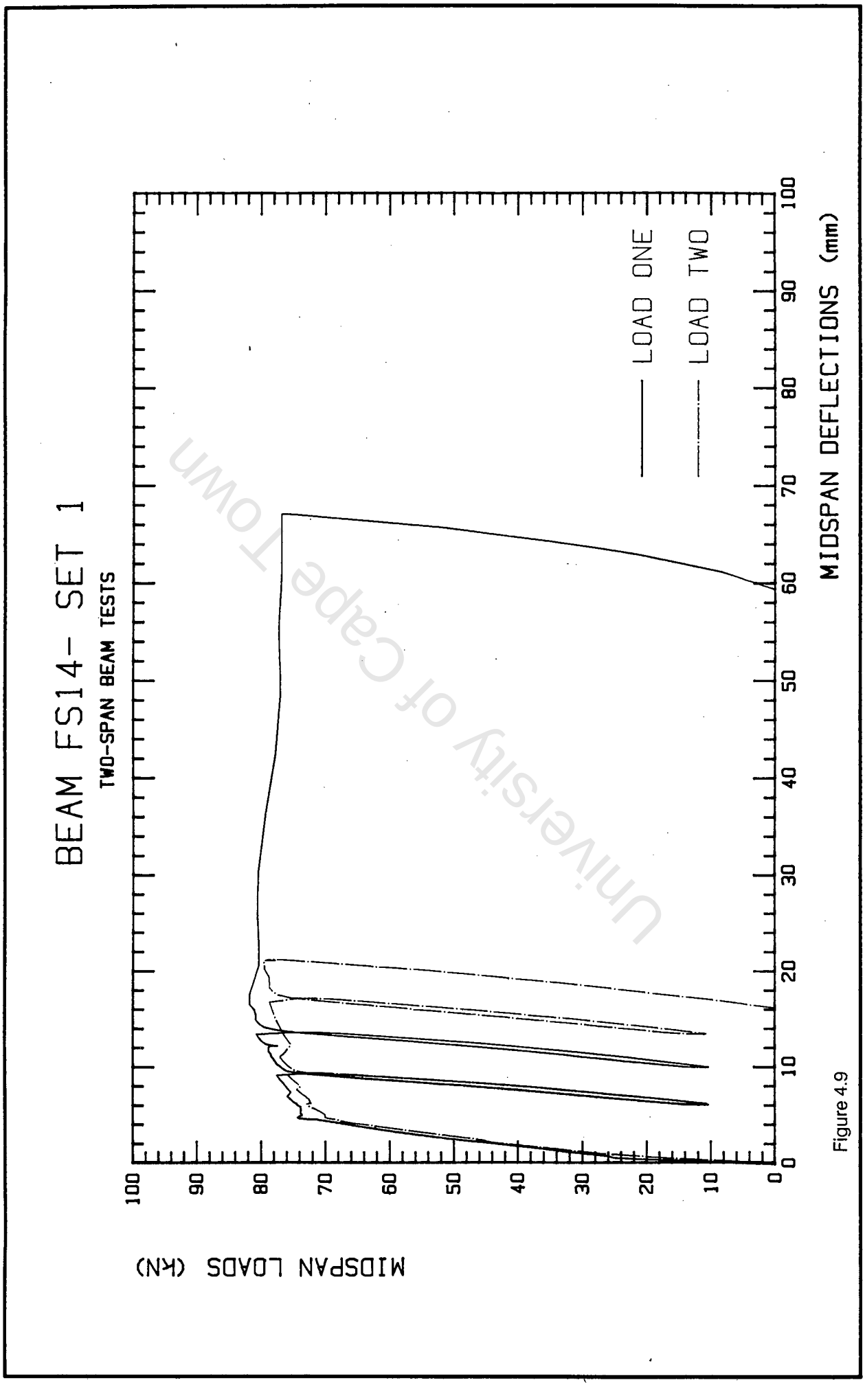

Figure 4.9

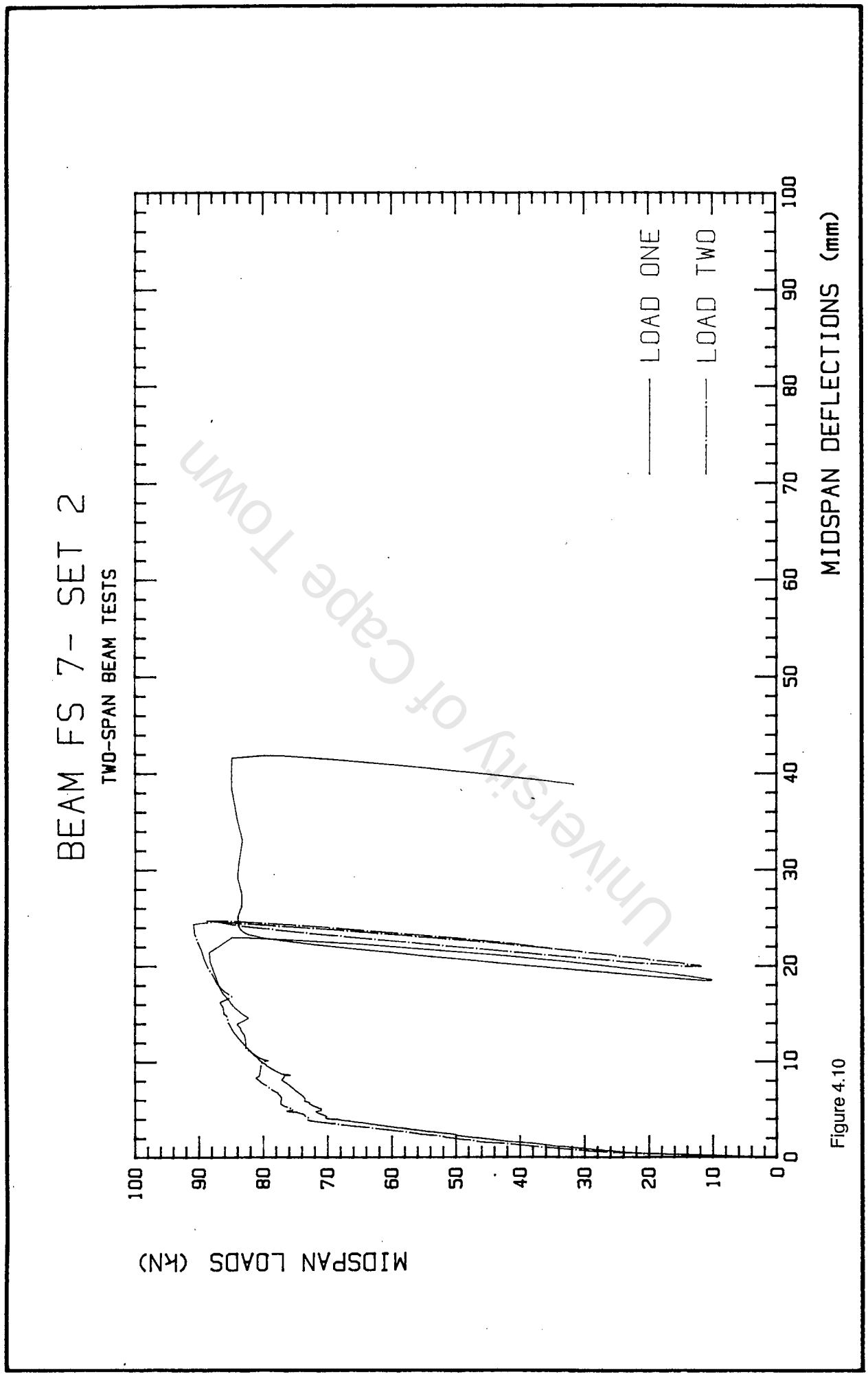

Figure 4.10

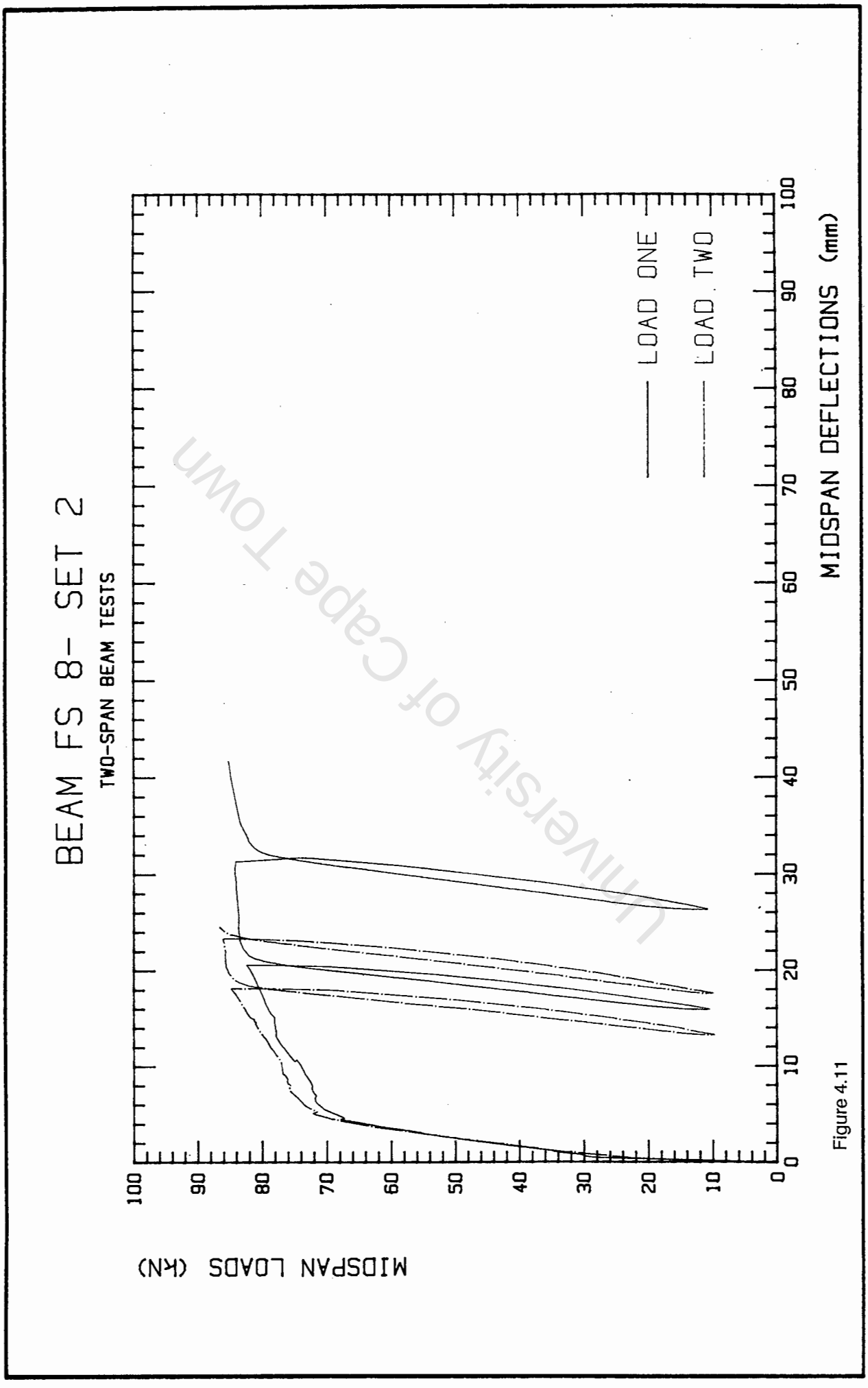

Figure 4.11

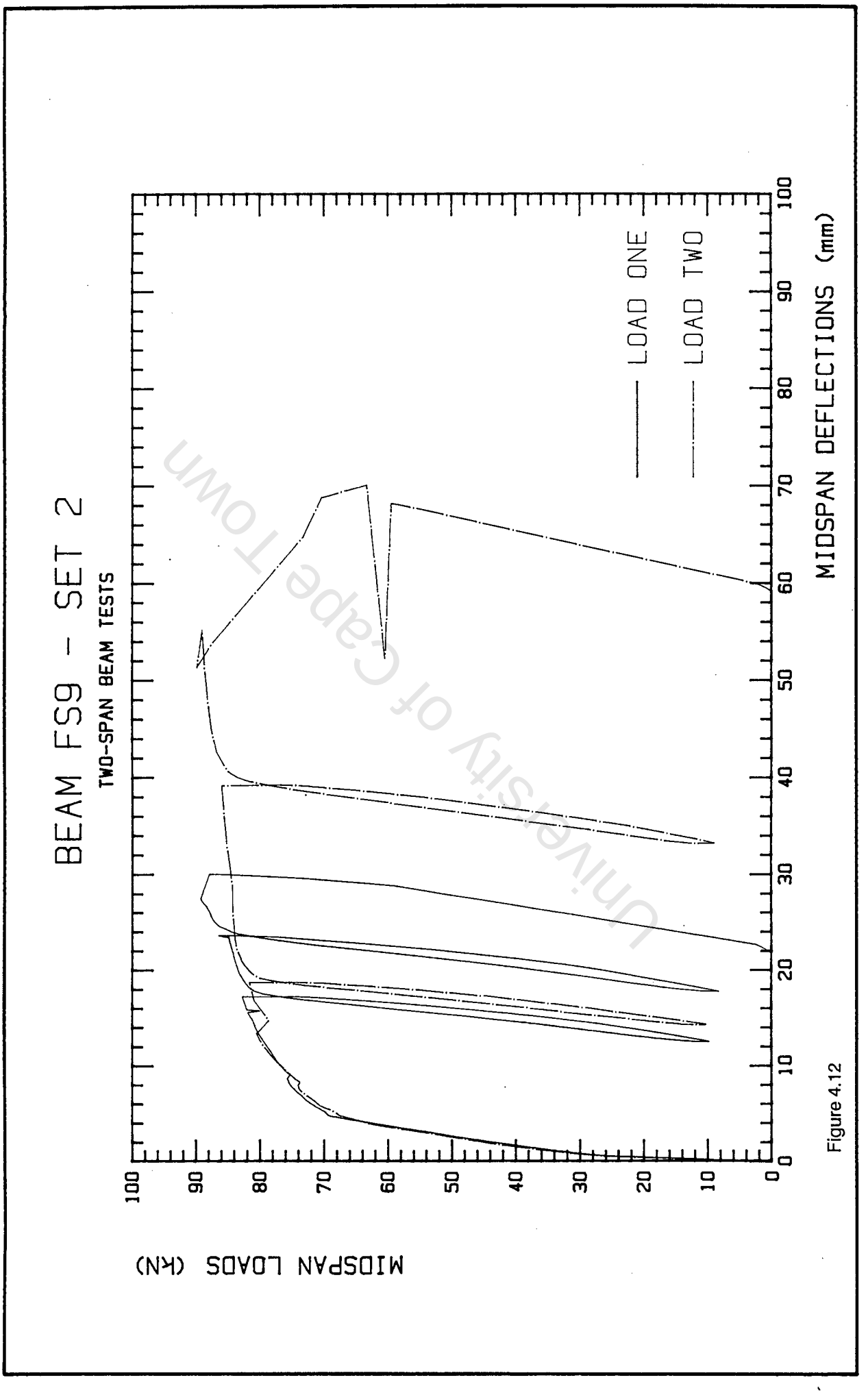

Figure 4.12

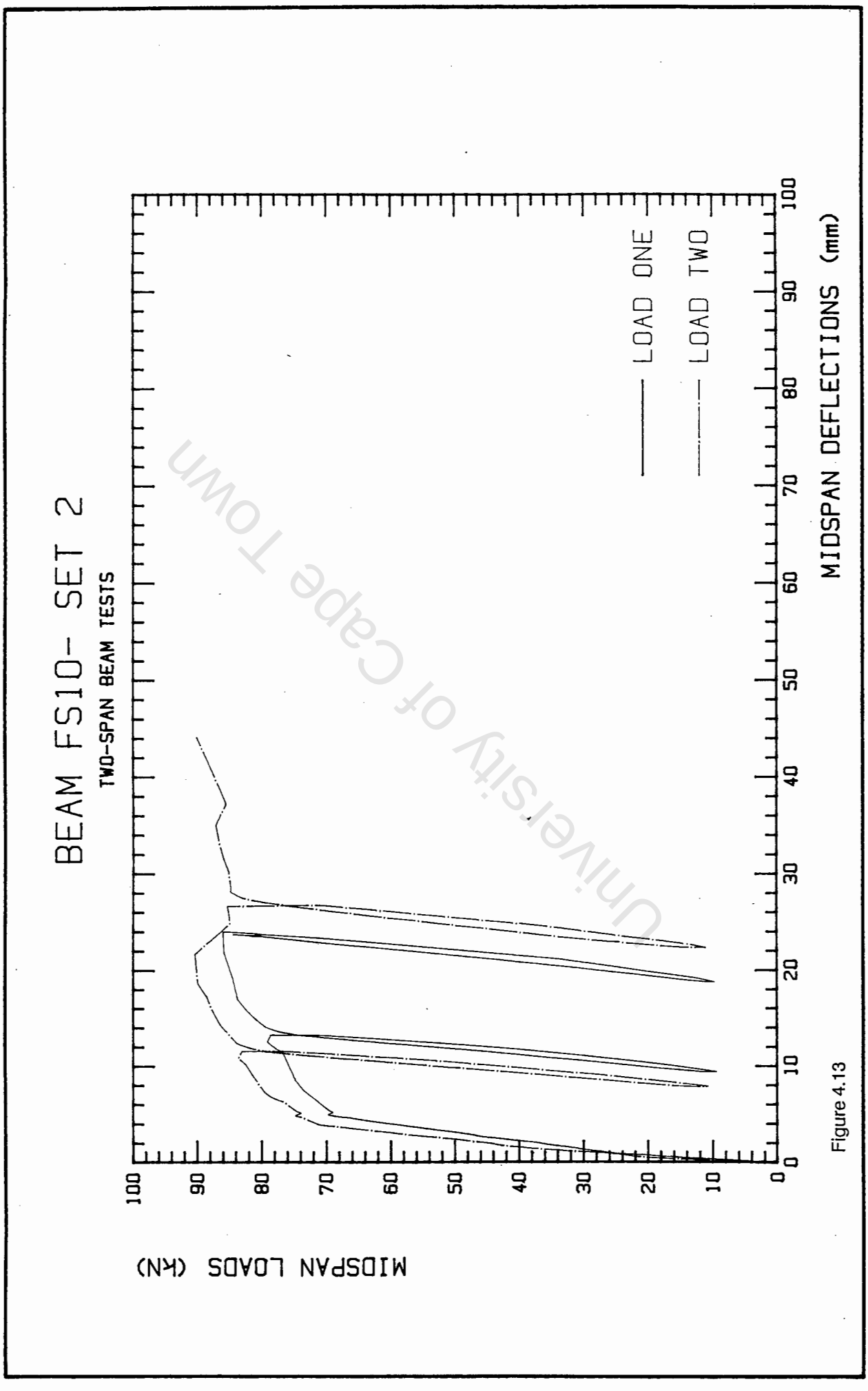

Figure 4.13

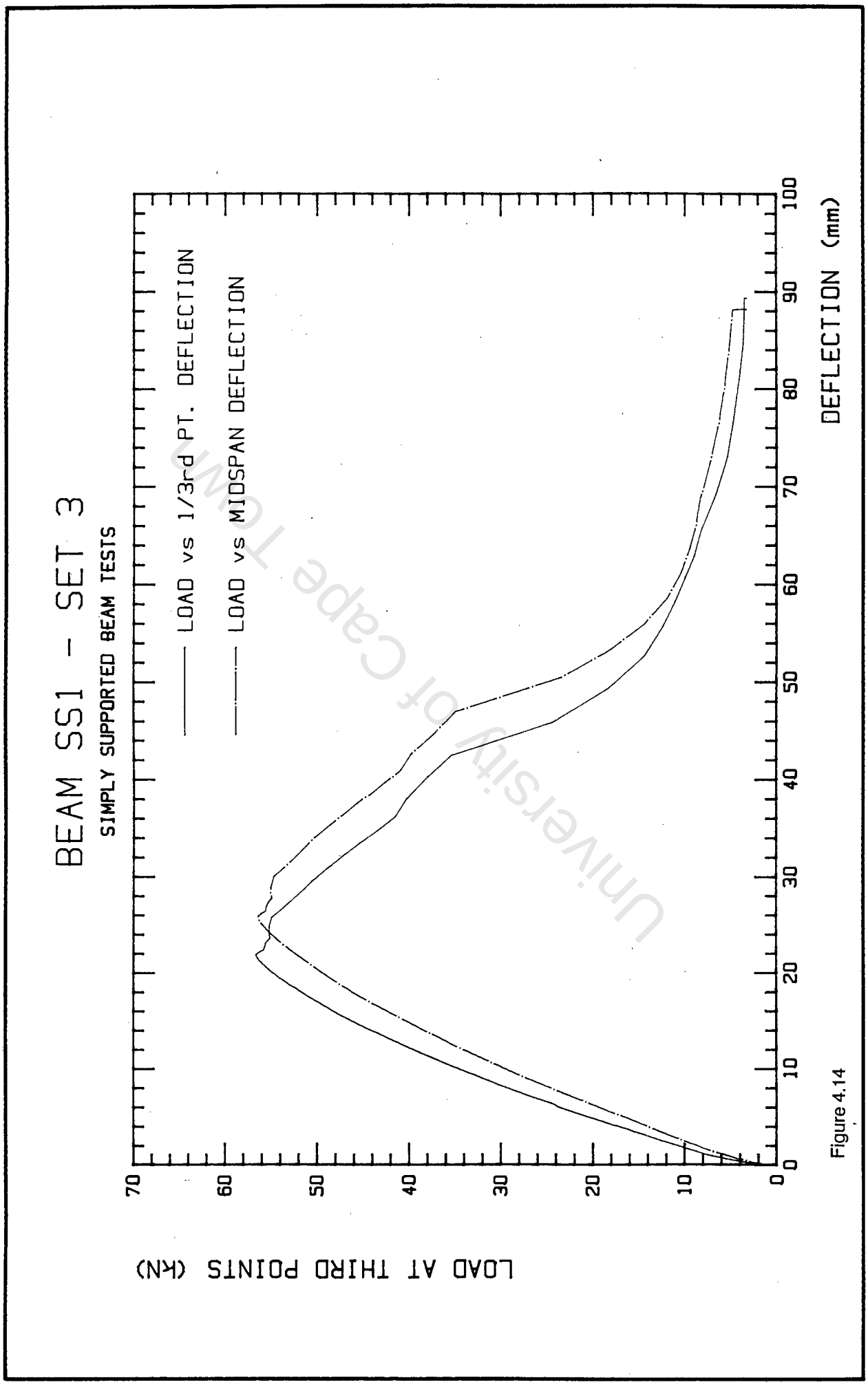

Figure 4.14

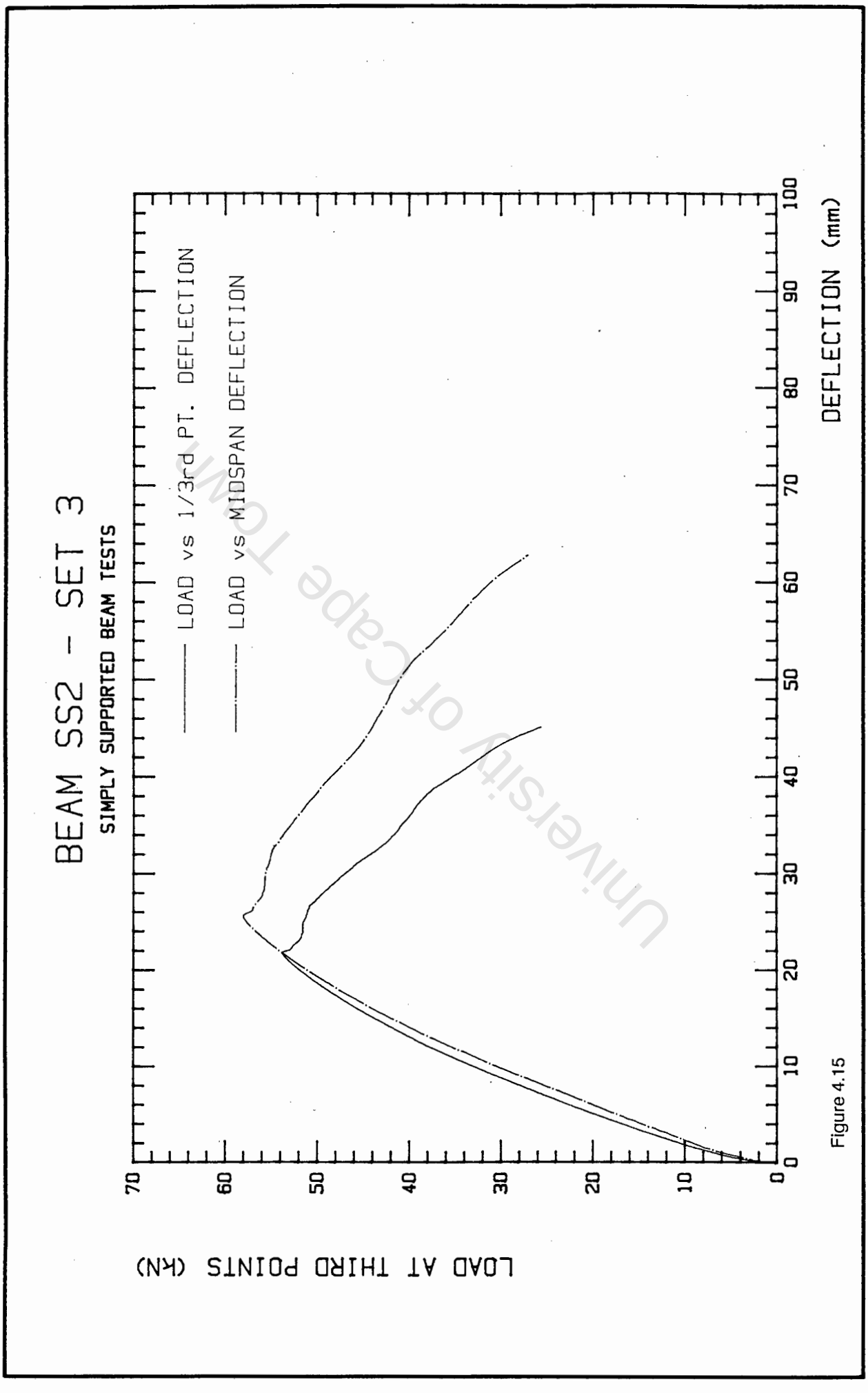

Figure 4.15

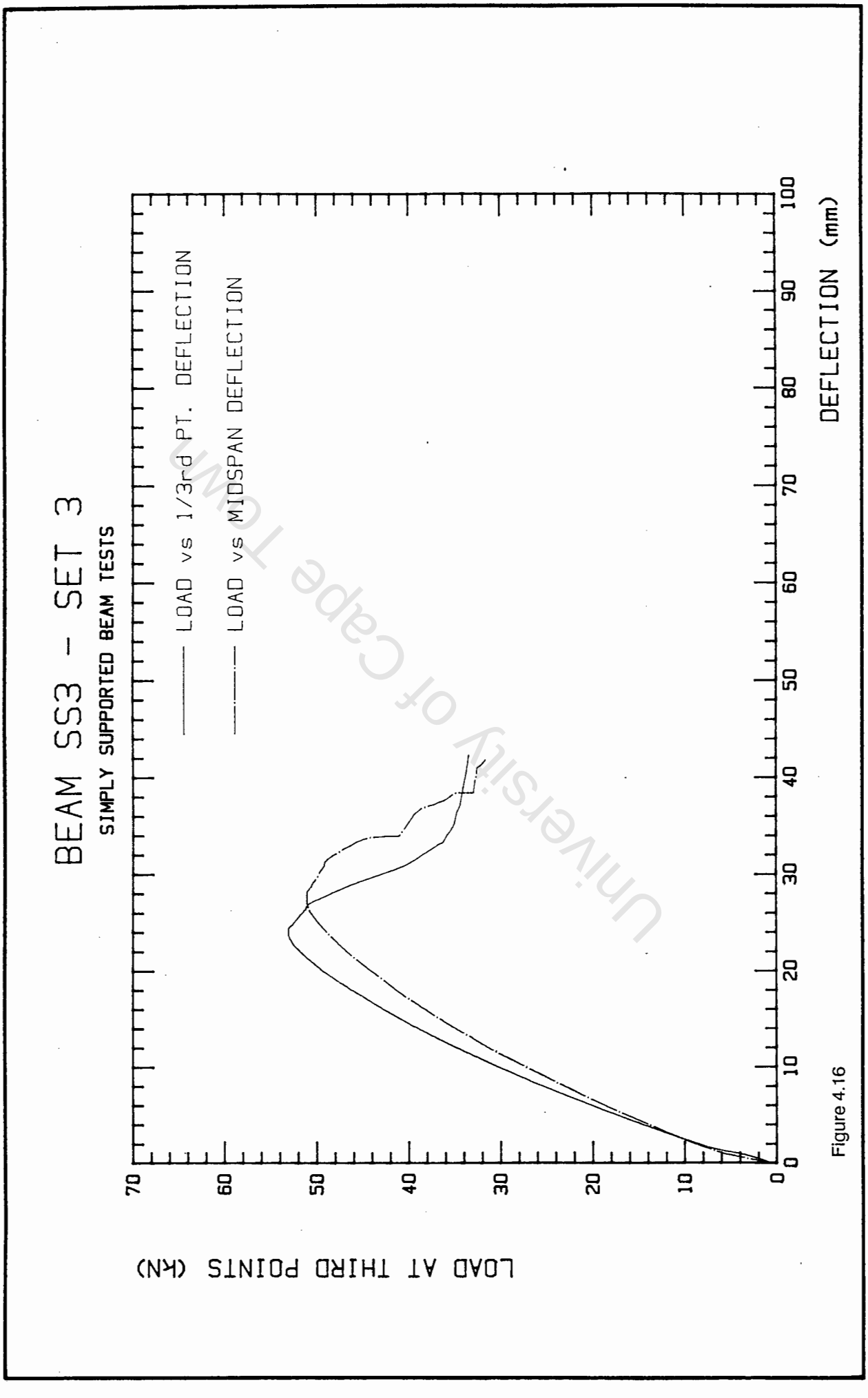

Figure 4.16

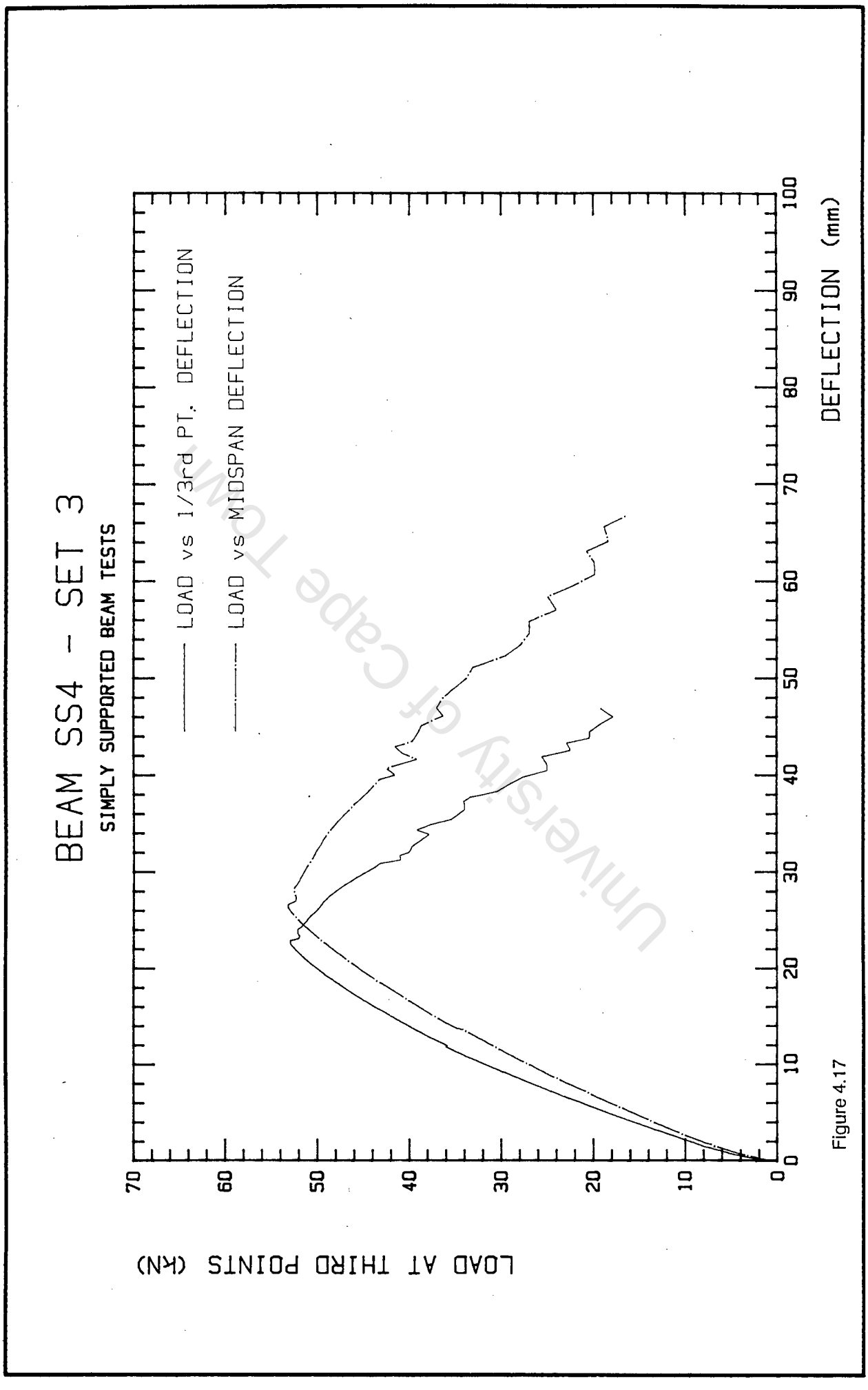

Figure 4.17

CHAPTER 5

THE FINITE ELEMENT PROGRAM, NLFRAM

5.1 Introduction

The finite element program, NLFRAM, was developed by Hawla [2,3,6] and is designed for static and transient response analysis of reinforced concrete plane frames exhibiting geometric and/or material non-linearities. The program may also be used to study time integration techniques, nonlinear equation solution techniques as well as nonlinear behaviour of various types of materials [6].

For static and dynamic analyses special procedures are required for the solution of the nonlinear equations and a number of options are available in NLFRAM. The program assumes that all loads, both static and dynamic, are functions of "time". This gives the user great flexibility since any programme of loading may be applied to the structure. The nonlinear solutions are then obtained by an incremental procedure in time. In static analysis this is essentially an incremental loading procedure. At the end of each increment it is possible to iterate for equilibrium and a number of options are available. These equilibrium iteration methods may also be used in the transient dynamic response analysis where the implicit trapezoidal rule is used for the time integration.

At present, two versions of the program NLFRAM are available. Both of these, called NLFRAM (VERSION 1)[2] and NLFRAM (VERSION 2) [3], are used in this thesis. For convenience, these will henceforth be referred to as NLV1 and NLV2 respectively. NLV2 only became available later in the investigation after considerable difficulties were experienced in reaching equilibrium solutions using NLV1. (These are discussed in Chapter 6 and 7). In NLV2, Hawla introduced additonal material models into the program which are not available in NLV1. He also made some structural changes to the program in NLV2 with the intention of improving the computational efficiency of the program. Prior to this thesis, NLV2 was virtually untested and it would be of interest to assess its performance when compared to NLV1.

In this thesis, NLFRAM is used to simulate the load-deflection behaviour of the reinforced concrete beams discussed in Chapters 3 and 4. By modelling these experimental beams under statically applied loading conditions, the validity and efficiency of the various material models in NLFRAM are investigated.

In this chapter, the theory relating to the static analysis in NLFRAM is first discussed. This is followed by a description of the elements, integration techniques, material models and solution methods presently incorporated into NLFRAM [2,3].

5.2 The Equilibrium Equations

The formulation of the equilibrium equations for static analysis is based on the principal of virtual work, this being suitable for nonlinear behaviour [37]. The virtual work principal states that the equilibrium of a body requires that for any compatible, small virtual displacements (which satisfy the essential boundary conditions) imposed onto the body, the total internal virtual work due to the stresses induced in the body is equal to the external virtual work due to the loads imposed on the body. In reaching the expression of virtual work used in developing NLFRAM, the following assumptions are made:

i) strains are small, although displacements and rotations may be large,

ii) plane cross-sections remain plane when the structure deforms,

iii) shear strains are negligible so that normal sections remain normal to a reference axis which is orientated lengthwise along the frame members and

iv) the displacements of any point on a cross-section can be adequately described in terms of the displacement of the reference axis.

The statement of virtual work is used as the basis of the finite element equations. The equilibrium condition at a general time increment, t, for a system of finite elements representing a body is obtained when the external nodal loads are equal to internal forces corresponding to the element stresses in the body. This is conveniently expressed in vector form as:

$$\underline{F}_t(K_T(\underline{u}),\sigma_e) = \underline{P}_t \qquad (1)$$

where $\underline{P}_t$ is a vector of externally applied nodal loads at "time" t, $\underline{F}_t$ is the internal nodal force vector equivalent to the element stresses (σ_e)in the structure at "time" t, K_T is the tangent stiffness matrix and $\underline{u}$ is the displacement vector.

The time t indicates the order of events, and is a parameter in terms of which the history of loading on the structure is expressed. The equilibrium equation in (1) must be satisfied for the complete time range of interest. Because of the nonlinear relationship between the applied loads and the internal element stresses, an incremental step-by-step analysis is used to establish equilibrium for a discrete time $t + \Delta t$, assuming that the solution at time t is known. That is, an approximate solution of equation (1) written at time $t + \Delta t$ is sought, given that the solution is known up to and including the previous time-step.

$$\underline{F}_{t+\Delta t}\,(K_T(\underline{u}),\sigma_\theta) = \underline{P}_{t+\Delta t} \qquad (2)$$

The virtual work equation is written for time $t+\Delta t$ but referred to the configuration at time t (consistent with an approximate updated Lagrangian description) [38, 39]. The following incremental equation is produced;

$$K_T\ \Delta\underline{u} = \underline{P}_{t+\Delta t} - \underline{F}_t \qquad (3)$$

where $\Delta\underline{u} = \underline{u}_{t+\Delta t} - \underline{u}_t$, the displacement increment.

Solving for $\Delta\underline{u}$ in (3), an approximation to the displacements at time $t + \Delta t$ can be calculated. Since the equilibrium equations are, in general, nonlinear (the deformed geometry is unknown and the material behaviour is nonlinear), the solution of equation (3) does not usually give an adequate approximation to equation (2) unless very small increments are used. To improve the solution, iterative procedures are used.

An iterative version of equation (3), for the i^{th} iteration is

$$K_T^i\ \Delta\underline{u}^i = \underline{P}_{t+\Delta t} - \underline{F}_{t+\Delta t} \qquad (4)$$

where

$$\Delta\underline{u}^i = \underline{u}_{t+\Delta t}^{i+1} - \underline{u}_{t+\Delta t}^{i} \qquad (5)$$

$\underline{F}^{i}_{t+\Delta t}$ is the i^{th} approximation to internal forces at $t+\Delta t$ and
K^{i}_{T} is the tangent stiffness matrix evaluation at the i^{th} approximation to equation (2).

Equation (4) is derived by writing the virtual work equation at time $t+\Delta t$ but now it is referred to the i^{th} approximation to the configuration at time $t+\Delta t$ [38]. This iterative method is identical to the Newton-Raphson method for systems of nonlinear equations, but is generally not used in its unmodified form, the main reason for this being the high cost involved in reforming and refactorising the tangent stiffness matrix [6]. Modified methods, based on the Newton-Raphson methods, are generally more economical. A number of these have been incorporated in NLFRAM and are discussed briefly in Section 5.3.6.

5.3 NLFRAM Finite Elements

5.3.1 Element Description

Two elements are available in NLFRAM (figure 5.1), both being straight and prismatic. These are:

i) The standard element. This is a two-noded beam element with cubic transverse and linear longitudinal displacement fields. The element uses linear interpolation to approximate the displacements of the reference axis in the local x-direction, $u_o(x)$.

ii) The special element. This is a two-noded beam element with cubic transverse and quadratic longitudinal displacement fields. The element, having an extra longitudinal degree of freedom at the element centre, uses quadratic Lagrangian interpolation to approximate the displacement of the reference axis in the local x-direction, $u_o(x)$.

In both elements cubic Hermite interpolation is used to approximate the displacement in the local y-direction, v(x) of the reference axis. According to the assumptions (ii) - (iv) given in Section 5.2, for both elements, the displacements are adequately described by:

$$u(x,y) = u_o(x) - y \frac{dv}{dx} \tag{6a}$$

$$v(x,y) = v(x) \tag{6b}$$

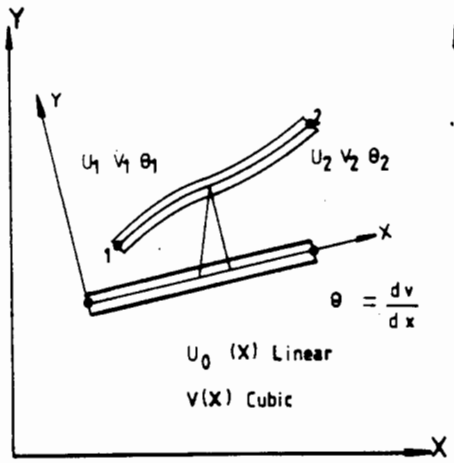

Figure 5.1(a): Standard Element

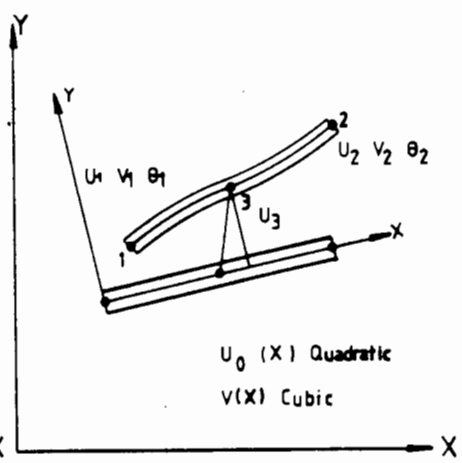

Figure 5.1(b): Special Element

5.3.2 Element Internal Forces and Stiffnesses

The calculation of the element internal forces and stiffness matrices in their local coordinate system is performed using the principle of virtual work. The internal force vector $\underline{f}$ is derived from

$$\delta\underline{\tilde{u}}\,\underline{f} = \int_0^L \int_A \delta\epsilon\sigma dA dx \tag{7}$$

where

σ is the longitudinal stress

$\delta\underline{\tilde{u}}$ is the transpose of the virtual displacement vector

and $\delta\epsilon$ is the virtual strain

The stress is calculated from:

$$\sigma = \sigma(\epsilon, H_\alpha) \tag{8}$$

where ϵ is the strain and H_α are parameters which record the history of strain in the material.

The strain is calculated from

$$\epsilon(x,y) = \frac{du_o}{dx} - y\frac{d^2v}{dx^2} \tag{9a}$$

which may be written as:

$$\epsilon = e - y\kappa \tag{9b}$$

The equation (7) may then be written as:

$$\delta\underline{\tilde{u}}\,\underline{f} = \int_0^L \delta e N dx + \int_0^L \delta\kappa M dx\,. \tag{10a}$$

where

$$N(x) = \int_A \sigma dA \qquad (10b)$$

$$M(x) = -\int_A y\sigma dA \qquad (10c)$$

are the stress resultants.

Within the assumption that, for an element, the displacements of the reference axis are small when referred to the current local coordinate system and that the integrations are performed in the current configuration, equations (7) - (10) hold for all materials. When geometric nonlinearity is not taken into account the current and original configurations are assumed to coincide and the analysis is greatly simplified.

When geometry changes are included, NLFRAM updates the local co-ordinate systems for each element after every displacement increment in such a way that the local x-axis passes through the nodes at the ends of the elements. The virtual work calculations are then performed in this coordinate system . To calculate the stresses in the element, NLFRAM uses strains computed from equation (9a) with the rigid body displacements removed from $u_o(x)$ and v(x). In this way the use of special stress increments to correct for rotations is avoided.

The element tangent stiffness matrices, $\underline{k}_T$, when calculated for materially nonlinear problems only, are found from the principle of virtual work formulation in which

$$\delta\tilde{\underline{u}}\,\underline{k}_T\Delta\underline{u} = \int_0^L\int_A \delta\epsilon\,\frac{d\sigma}{d\epsilon}\Delta\epsilon dA dx. \qquad (11)$$

Using equation (9b) again we may rewrite equation (11) in a computationally more efficient form as

$$\delta\tilde{\underline{u}}\,\underline{k}_T\Delta\underline{u} = \int_0^L(\delta e E_1\Delta e + \delta e E_2\Delta\kappa + \delta\kappa E_2\Delta e + \delta\kappa E_3\Delta\kappa)dx \qquad (12a)$$

Where

$$E_1(x) = \int_A \frac{d\sigma}{d\epsilon}dA \qquad (12b)$$

$$E_2(x) = -\int_A y\frac{d\sigma}{d\epsilon}dA \tag{12c}$$

$$E_3(x) = \int_A y^2\frac{d\sigma}{d\epsilon}dA \tag{12d}$$

The tangent modulus $\frac{d\sigma}{d\epsilon}$ is calculated from

$$\frac{d\sigma}{d\epsilon} = \frac{\partial\sigma}{\partial\epsilon}\Bigg|_{H\alpha \text{ fixed}} \tag{13}$$

When geometric nonlinearity is included, the tangent stiffness matrix is calculated by specialising the general continuum incremental virtual work formulation [37,38] to plane frames and only then introducing the assumption of small strain. This will lead to an "elastic" tangent stiffness matrix, $\underline{k}_E$ given above as $\underline{k}_T$, and a geometric stiffness matrix, $\underline{k}_G$, which is found from

$$\delta\underline{\tilde{u}}\,\underline{k}_G\Delta\underline{u} = \int_0^L\int_A \delta\theta\sigma\Delta\theta dAdx + \int_0^L\int_A (\delta e\tau\Delta\theta + \delta\theta\tau\Delta e)dAdx \tag{13a}$$

where

$$\theta = \frac{dv}{dx} \tag{13b}$$

and

τ = shear stress in the element .

By using stress resultants and the fact that, for elements in NLFRAM the shear force is constant over the element, the following equation results.

$$\delta\underline{\tilde{u}}\,\underline{k}_G\,\Delta\underline{u} = \int_0^L \delta\theta N\Delta\theta dx + S\int_0^L (\delta e\Delta\theta + \delta\theta\Delta e)dx \tag{14a}$$

where $S = \int_A \tau dA$ (14b)

However, since no shear stresses are calculated in NLFRAM, the program uses the shear force which would be obtained from the virtual work calculation for the element internal force vector.

The total tangent stiffness for the element is then given by;

$$\underline{k}_T = \underline{k}_E + \underline{k}_G \,. \tag{15}$$

A feature of NLFRAM, which can be useful, is the option to include the effects of geometry changes by updating the local coordinate systems and removing rigid body displacements of elements, but excluding the formulation of the geometric stiffness, $\underline{k}_G$.

After the internal forces or stiffness matrices have been formed in their local coordinate systems, they are transformed to the global internal force vector or tangent stiffness matrix,respectively. These procedures are fairly standard in finite element programs.

5.3.3 Numerical Integration

Over the member cross-section, the strain distribution is assumed to be linear. However, because of the use of a nonlinear constitutive law, the stress distribution and tangent modulus distribution will be nonlinear. In order that very general constitutive laws may be used, NLFRAM uses numerical integration to evaluate the integrals in equations (10b-c) and (12b-d). This numerical integration is done via Newton-Cotes integration through the member depth.

The Newton-Cotes integration method uses the trapezoidal rule, Simpson's rule or multi - Simpson's rule to perform the integration piecewise over the cross-section. This implies that complex cross-sections such as one shown in figure 5.2 may be used in NLFRAM. However, a cross-section used should be symmetrical about the plane of bending and be composed of a matrix material (usually concrete) with (or without) embedded layers (usually steel), as shown in figure 5.2.

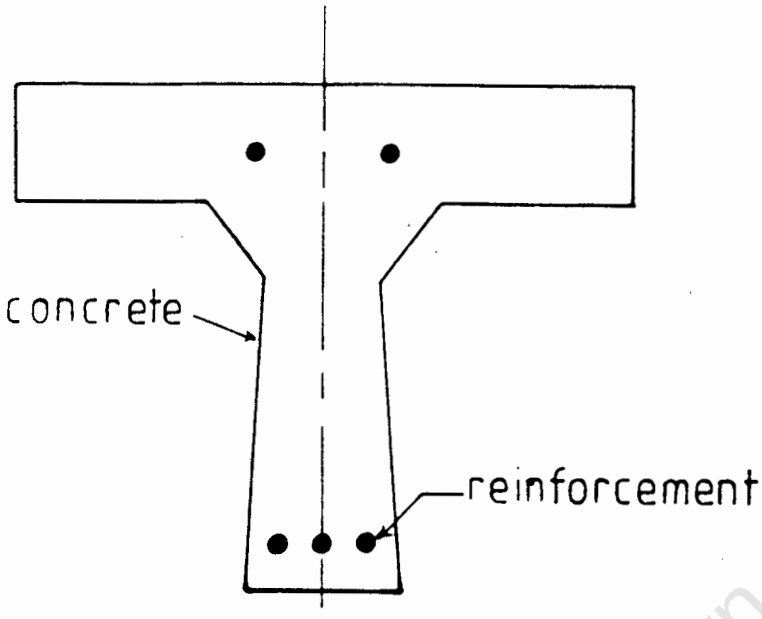

Figure 5.2 Typical cross-section in NLFRAM

The effects of nonlinearity also require that integrals for the element stiffnesses and internal forces in equations (10a), (12a) and (14a) be performed numerically. This is done via Gaussian quadrature using the two-point rule.

5.4 Material Models in NLFRAM

In the current version of NLFRAM [3], one linear and seven non-linear material models are incorporated into the program. These models are essentially uniaxial, thus placing a restriction on the type of problem which may be accurately analysed. The models available are:

Model 1: A Linear-Elastic Material Model - This model is applicable to all linear - elastic materials. The only parameter required to define this model is E_S, the Young's Modulus.

Model2: An Elastic-Linear Kinematic Hardening Model - This model, shown in figure 5.3, may be used for both concrete and steel. Unloading is elastic in both tension and compression. The parameters required to define this model are:

i) Young's Modulus, E_S
ii) Hardening modulus, E_H
iii) Initial compressive yield stress, f_y
iv) Initial tensile yield stress, f'_y

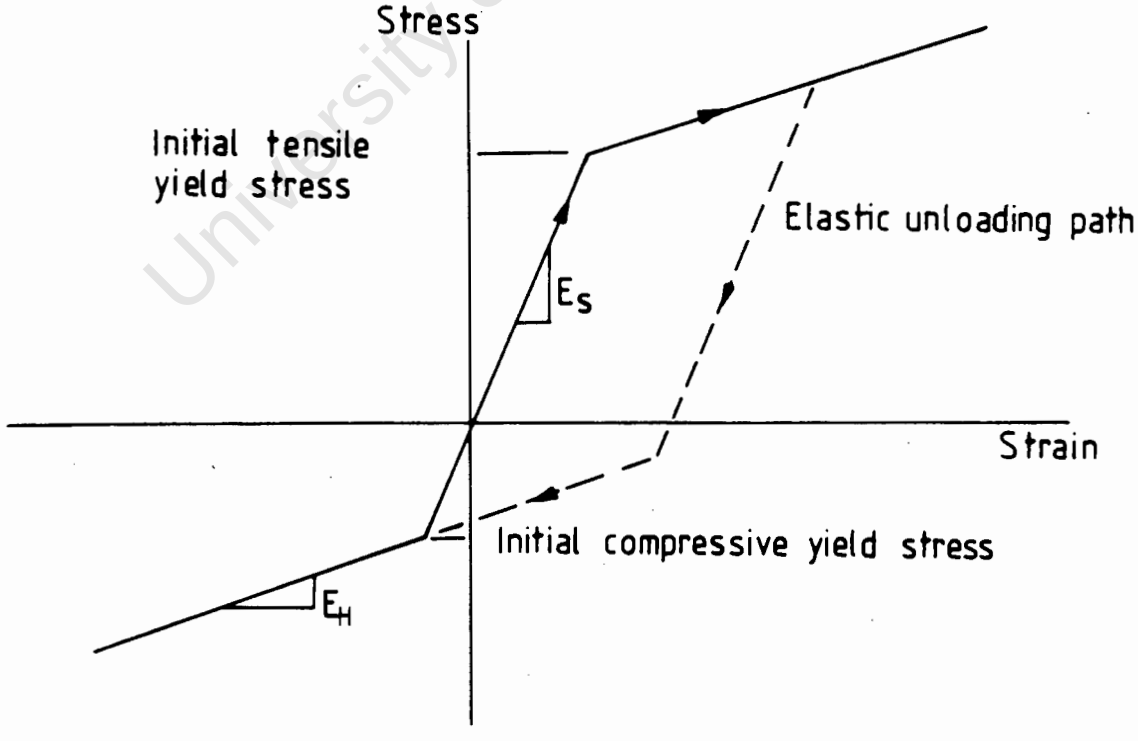

Figure 5.3: Model 2 - Elastic-Linear Kinematic Hardening Model.

Model 3: A Trilinear Elastic-Kinematic Hardening Model - This model is an extension of Model 2 above. The model is trilinear elastic (figure 5.4), and has an elastic unloading path. The model, used primarily for steel reinforcement, requires the following parameters to define its stress-strain path:

i) Young's Modulus, E_S

ii) Transition modulus, E_T

iii) Hardening modulus, E_H

iv) First yield stress, f_y^1

v) Second yield stress, f_y^2

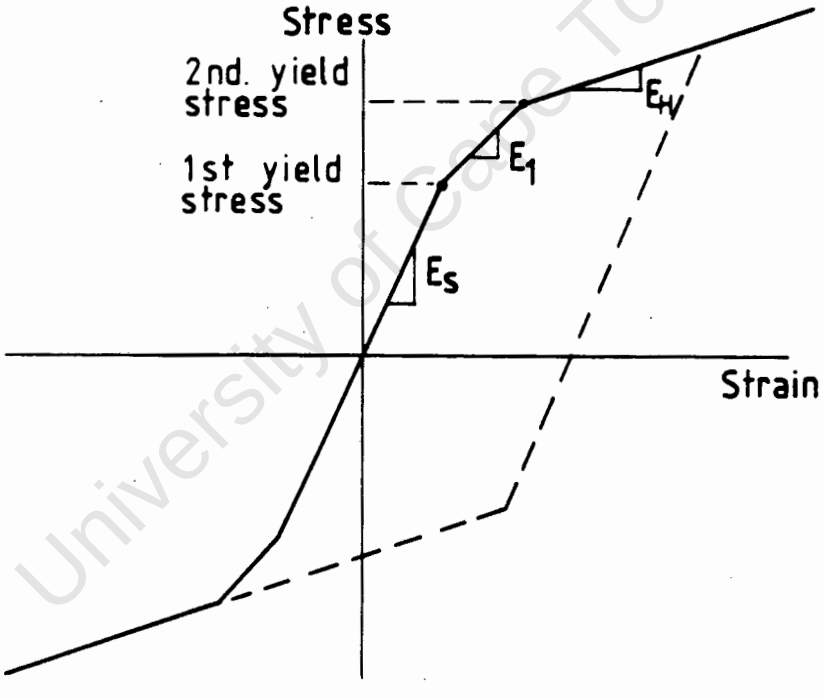

Figure 5.4: Model 3 - Trilinear Elastic Kinematic Hardening Model.

Model 4: Quadratic Compression Yield Envelope and Tensile Failure Model.

This is primarily a concrete model (figure 5.5). Unloading is elastic, at the same slope as the initial modulus. The ultimate compression stress is assumed to occur at a strain such that the secant modulus is half of the initial modulus. In tension, the model is quadratic up to the tensile failure stress, at which point the material is assumed to lose all its strength. The parameters required to define this model are:

i) Young's modulus for concrete, E_c

ii) Maximum compressive stress, f_c

iii) Tensile failure stress, f'_{ct}

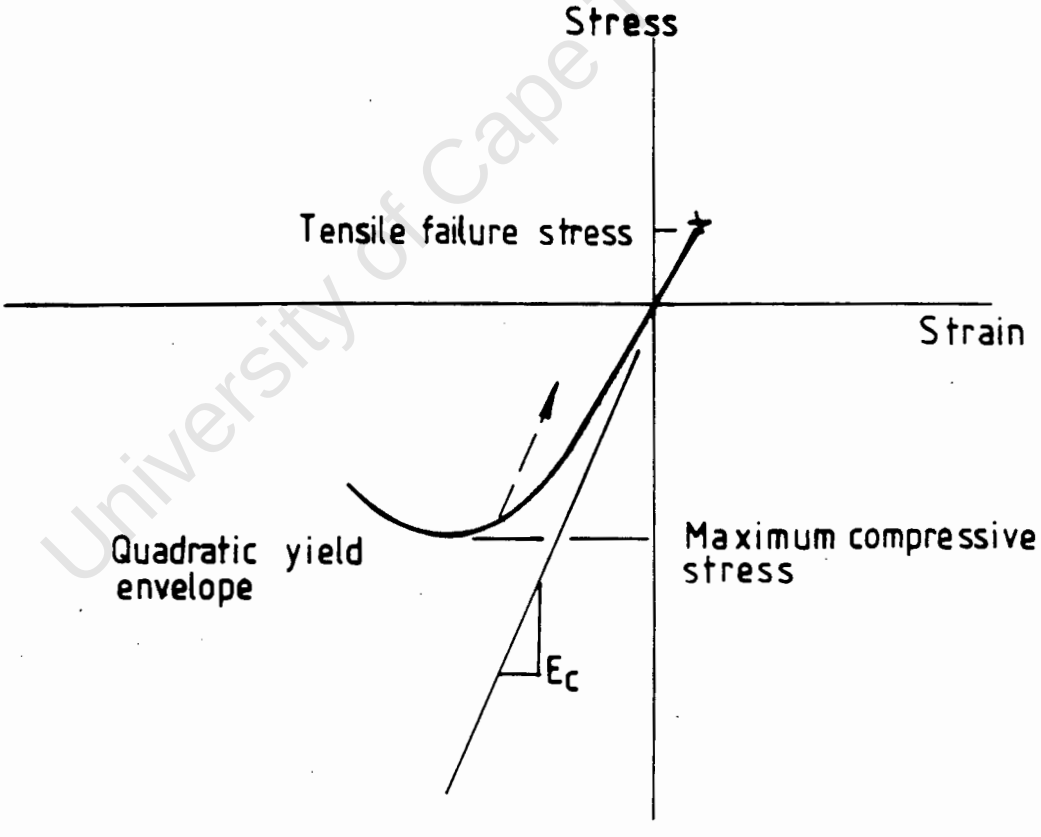

Figure 5.5: Model 4 - Quadratic Compression Yield Envelope and Tensile Failure Model.

Model 5: Quadratic Yield Compression with Lower Limit and Linear/Rational Progressive Tensile Fracture Model.

This concrete model, figure 5.6, is an extension of model 4. The model describes a stress-strain path beyond the maximum tensile and compressive stress. In tension, the concrete is assumed to lose its strength gradually after the maximum tensile stress is reached (tension stiffening). In Model 5 Hawla describes this path of tensile stress release as a constant/rational progressive fracture envelope. In compression, the quadratic yield envelope has a limit, the compressive stress limit. When this limit is reached the stress-path is constant with increasing strain. To define Model 5 in NLFRAM, the following parameters are required:

i) Young's modulus for concrete, E_c

ii) Maximum compressive stress, f_c

iii) Maximum tensile stress, f'_{ct}

iv) Compressive stress limit, f_{cl}

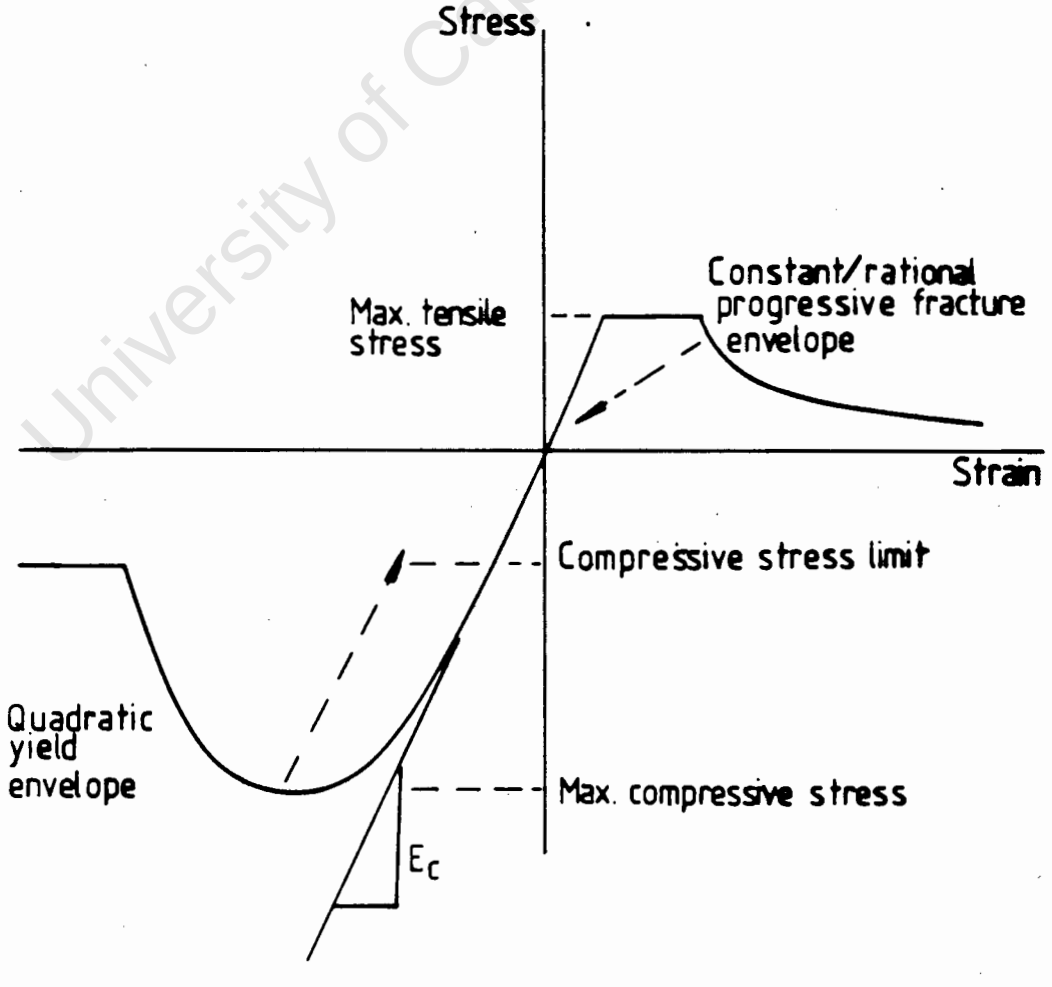

Figure 5.6: Model 5 - Quadratic Compression Yield Envelope with Limit Stress and Elastic - Constant/Rational Progressive Tensile Fracture Model.

Model 6: Quadratic Compressive Yield Envelope and Tensile Progressive Fracture/ Permanent Straining Model.

This model, shown in figures 5.7 has the same envelopes in tension and compression as Model 5, but allows for limited tensile permanent straining to occur. The parameters required to define this model are:

i) Young's modulus for concrete, E_c

ii) Maximum compressive stress f_c

iii) Maximum tensile stress f'_{ct}

iv) Compressive stress limit f_{cl}

v) Maximum tensile permanent strain ϵ_m^p

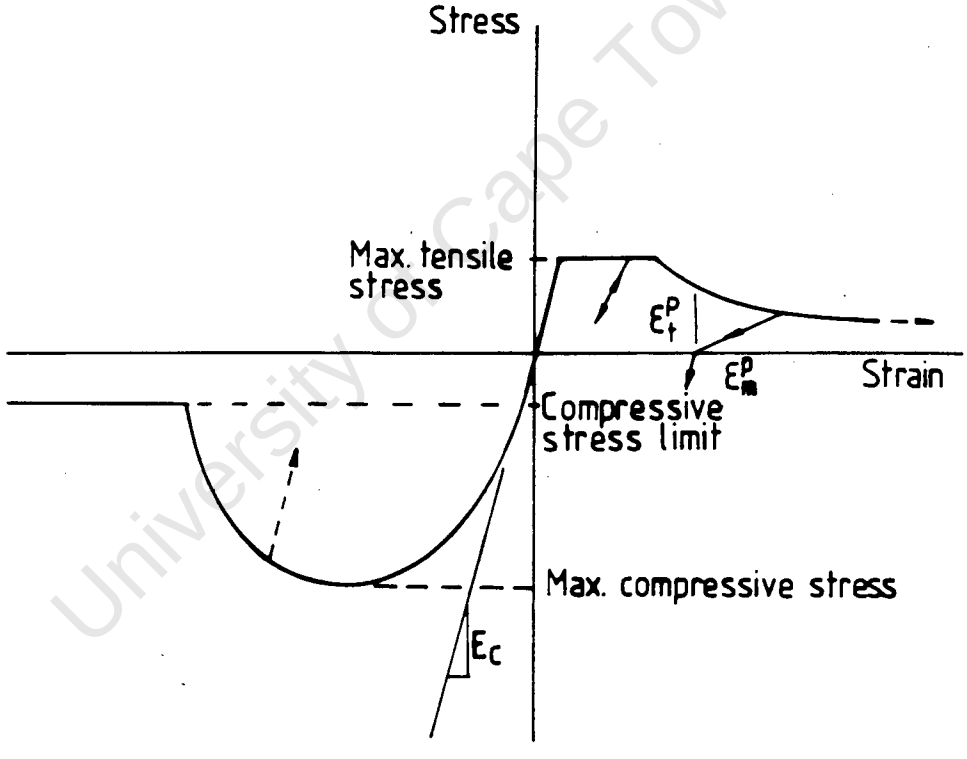

Figure 5.7: Model 6 - Quadratic Compressive Yield Envelope and Tensile Progressive Fracture/Permanent Straining Model.

Model 7: Progressive Damage Model with Permanent Compressive Strain.

This model, shown in figure 5.8, has the same stress-strain envelope in tension as Model 5. The compression envelope is defined in terms of the initial modulus (which is automatically calculated), the maximum compressive stress and the strain corresponding to this stress. After the maximum compressive stress is reached, the stress decreases gradually with increasing strain. No compressive stress limit is defined (as in the case of Model 5). To define the complete stress-strain relationship for this model, the following parameters are required

i) Maximum compressive stress, f_c

ii) Strain corresponding to fc, ϵ_{mc}

iii) Fraction of the Initial Modulus at 2x ϵ_{mc}

iv) Maximum Tensile Stress, f'_{ct}

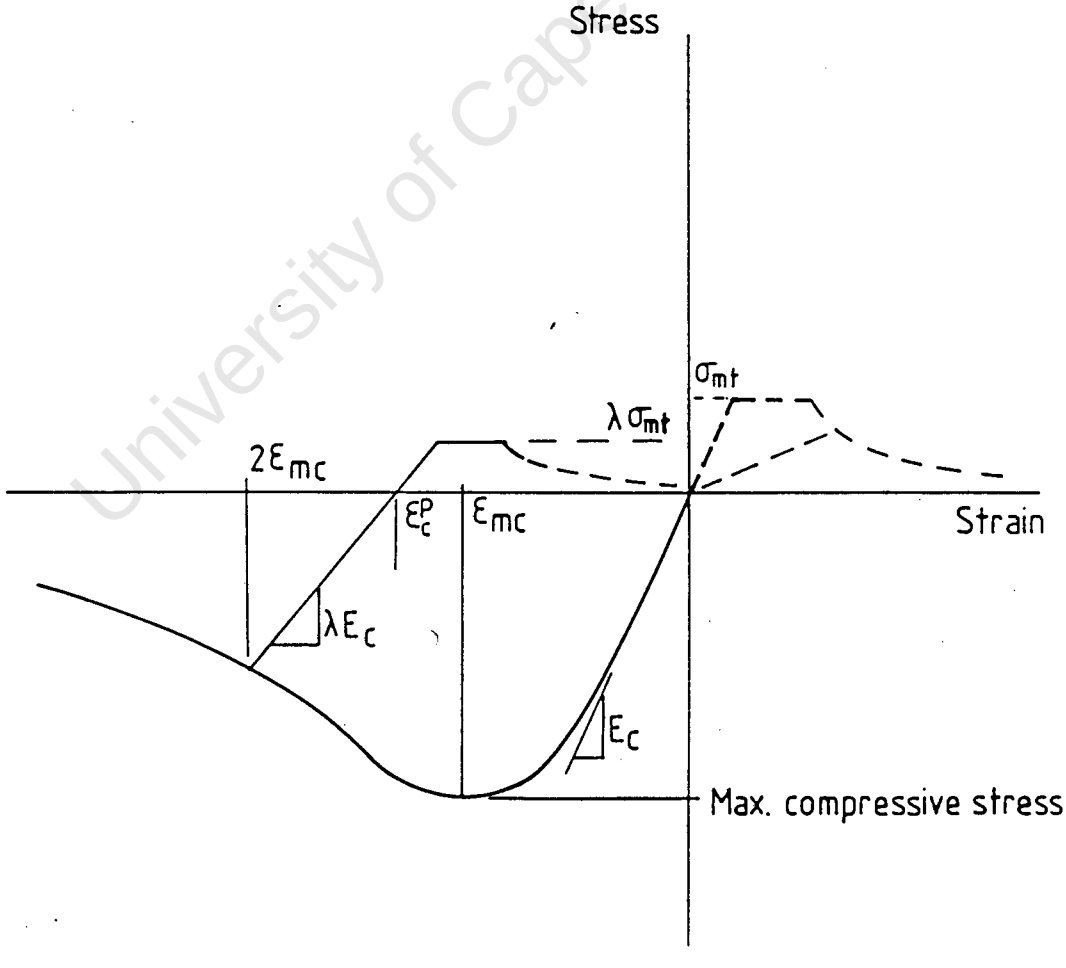

Figure 5.8 **Model 7: Progressive Damage Model with Permanent Compressive Strain.**

Model 8: Quadratic Compressive Envelope and Linear Tensile Stress Release with Permanent Straining Model.

In compression, the stress-strain behaviour of this model is the same as Models 5 and 6. In tension, the model differs from these two models in that the tensile stress release, after the maximum tensile stress is reached, is linear (figure 5.9). The slope of this stress release is defined in terms of a stress release factor, α. The model also allows for limited tensile permanent straining. In order to describe the stress-strain behaviour of this model, the following parameters are required:

i) Young's modulus for concrete, E_c
ii) Maximum compressive stress, f_c
iii) Maximum tensile stress, f'_{ct}
iv) Compressive stress limit, f_{cl}
v) Tensile stress release factor, α
vi) Maximum tensile permanent strain, ϵ^p_m

Note that α is usually between 4 and 8

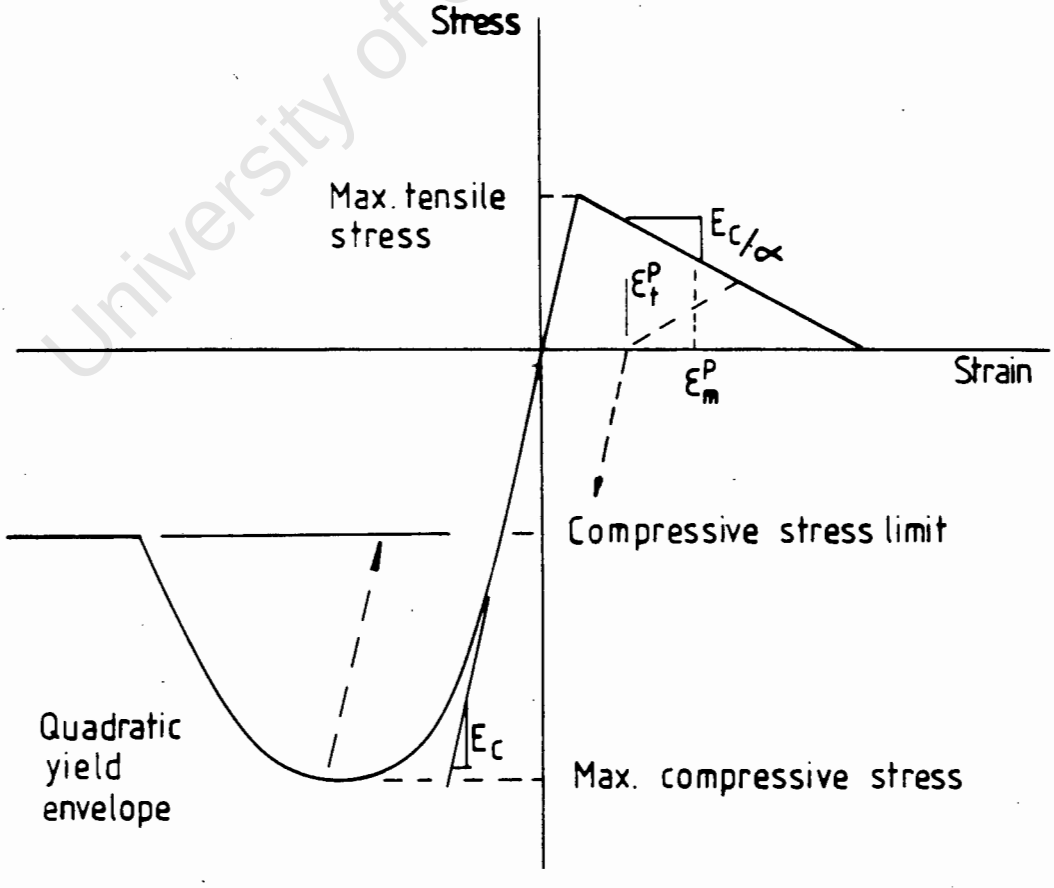

Figure 5.9 Model 8: Quadratic Compressive Envelope and Linear Tensile Stress Release with Permanent Straining Model.

5.5 Solution Methods

With nonlinear material behaviour or nonlinear geometric effects, equation (4) in Section 5.2 is solved using one of a number of iteration methods, based on the standard Newton-Raphson method. Application of the full Newton-Raphson method is, however, expensive, and acceleration techniques based on generalisations of the secant method generally produce more economical solutions. A number of these methods have been incorporated in NLFRAM.

i) Modified Newton-Raphson
ii) Full Newton-Raphson
iii) Modified Newton-Raphson but with stiffness reformed only at the start of the second iteration
iv) Modified Newton-Raphson with Aitken acceleration
v) Modified Newton-Raphson with Jenning's symmetrical modification of Aitken acceleration.
vi) Modified Newton-Raphson with Jenning's anti-symmetrical modification of Aitken acceleration.
vii) Crisfield's faster modified Newton-Raphson
viii) BFGS matrix updating

In all of the above iteration methods a matrix solution is required. NLFRAM stores the coefficient matrix in a compacted skyline form and factorises it into its LDL factors [38]. A useful feature of NLFRAM is the ability to perform displacement controlled tests, even on a single element with all boundary displacements prescribed. This latter facility enables easy checking of new material models.

A full description of these solution methods is given in [40].

CHAPTER 6

NUMERICAL EXAMPLES USING NLFRAM

6.1 Introduction

In this section, an investigation into the behaviour of the material models in NLFRAM is undertaken. In order to do this, NLFRAM is used to simulate the load-deflection behaviour of the experimental beams tested in the laboratory. Two finite element models are used for this purpose:

i) a finite-element model, called Model A, based on the under-reinforced two-span beams in Set 1 and Set 2, discussed in Section 3.3.

ii) a finite-element model, called Model B, based on the slightly over-reinforced simply-supported beams in Set 3, discussed in Section 3.3.

The beams tested in Set 1, Set 2 and Set 3 represent a range of conditions where either the tensile or compressive properties of the constituent materials play a major role in determining the load-deflection behaviour. By modelling these beams in NLFRAM, the tensile and compressive material parameters under different conditions are assessed.

Both NLV1 and NLV2, discussed in Section 5.1, are used in the analysis. The beam elements are the same in both versions. The constituent materials are however, modelled using different material models. In NLV1, material Model 3 and Model 5 are used to model the reinforcement and the concrete respectively. In NLV2, the reinforcement is also modelled using Model 3 but the concrete is modelled using Model 8. These models are discussed in Section 5.4.

The concrete models, Model 5 and Model 8 differ only in the way that the tension-stiffening envelope in tension is described after the maximum tensile stress is reached (compare these models in figures 6.1 and 6.2). In Model 5, on reaching the maximum tensile stress, the stress initially remains constant with increasing strain. After a certain strain level is reached, the stress is gradually released along a hyperbolic curve. This envelope is described by Hawla [2] as a "constant/rational progressive fracture envelope". In Model 8, the stress is released linearly immediately after the maximum tensile stress is reached. The slope of this stress release is a function of the elastic modulus of the concrete. The difference in the shape of these models is not so much based on experimental observations but rather on numerical efficiency criteria.

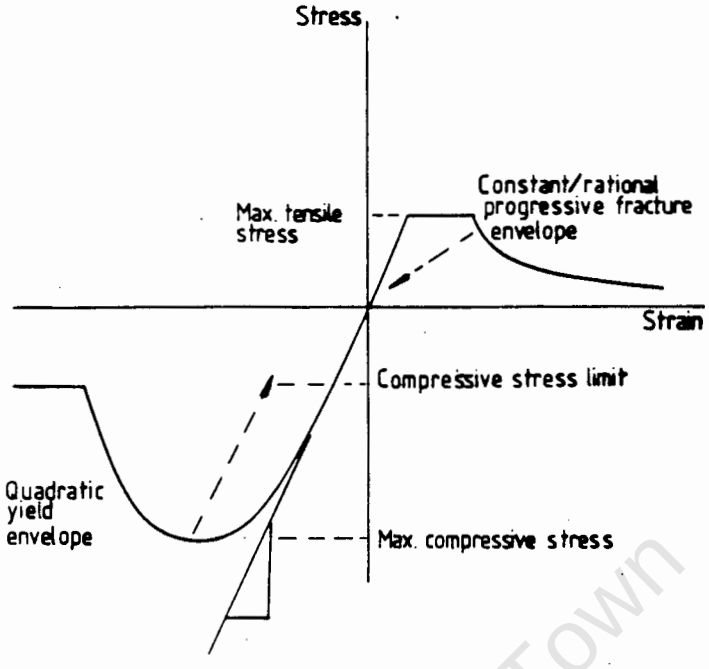

Figure 6.1: Model 5 - Quadratic Compression Yield Envelope - with Limit Stress and Elastic - Constant/-Rational Progressive Tensile Fracture Model.

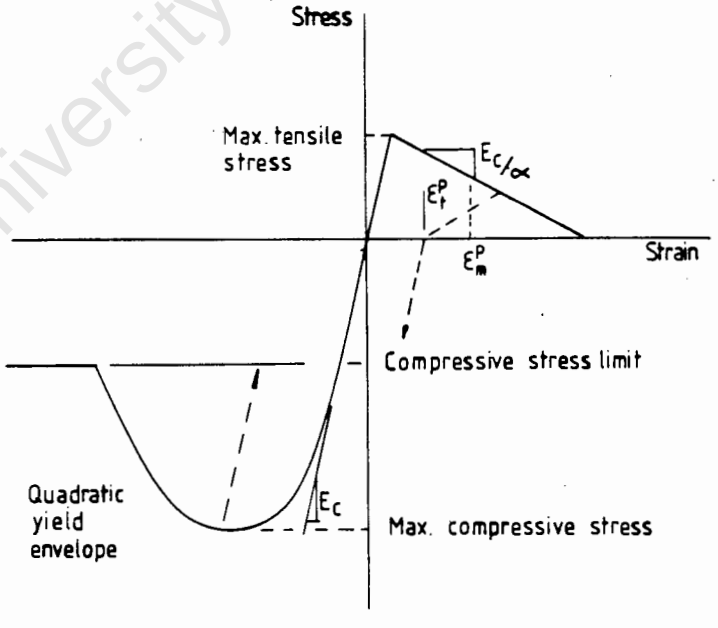

Figure 6.2: Model 8 - Quadratic Compressive Envelope and Linear Tensile Stress Release with Permanent Straining Model.

In investigating the material behaviour in NLFRAM, the numerical efficiency of the combination of Model 3 and Model 5 in NLV1, and Model 3 and Model 8 in NLV2 is first compared. The sensitivity to variation of the various material parameters is then studied. This is done by systematically changing the values of the material parameters specified in the NLFRAM examples and then plotting and comparing the relevant load-deflection curves. In this way the effects of a particular parameter on the beam model may be assessed.

In this chapter, the finite element modelling of the two span beams in Set 1 and Set 2 and the simply-supported beams in Set 3 is first discussed. Then the results of the material parameter study are presented and discussed. However, it should be noted that only behavioural trends of the various material models are investigated here. In Chapter 7, the validity of these results will be assessed when compared directly to numerical observations.

6.2 Finite Element Modelling of the Two-Span Beams using Model A.

In NLV1 and NLV2, the finite-element model, Model A, is used to model the beams in Set 1 and Set 2. The two spans in these beams are equal and the loads are symmetrically applied about the interior support (see figure 3.3). For this reason, Model A only models a single span. The beam is modelled using fourteen 2-noded special elements, with two-point Gaussian quadrature along the element length (figure 6.3). The elements between nodes 1 and 9 are 150mm in length while the elements between nodes 9 and 15 are 100mm in length, thus giving a span of 1800mm (figure 6.3). The first few examples executed in NLV1 indicated that increasing the number of elements did not have a significant effect on the load-deflection behaviour of the beam. Similar observations were made in reference [6] and [41]. The number of elements is kept at fourteen throughout the analysis.

The beam cross-section is uniform; the cross-sectional dimensions being b = 152mm and h = 250mm (consistent with the overall concrete dimensions of the beams in Set 1 and Set 2). The longitudinal reinforcement is modelled as two layers representing the areas of the 3Y12 and the 2Y12 bars in the top and bottom faces of the beam cross-section respectively (figure 6.3). The eccentricity of these layers is varied in the analysis to observe its influence on the load-deflection curves. NLFRAM uses these dimensions to calculate the effective concrete and steel areas in the cross-section. The vertical stirrups used in the beams in Set 1 and Set 2 are not modelled in NLFRAM. Also, no distinction is made between the area of concrete confined by the reinforcing stirrups and the unconfined concrete area outside of the stirrups. Because of the highly non-linear stress distribution over the element cross-section, five or seven point Newton-Cotes integration is used to evaluate the stress distribution over the element cross-section.

The materials, concrete and steel are modelled as non-linear. No geometric effects are considered. The reinforcement is modelled using material Model 3 (see Section 5.4). The concrete is modelled using Model 5 in NLV1 and Model 8 in NLV2 (see figures 6.1 and 6.2 respectively). The parameters used in these models are based on uniaxial tensile tests performed on samples of reinforcement and compressive tests performed on samples of concrete cubes.

For concrete, the maximum compressive stress, f_c, is taken to be:

$$f_c = 0.8 \times f_{ck} \tag{1}$$

where f_{ck} is the average compressive cube strength of the concrete.

Since the maximum tensile strength, f'_{ct}, and the elastic modulus, E_c, for concrete were not experimentally measured, the equations (2) and (3) are used to obtain an initial estimate of these quantities.

$$E_c = 5000\sqrt{f_{ck}} = \text{constant} \tag{2}$$

$$f'_{ct} = 0.26\sqrt{f_{ck}} \tag{3}$$

where f_{ck} is measured in MPa

The equation (1) is obtained from reference [5] and the equations (2) and (3) from reference [25].

The point load is applied at node 7(figure 6.3). This load is increased from 0 to 96kN using the time functions described in [2] and [3] for examples in NLV1 and NLV2 respectively. The stiffness matrix is reformed at the beginning of each load increment and iteration with BFGS matrix updating is used to ensure equilibrium. The input files of two typical examples in NLV1 and NLV2 are shown in figures 6.4 and 6.5 respectively.

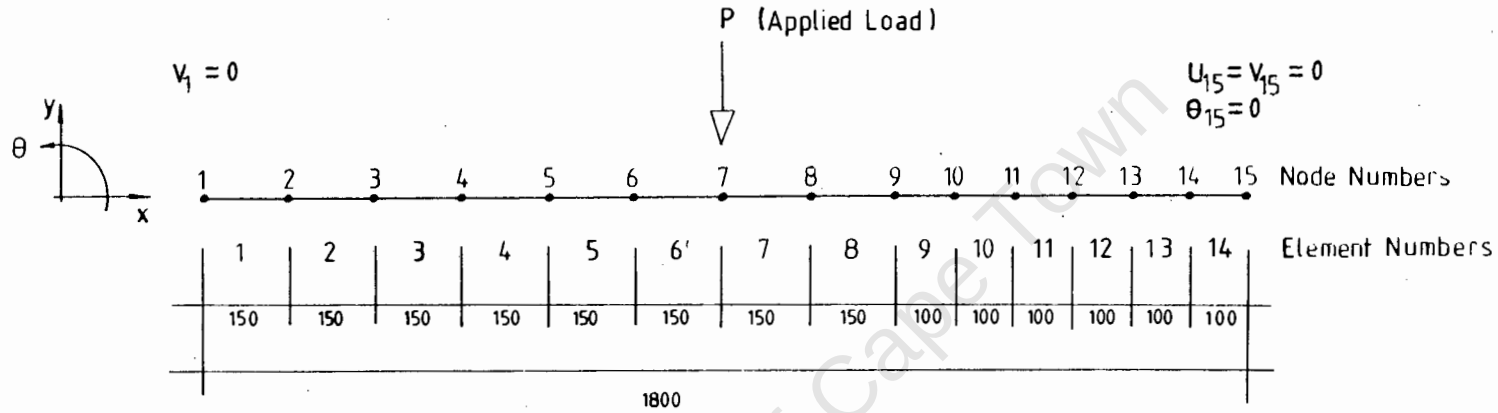

Finite element modelling of the Two-Span Beams in Sets 1 & 2

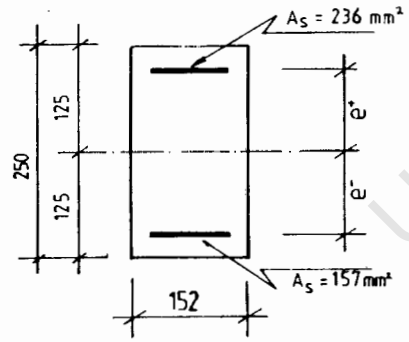

beam cross-section

BOUNDARY CONDITIONS			
NODE	U	V	θ
1	Free	Fixed	Free
15	Fixed	Fixed	Fixed

all dimensions are in millimetres

Figure 6.3: Model A - Finite Element Beam Model based on Two-Span Beams in Set 1 and Set 2.

IDENTICAL COPY OF INPUT DATA

```
1.    NSMRU R.C. 2-SPAN BEAMS TESTED BY FAIDI- EC2
2.    CONTROL DATA
3.    14  15  2  0  1
4.    NONLINEAR ANALYSIS
5.    3
6.    STATIC ANALYSIS
7.    0.0  1.0  112  1  2  50  0.04  0.04  7  1
8.    PRINT CONTROL
9.    DISPLACEMENTS
10.   3
11.   1  3  6  8  14  15
12.   NODAL COORDINATES
13.   1  0.0  0.0
14.   9  1.200  0.00
15.   10  1.30  0.0
16.   15  1.80  0.0
17.   TOPOLOGY
18.   LINES OF ELEMENTS
19.   1  8  1  9  1  1
20.   9  14  9  15  1  1
21.   SECTION PROPERTIES
22.   1  2  2
23.   -0.125  .152  5  0.125  0.152
24.   -.100  .000157  2  .096  1.000236  2
25.   MATERIAL PROPERTIES
26.   5  2400.0
27.   30.0E9  -40.0E6  1.5E6  -3.0E6
28.   3
29.   200.0E9  110.0E9  5.0E9  410.0E6  520.0E6
30.   BOUNDARY CONDITIONS
31.   1  0  1  0
32.   15  1  1  1
33.   LOADING
34.   STATIC LOADS
35.   POINT LOADS
36.   7  0.0  -1000.  0.0  1
37.   TIME FUNCTIONS
38.   1  4
39.   0  0.0  32  64.0  72  88.0  112  96.0
40.   INITIAL CONDITIONS
41.   END OF DATA
```

Figure 6.4: Input Data for NLV1 example: TSB19

IDENTICAL COPY OF INPUT DATA

```
 1.   2-SPAN BEAM TEST9 WITH CHANGE IN CONCRETE PROPERTIES
 2.   CONTROL DATA
 3.   14  15  2  0  1
 4.   NONLINEAR ANALYSIS
 5.   3
 6.   STATIC ANALYSIS
 7.   96.  4.  .5  0.0  7  -10  0.005  0.005  .5  30  0.  1  1  0  0  1  1  0
 8.   PRINT CONTROL
 9.   DISPLACEMENTS
10.   3
11.   1  3  6  8  14  15
12.   FORCE
13.   3
14.   1  2  5  6  13  14
15.   NODAL COORDINATES
16.   1  0.0  0.0
17.   9  1.200  0.00
18.   10  1.30  0.0
19.   15  1.80  0.0
20.   TOPOLOGY
21.   LINES OF ELEMENTS
22.   1  8  1  9  1  1  0.
23.   9  14  9  15  1  1  0.
24.   SECTION PROPERTIES
25.   1  2  2
26.   -0.125  .152  3  0.125  0.152
27.   -.100  .000157  2  .096  -.000236  2
28.   MATERIAL PROPERTIES
29.   8. 2400.0
30.   32.0E9  -36.0E6  2.2E6  -3.0E6  8.0  0.4E-3
31.   3
32.   200.0E9  70.0E9  5.0E9  410.0E6  520.0E6
33.   BOUNDARY CONDITIONS
34.   1  0  1  0
35.   15  1  1  1
36.   LOADING
37.   STATIC LOADS
38.   POINT LOADS
39.   7  0.0  -1000.  0.0  1
40.   TIME FUNCTIONS
41.   1  2
42.   0  0.0  200  200.0
43.   INITIAL CONDITIONS
44.   END OF DATA
```

Figure 6.5: Input Data for NLV2 example: TSPAN18

6.3 Finite Element Modelling of the Simply-Supported Beams Using Model B

In NLV1 and NLV2, the finite element model, Model B, is used to simulate the behaviour of the beams in Set 3 (see Section 3.3.2). Because of symmetry, only half the beam is modelled. Model B consisted of six 2 noded special elements, each element being 250mm in length (figure 6.7). The stiffness and internal force evaluations are made using the 2-point Gaussian quadrature formula.

The beam cross-section is uniform and the cross-sectional dimensions are given as b=152mm and h=250mm. The embedded reinforcement is modelled as a smeared layer representing the area of the 3Y16 bars in the bottom of the beam (figure 6.6). Five and seven point Newton-Cotes integration is used to evaluate the stress-distribution over the element cross-section.

In Model B, the constituent materials are also modelled as non-linear with only material nonlinearities being considered. The reinforcement is modelled using the Trilinear Elastic-Kinematic Hardening Model (Model 3), described in Section 5.4. The concrete is modelled by Model 5 in NLV1 and by Model 8 in NLV2. The point load is applied at node 5 and is increased from 0 to 50 kN in NLV1 and NLV2 using the time-functions as described in references [2] and [3] respectively. At the beginning of each load increment, the stiffness matrix is reformed. Iteration with BFGS matrix updating is used to obtain equilibrium in the non-linear analysis. The input files of two typical examples from NLV1 and NLV2 are shown in figures 6.7 and 6.8 respectively.

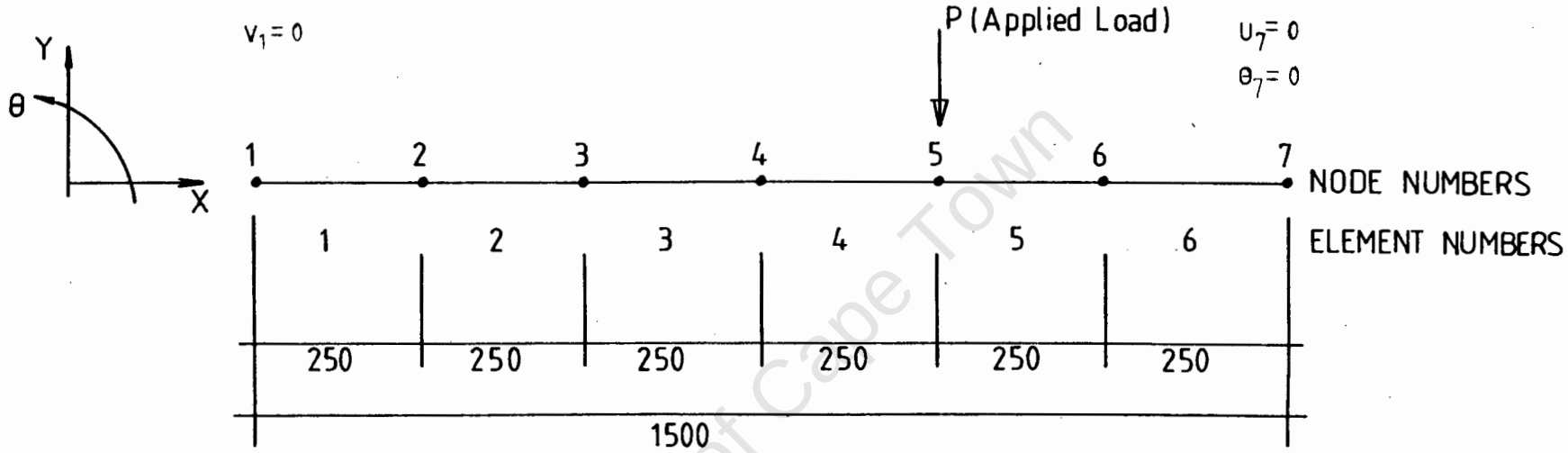

Finite Element Modelling of the Simply-Supported Beams in Set 3

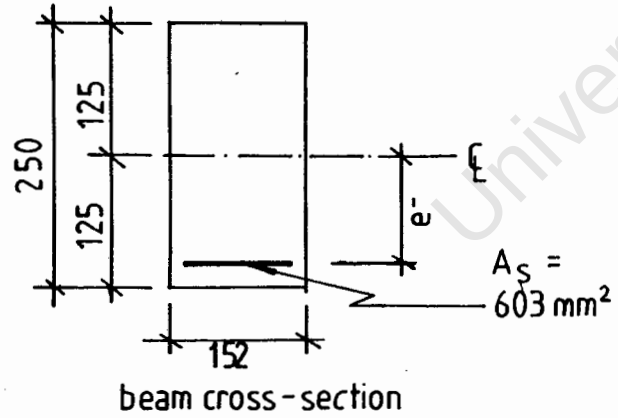

BOUNDARY CONDITIONS			
NODE	U	V	θ
1	FREE	FIXED	FREE
7	FIXED	FREE	FIXED

all dimensions in mm

Figure 6.6: Model B - Finite Element Beam Model based on Simply-Supported Beams in Set 3.

```
IDENTICAL COPY OF INPUT DATA
----------------------------


 1.   NSMRU R.C. SS BEAMS TESTED BY FALDT  -FSS1
 2.   CONTROL DATA
 3.   6   7   2   0   1
 4.   NONLINEAR ANALYSIS
 5.   3
 6.   STATIC ANALYSIS
 7.   0.0   1.0   50   1    1   50   0.04   0.04   7   1
 8.   NODAL COORDINATES
 9.   1   0.0   0.0
10.   7   1.500   0.00
11.   TOPOLOGY
12.   LINES OF ELEMENTS
13.   1   6   1   7   1   1
14.   SECTION PROPERTIES
15.   1   2   1
16.   -0.125   .152   5   0.125   0.152
17.   -.095   .000603   2
18.   MATERIAL PROPERTIES
19.   5   2400.0
20.   28.0E9   -24.0E6   1.3E6   -2.4E6
21.   3
22.   230.0E9   125.0E9   1.5E9   420.0E6   540.0E6
23.   BOUNDARY CONDITIONS
24.   1   0   1   0
25.   7   1   0   1
26.   LOADING
27.   STATIC LOADS
28.   POINT LOADS
29.   5   0.0   -1000.   0.0   1
30.   TIME FUNCTIONS
31.   1   2
32.   0   0.0   50   50.0
33.   INITIAL CONDITIONS
34.   END OF DATA
```

Figure 6.7: Input Data for NLV1 example: SSPLOT1

```
IDENTICAL COPY OF INPUT DATA
----------------------------


 1.   RC SS BEAM-TESTED BY FALDI EX5
 2.   CONTROL DATA
 3.   6  7  2  0  1
 4.   NONLINEAR ANALYSIS
 5.   3
 6.   STATIC ANALYSIS
 7.   50.0  4.0  .5  0.0  7  -10  .001  .001  .5  30  0.  1  1  0  0  1  1  0.
 8.   NODAL COORDINATES
 9.   1  0.0  0.0
10.   7  1.5  0.0
11.   TOPOLOGY
12.   LINES ON ELEMENTS
13.   1  6  1  7  1  1  0.
14.   SECTION PROPERTIES
15.   1  2  1
16.   -.125  .152  3  .125  .152
17.   -0.096  0.000603  2
18.   MATERIAL PROPERTIES
19.   8  2400.0
20.   28.0E9  -26.0E6  1.4E6  -2.0E6 8.0  0.4E-3
21.   3
22.   230.0E9  120.0E9  1.5E9  420.0E6  550.0E6
23.   BOUNDARY CONDITIONS
24.   1  0  1  0
25.   7  1  0  1
26.   LOADING
27.   STATIC LOADS
28.   POINT LOADS
29.   5  0.0  -1000.0  0.0  1
30.   TIME FUNCTIONS
31.   1  2
32.   0  0.0  200  200.0
33.   INITIAL CONDITIONS
34.   END OF DATA
```

Figure 6.8: Input Data for NLV2 example: SSPLOT18

6.4 Discussion of the Model A finite element results.

The finite element model, Model A, is used in NLFRAM to model the under-reinforced two-span beams in Set 1 and Set 2. In these examples the tensile properties of the constituent materials are expected to dominate the load-deflection behaviour.

Various examples are executed using both NLV1 and NVL2. These, together with their material properties, are tabulated in Table 6.1 and 6.2 respectively. The load-deflection plots of these examples are shown in figures 6.9 to 6.18. In these examples, the material parameters are systematically varied and examples in which the same parameter is varied are plotted on the same graph. These are done in order to determine:

i) the numerical efficiency of both NLV1 and NLV2

ii) the sensitivity of the load-deflection results due to variations in the material parameters.

Examining the plots in figures 6.9 to 6.18 with regard to (i) above, it is noted that the general load-deflection paths are similar in all the examples. However, the rate of convergence of the equilibrium iterations and also the actual computing time are significantly improved in the examples in NLV2. The computing time for the NLV2 examples is, on average, reduced by 50% when compared to the NLV1 examples. (Note that the NLV1 examples are plotted in the left column and the NLV2 examples in the right column).

Examining the plots in figures 6.9 to 6.18 and considering (ii), the following are observed with respect to a variation in:

i) the Initial Modulus of the Concrete, E_c (refer to figures 6.9 and 6.10): The load-deflection behaviour of the beam Model A is relatively insensitive to variations in the concrete modulus, E_c, in both the NLV1 and NLV2 examples. In these examples, E_c is varied between 20 and 32 GPa with very little change in the load-deflection plots being observed.

ii) the Maximum Compressive Strength of the Concrete, f_c (refer to figures 6.11 and 6.12): Varying the maximum compressive strength of the concrete also has little effect on the load-deflection results. In the figures above, f_c is varied between -32 and -40 MPa with very little change in the load-deflection plots being observed.

Table 6.1 Material Parameters for examples using Model A in NLFRAM (version1)-NLV1

Example	Concrete Parameters			Steel Parameters						
	Ec(GPa)	fc(MPa)	f'_{ct}(MPa)	E_S(GPa)	E_T(GPa)	E_H(GPa)	f_y^1(MPa)	f_y^2(MPa)	e^-(mm)	e^+(mm)
TSB2	28	-40	1.5	200	60	15	410	570	-105	105
TSB7	30	-40	1.5	200	110	5.0	420	520	-105	105
TSB8	30	-40	1.5	200	140	5.0	410	520	-105	105
TSB10	30	-40	1.5	200	70	5.0	410	520	-105	105
TSB12	30	-40	1.0	200	110	5.0	420	520	-105	105
TSB13	30	-40	2.0	200	110	5.0	420	520	-105	105
TSB14	20	-40	1.5	200	110	5.0	410	520	-105	105
TSB15	32	-40	1.5	200	110	5.0	410	520	-105	105
TSB17	30	-40	1.5	195	110	5.0	410	520	-105	105
TSB18	30	-40	1.5	200	110	5.0	410	520	-100	96
TSB26	30	-40	1.5	200	110	5.0	410	520	-104	104
TSB28	30	-40	1.5	200	110	5.0	410	520	-102	96
TSB37	30	-32	1.5	200	110	5.0	410	520	-100	96

Table 6.2 Material Parameters for examples using Model A in NLFRAM (version2)-NLV2

Example	Concrete Parameters			Steel Parameters						
	Ec(GPa)	fc(MPa)	f'_{ct}(MPa)	E_S(GPa)	E_T(GPa)	E_H(GPa)	f'_y(MPa)	f^z_y(MPa)	e^-(mm)	e^+(mm)
TSPAN1	30	-40	1.5	200	110	5	410	520	-100	96
TSPAN3	34	-40	1.5	200	110	5	410	520	-100	96
TSPAN4	28	-40	1.5	200	110	5	410	520	-100	96
TSPAN5	26	-40	1.5	200	110	5	410	520	-100	96
TSPAN6	28	-34	1.5	200	110	5	410	520	-100	96
TSPAN9	32	-36	2.2	200	110	5	410	520	-100	96
TSPAN18	32	-36	2.2	200	70	5	410	520	-100	96
TSPAN19	28	-34	2.0	200	70	5	410	520	-100	96

iii) the Maximum Tensile Stress of the Concrete, f'_{ct} (refer to figures 6.13 and 6.14): This parameter exerts a major influence on the load-deflection results. The parameter is varied between 1,0 and 2,0 MPa for the NLV1 examples and between 1,5 and 2,0 MPa for the NLV2 examples. The value specified for f'_{ct} determines the load at which the first kink in the load-deflection curve occurs as well as the load-deflection behaviour of the beam thereafter. This kink symbolises the initial cracking of the concrete.

iv) the Initial Modulus of the Steel, E_S (refer to figure 6.15): This parameter also exerts a small influence on the results after the first kink in the load-deflection curve is reached.

v) the Transition Steel Modulus, E_T (refer to figures 6.16 and 6.17): This parameter only influences the results just prior to the second kink in the curve. This is understandable since the parameter was introduced to smoothen the load-deflection curve in this region.

vi) the Yield Stress of the Steel, f'_y and f^2_y (refer to figure 6.18): The yield stress of the steel determines the load-deflection path from just prior to the yielding of the steel. In figure 6.17, f^2_y is reduced from 570 to 520 MPa and the load-deflection path changes quite substantially. From the figure it is evident that the yield stress specified should accurately reflect the yield stress of the reinforcement used in the experimental beams in order to model the load-deflection behaviour of these beams in the yielding range.

From the above observations it can also be concluded that NLV2 with material Models 3 and 8 is numerically more efficient than NLV1. As expected, the tensile properties of the concrete and the ductile properties of the steel exert the major influences on the load-deflection behaviour of the beam model, Model A. At low load levels, the initial modulus of the steel dominates the load-deflection behaviour. When concrete cracking begins, the maximum tensile stress of the concrete becomes important. As the loads are increased and the concrete cracks open wider, the yield stress of the steel, the steel transition and hardening moduli become important because by this time, the beam relies entirely on the reinforcement for its stiffness.

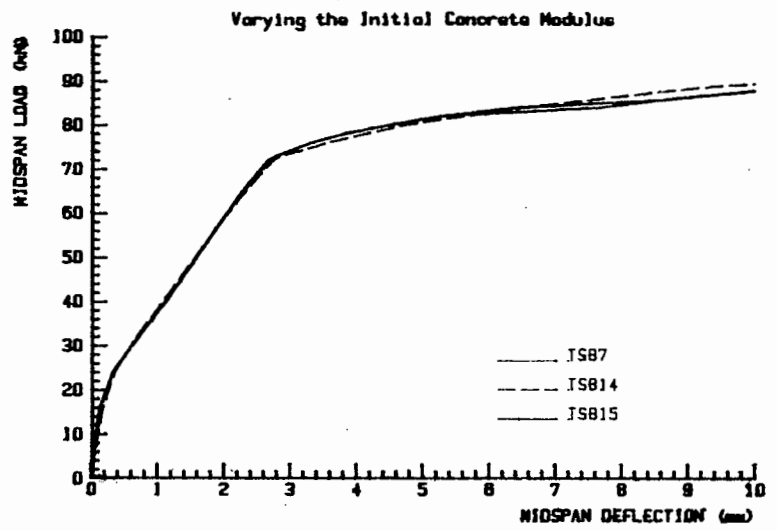

Figure 6.9

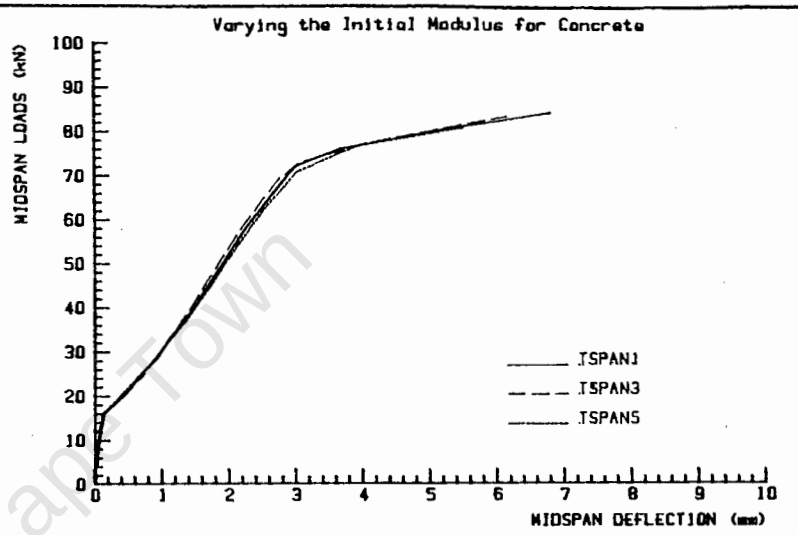

Figure 6.10

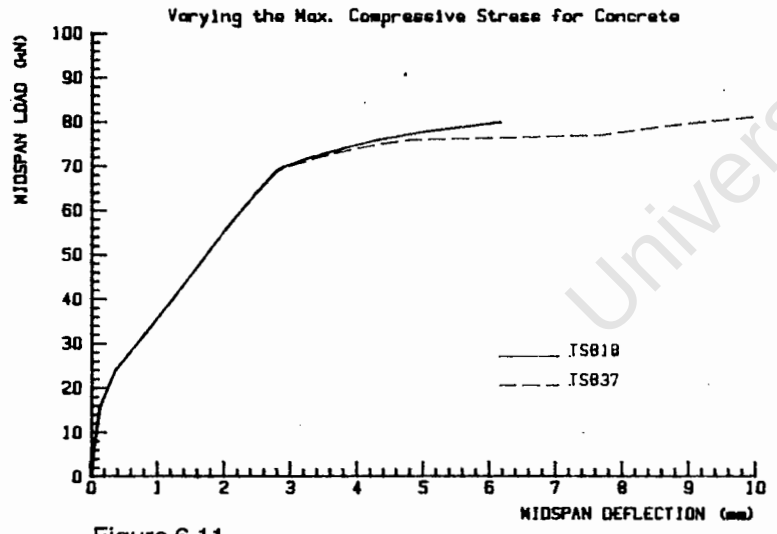

Figure 6.11

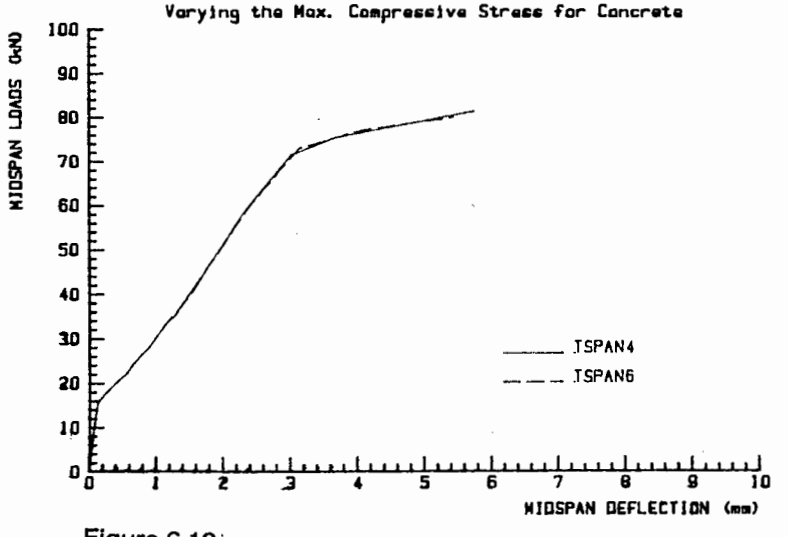

Figure 6.12

MODEL A-NLV1

MODEL A-NLV2

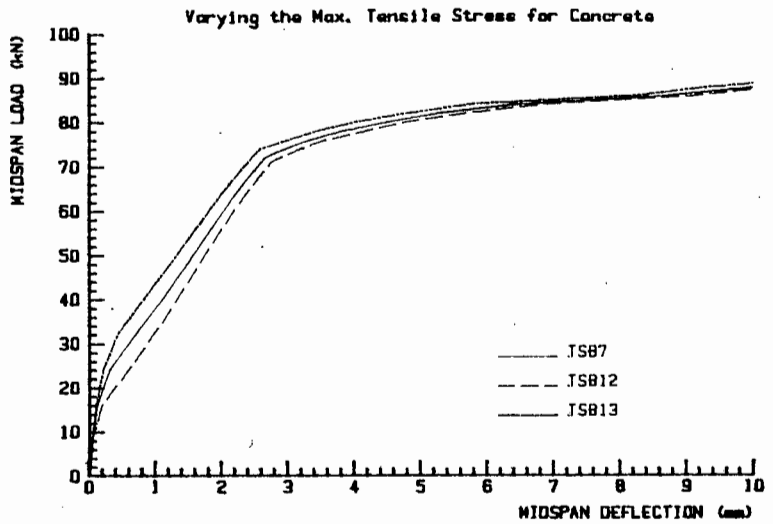

Figure 6.13

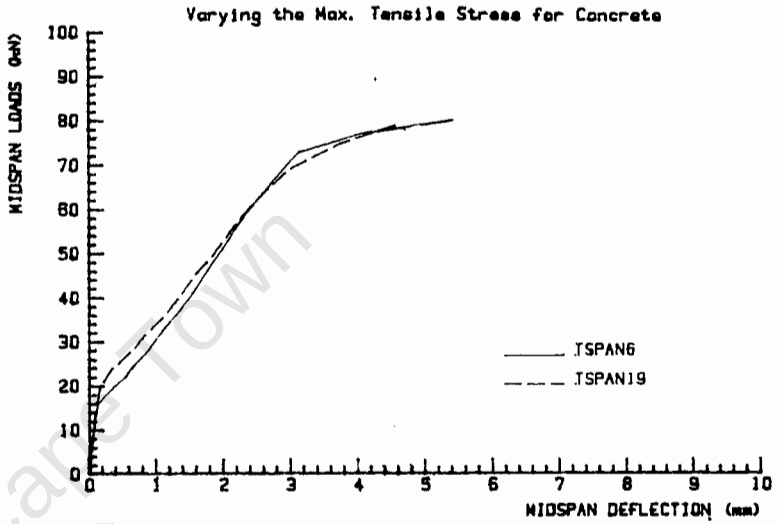

Figure 6.14

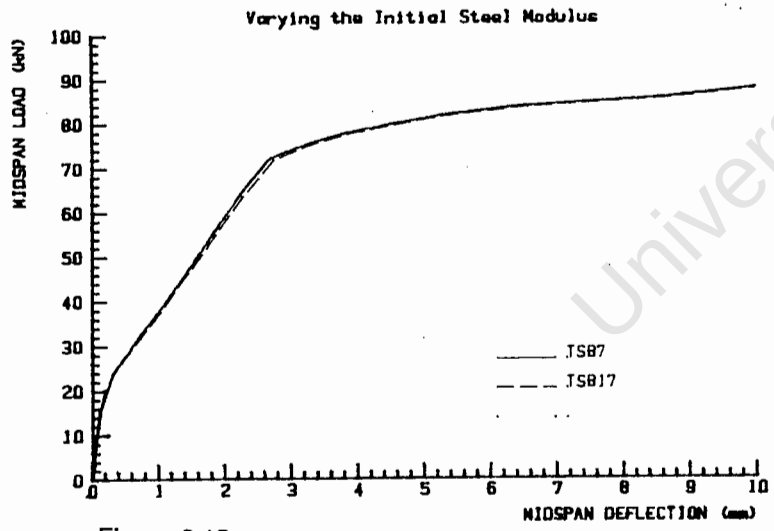

Figure 6.15

MODEL A-NLV1

MODEL A-NLV2

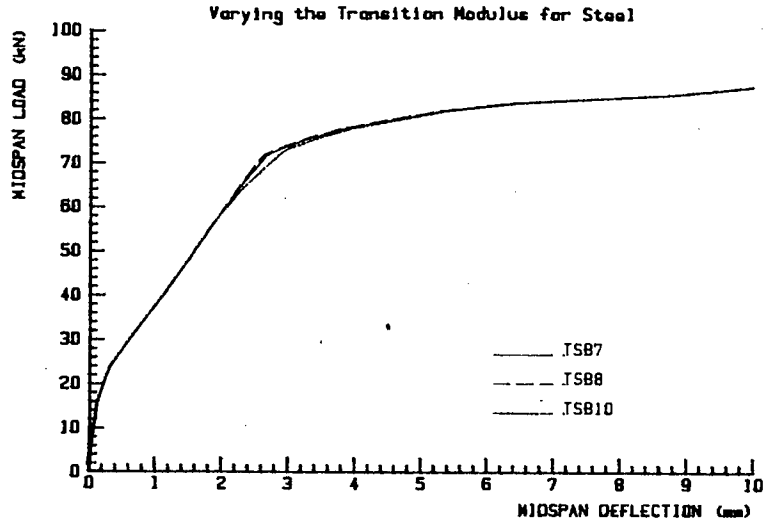

Figure 6.16

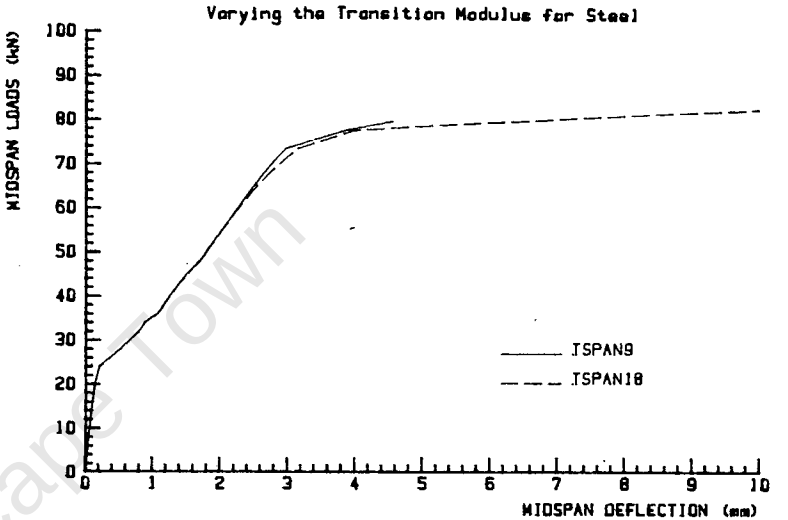

Figure 6.17

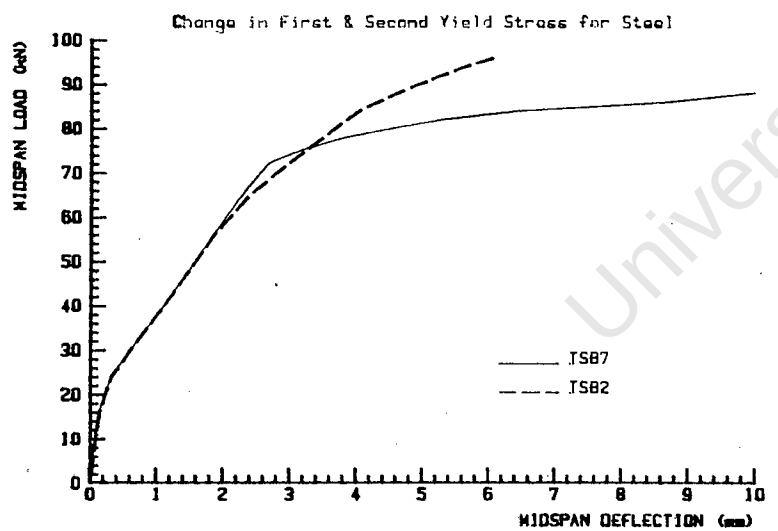

Figure 6.18

MODEL A-NLV1

MODEL A-NLV2

6.5 Discussion of the Model B results

The finite element model, Model B, is used in NLFRAM to model the slightly over-reinforced simply-supported beams in Set 3. In these examples the compressive properties of the concrete are expected to play a greater role in influencing the load-deflection behaviour.

The examples executed in NLV1 and NLV2, together with their material properties, are tabulated in Tables 6.3 and 6.4. The load-deflection plots of these examples are shown in figures 6.19 to 6.24. Again, the material parameters are systematically varied and examples in which the same parameter is varied are plotted on the same graph.

Examining these plots and considering the objectives set out in Section 6.4, it is again noted that the general load-deflection paths are similar for all the examples. The rate of convergence of the equilibrium iterations as well as the computing time are improved by about 60% in examples using NLV2 when compared to examples from NLV1. Furthermore, the following observations are made with respect to a variation in:

i) the Maximum Compressive Stress of the Concrete, f_c, (figures 6.19 and 6.20): The load-deflection behaviour of the beams modelled in NLV1 and NLV2 remains relatively insensitive to variation in this parameter until the load reaches about 70% of the ultimate capacity of the beam. Thereafter, the examples with the higher f_c values produce stiffer load-deflection results. (The parameter f_c is varied between -22 and -26 MPa). Although the variation in the results is small, the plots do indicate that the maximum compressive stress of the concrete has an influence on the results in the region close to the ultimate load capacity of the finite element beam.

ii) the Maximum Tensile Stress of the Concrete, f'_{ct} (figures 6.21 and 6.22): This parameter exerts an influence on the results especially in the region of the first kink in the curve. The plots show that for examples with a higher f'_{ct}, the results in this region become stiffer (f'_{ct} was varied between 1.2 and 2.0 MPa). The first kink in the curve represents the initial cracking of the beams. The parameter, f'_{ct}, determines the load at which this initial cracking takes place and the stiffness of the beam immediately after.

Table 6.3 Material Parameters for examples using Model B in NLFRAM (version1)-(NLV1)

Example	Concrete Parameters			Steel Parameters					
	Ec(GPa)	fc(MPa)	f'_{ct}(MPa)	E_S(GPa)	E_T(GPa)	E_H(GPa)	f'_y(MPa)	f^z_y(MPa)	e^-(mm)
SSPLOT1	28	-24	1.3	230	125	1.5	420	540	95
SSPLOT2	28	-24	1.4	230	110	5.0	410	520	95
SSPLOT3	28	-24	1.4	230	110	5.0	410	520	95
SSPLOT4	28	-24	1.2	230	125	1.5	420	540	95
SSPLOT5	28	-24	2.0	230	125	1.5	420	540	95
SSPLOT6	28	-22	1.3	230	125	1.5	420	540	95
SSPLOT7	28	-26	1.3	230	125	1.5	420	540	95

Table 6.4 Material Parameters for examples using Model B in NLFRAM (version2)-(NLV2)

Example	Concrete Parameters			Steel Parameters					
	Ec(GPa)	fc(MPa)	f'_{ct}(MPa)	E_S(GPa)	E_T(GPa)	E_H(GPa)	f'_y(MPa)	f^2_y(MPa)	e^-(mm)
SSPLOT10	30	-24	1.4	230	120	1.5	420	550	96
SSPLOT11	32	-24	1.4	230	120	1.5	420	550	96
SSPLOT12	28	-24	1.4	230	120	1.5	420	550	96
SSPLOT14	28	-22	1.4	230	120	1.5	420	550	96
SSPLOT18	28	-26	1.4	230	120	1.5	420	550	96
SSPLOT19	28	-24	1.3	230	120	1.5	420	550	96
SSPLOT20	28	-24	1.5	230	120	1.5	420	550	96
SSPLOT21	28	-24	1.4	220	120	1.5	420	550	96
SSPLOT29	28	-24	2.4	215	110	1.5	420	550	96

iii) the Elastic Modulus of the Concrete, E_C, (figure 6.23): For the NLV2 examples, E_C is varied between 28 and 32 MPa. The load-deflection results are insensitive to this variation until after the initial cracking of the beam.

iv) the Elastic Modulus of the steel, E_S (figure 6.24): In figure 6.24, E_S is varied between 220 and 230 MPa. This variation also influences the results after the initial cracking of the beam (the beam with the higher E_S value produces a stiffer result).

From the observations above it can again be concluded that NLV2 is numerically more efficient than NLV1. Also, the compressive parameters of the material models play the major role in influencing the results. However, the maximum tensile stress of the concrete determines the beam behaviour at the commencement of tensile cracking of the beam. The compressive parameters only become significant thereafter. This is as expected since the stiffness of the beam then becomes dependent on the parameters such as E_S and E_C. Near failure, the influence of f_C becomes dominant because the load capacity of the beam is dependent on the maximum compressive stress of the concrete.

From these observations and those in Section 6.4, it is clear that the examples in NLV1 and NLV2 utilize the stress-strain properties of the constituent materials in both tension and compression. The significance of the material parameters under these conditions is determined. It should be noted however, that only trends in the material models are investigated here. In Chapter 7, the validity of these numerical examples is tested when the results are directly compared to the results of the experimental beams.

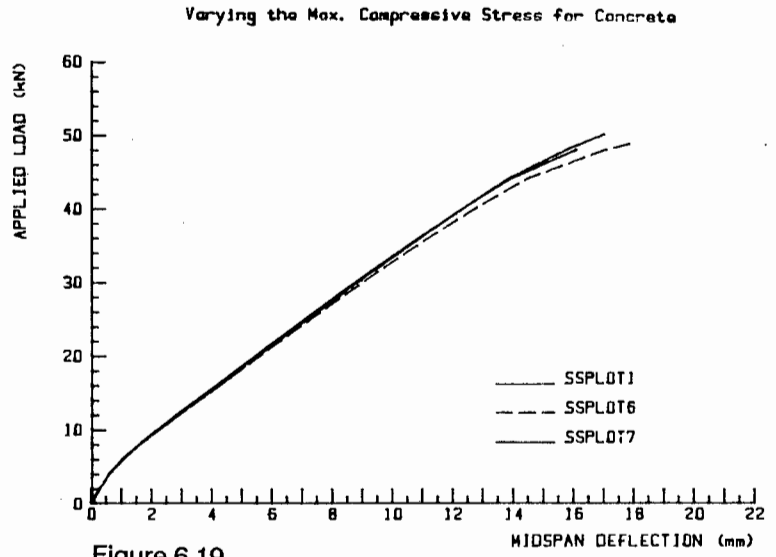

Figure 6.19

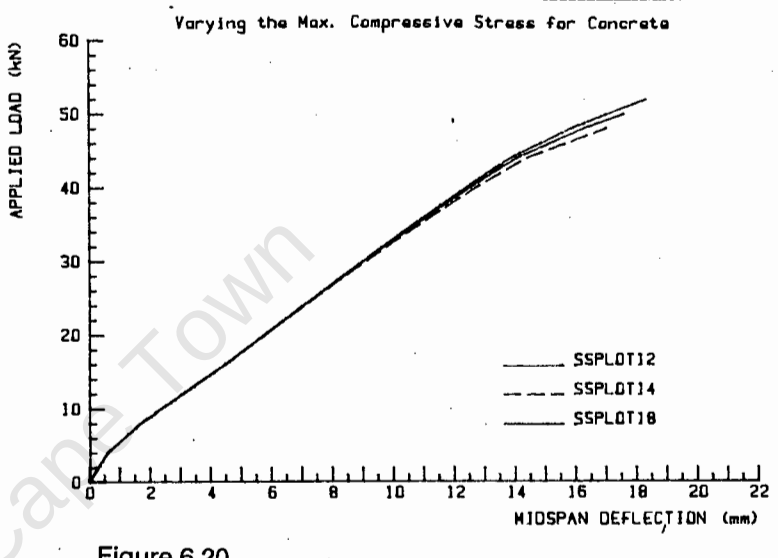

Figure 6.20

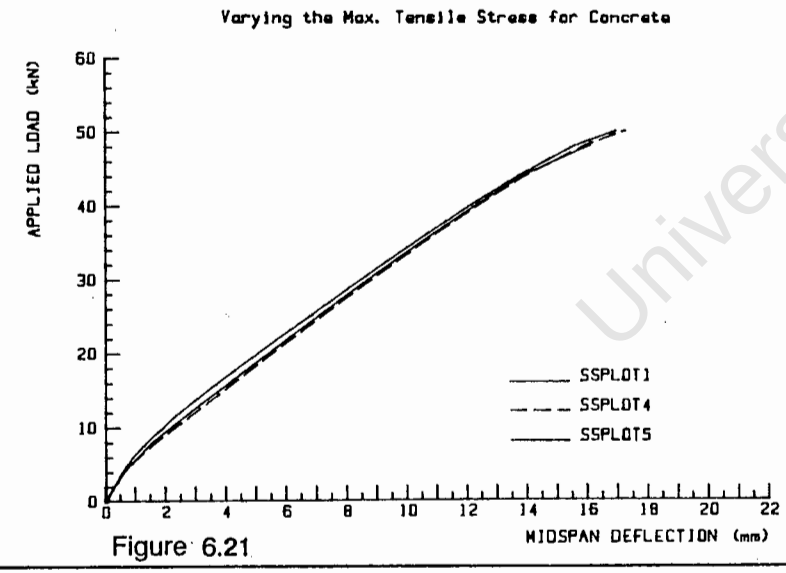

Figure 6.21

MODEL B-NLV1

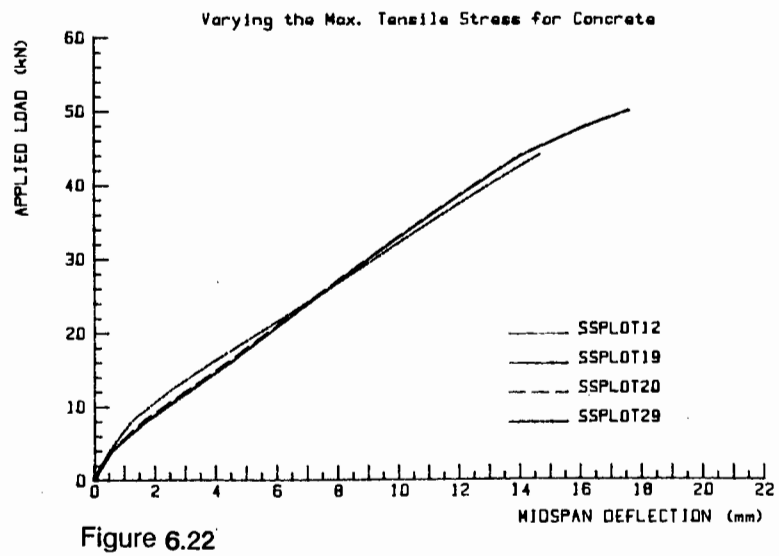

Figure 6.22

MODEL B-NLV 2

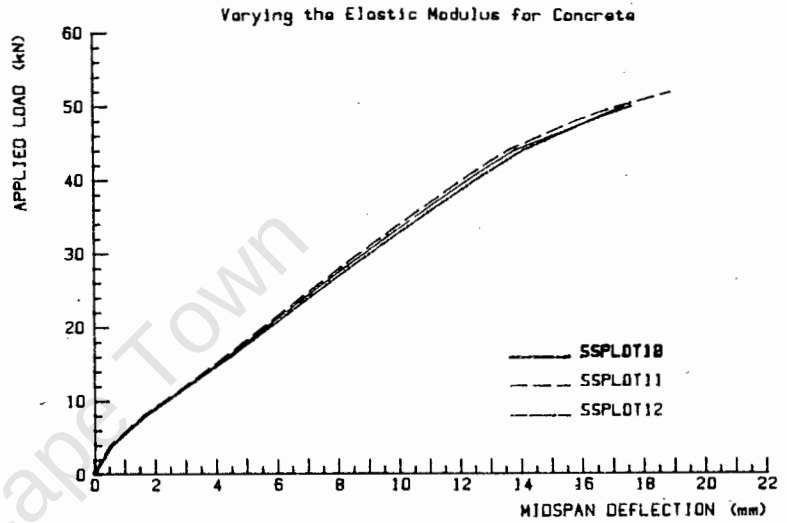

Figure 6.23

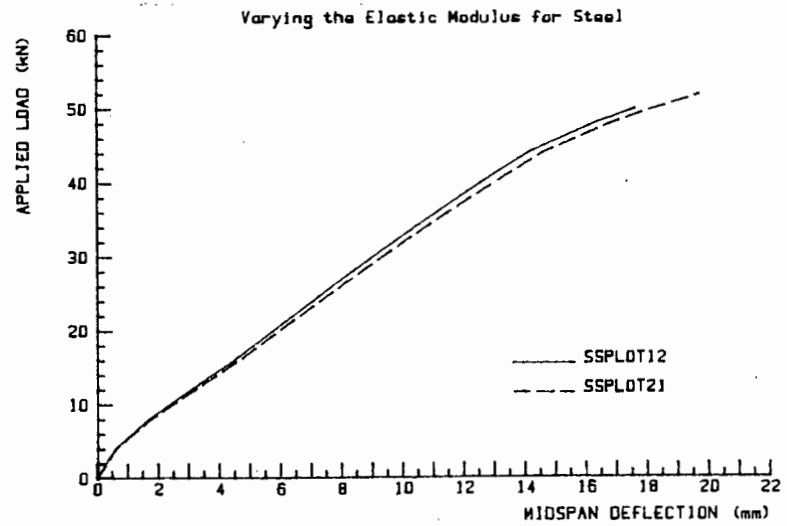

Figure 6.24

MODEL B NLV-2

CHAPTER 7

COMPARISON OF THE EXPERIMENTAL AND FINITE ELEMENT RESULTS

7.1 Introduction

In this chapter, the load-deflection results of the experimental beams, discussed in Chapter 3, are directly compared with the finite-element results from NLFRAM (discussed in Chapter 6). The comparisons of the two-span beam results are discussed in Section 7.2 while the comparisons of the simply supported beams are discussed in Section 7.3.

7.2 Comparison of the experimental two-span beams and the finite element results in NLFRAM.

In this section, the load-deflection results of typical two-span beams from the experimental investigation are compared to the finite element examples from NLFRAM. The NLFRAM examples used in the comparisons are based on the finite element model, Model A, presented in Chapter 6. The two-span beams, FS7 (Set 2) and FS11 (Set 1) form the basis of the experimental comparisons. These beams are compared to the results from NLV1 (figures 7.1 to 7.3) and to the results from NLV2 (figures 7.4 to 7.8). These figures show the midspan deflections as functions of the midspan applied loads.

To begin with, the load-deflection plot of an NLV1 example simulating the behaviour of the beam FS7, is superimposed on the FS7 results (figure 7.1). The material properties used in the NLV1 example are also shown. Examining the two curves, it is evident that there are distinct similarities as well as discrepancies in the results.

The results are similar in that the general load-deflection paths for the two curves are divided into three distinct regions. These regions are marked O,A,B,C on the FS7 curve and O,A′ ,B′ ,C′ on the NLV1 curve (figure 7.1). The region from O to A and O to A′ represents the initial load-deflection response of the experimental and finite element beams respectively. In this region the concrete is virtually in an uncracked state and the beams behave elastically. The kinks at A and A′ in the curves, represent the initial cracking of the concrete.

The second region, from A to B and A′ to B′ for beam FS7 and the NLV1 example respectively, represents the load-deflection behaviour of the beam when the concrete is undergoing progressive tensile cracking under increasing applied load. The kinks at B and B′ represent the physical and simulated yielding of the steel respectively. The third region, from B to C and B′ to C′ represents the behaviour of the beams after the initial yielding of the steel has occurred.

The general load-deflection path of beam FS7 thus seems to be reasonably well simulated by the NLV1 example. However, some discrepancies are also evident in the results. These are:

i) the NLV1 example appears to under-estimate the measured displacements of beam FS7. This occurs throughout the loading range. The predicted displacement is about 0.2mm lower than the measured displacements when the loads reached 24kN. When the loads reach 70kN the predicted displacement is about 1.0mm lower. This represents a substantial discrepancy if it is considered that the overall displacement of beam FS7 is only 4mm just prior to the yielding of the steel.

ii) The elastic region (the loading range between O and A′) for the NLV1 example appears to be bilinear. A minor kink in the curve occurs when the loads reach 16kN. This phenomenon is not observed in the results for beam FS7.

iii) A tensile strength of 1.5MPa is used in the material modelling of the NLV1 example (figure 7.1). This value is only half the initial estimated value of 3.0 MPa obtained from equation 3 given in Section 6.2. Increasing the tensile strength above 1.5 MPa results in the curve becoming even stiffer. This effect is illustrated in Section 6.2. Hawla made a similar observation when he simulated under-reinforced simply-supported concrete beams using NLV1 [6].

In order to establish the causes of these discrepancies, various load-deflection plots used in the material parameter study for NLV1 (See Section 6.2), are superimposed on the FS7 results. In these NLV1 plots, the material parameters are systematically varied to determine how these affect the load-deflection curves. Comparing these plots with the FS7 results, it is observed that with the exception of the elastic modulus of the steel, E_S and the tensile strength of the concrete, f'_{Ct}, none of the other material parameters are sensitive enough to influence the results so significantly. However, in order to increase the predicted displacements so as to match the FS7 curve, the elastic modulus of the steel may be reduced from 200 GPa to 150 GPa and/or the concrete tensile strength may be reduced from the already low 1.5 MPa to below 1.0 MPa.

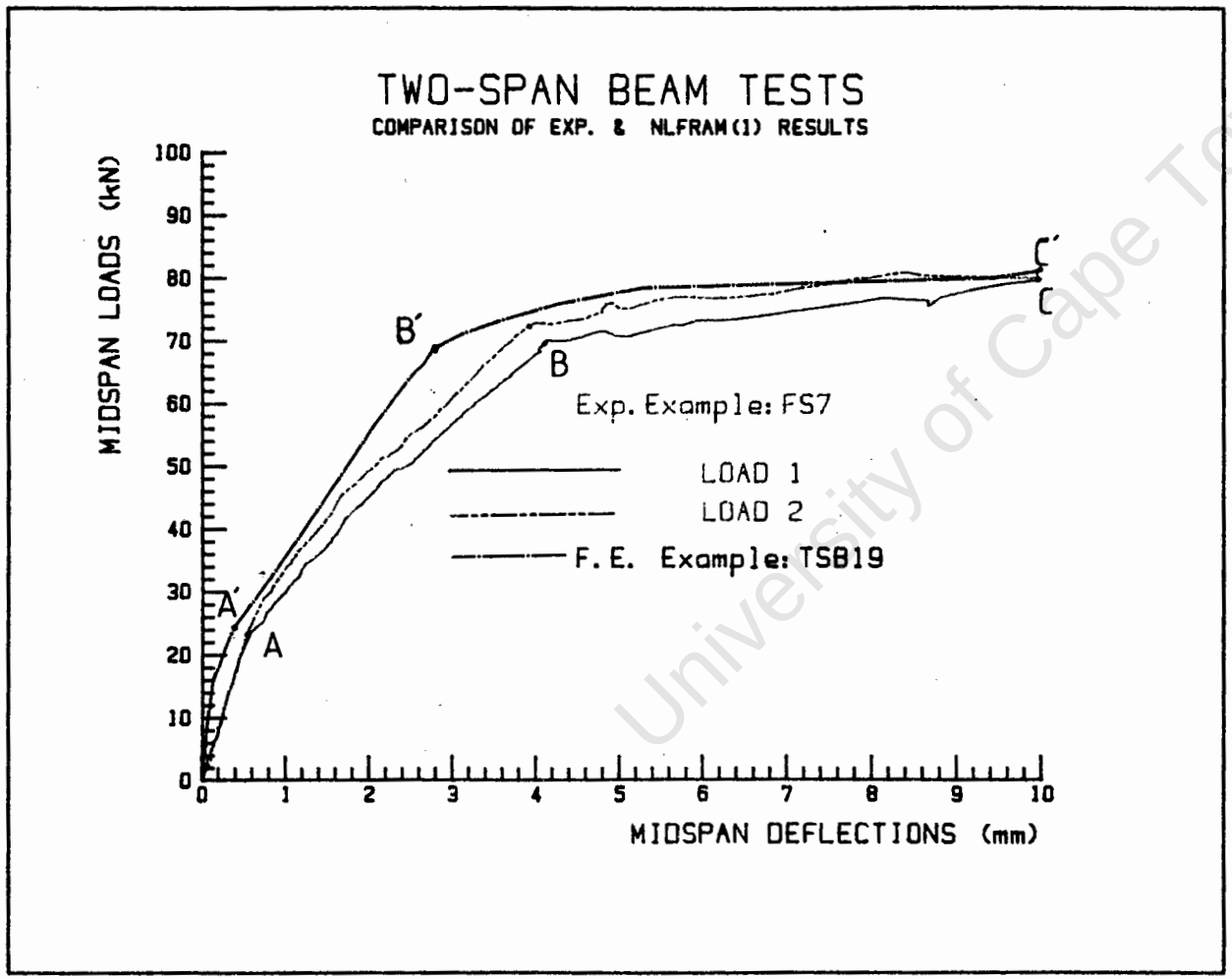

Figure 7.1: Comparison of Results of Beam FS7 (Set 2) and F.E. Example TSB19 (NLV1).

F. E. EXAMPLE : TSB19

MATERIAL PROPERTIES

STEEL-MODEL 3

E_S =200 GPa
E_T =110 GPa
E_H = 5 GPa
f_y' =410 MPa
f_y^2 =520 MPa

CONCRETE-MODEL 5

E_C = 30 GPa
f_c =-40 MPa
f_{ct}' =1.5 MPa

These conditions are unrealistic because:

i) the elastic modulus of the steel was experimentally determined from stress-strain curves. These curves were derived from uniaxial tensile tests performed on a selection of bars from the batch of reinforcing steel used in the manufacture of the experimental beams (See Section 4.3).

ii) reducing the tensile strength below 1,5 MPa would not only reduce the stiffness of the beam but also reduce the elastic range of the load-deflection curve (See Section 6.2). This implies that the predicted initial cracking of the concrete would occur at a much lower load than experienced by FS7. Although the tensile strength of beam FS7 was not determined experimentally, it was expected to be in the region of 2.5 to 3.0 MPa. This range is based on the formulae given in references [25] and [35].

A similar investigation is performed using examples from the NLV1 parameter study to simulate the behaviour of the Set 1 beam, FS11. In these NLV1 examples, the compressive strength is reduced from 40 MPa to 32 MPa to account for the lower cube strength of beam FS11. The compared results are similar to those for FS7 (see figure 7.2). This is not really unexpected since it has been shown in Section 6.2 that a reduction in the compressive strength of the concrete has little effect on the predicted load-deflection results. This effect is also observed experimentally when the results of FS7 and FS11 are compared (figure 7.3).

From the above observations, it is clear that the parameters used in modelling the constituent materials in the NLV1 examples are not sensitive enough to variation to cause the discrepancy between the actual and predicted responses. This leads to the conclusion that either:

i) the material models used in NLV1 do not reflect the load-deflection behaviour of the experimental beams correctly

and/or

ii) the experimental load-deflection results were measured incorrectly or influenced by factors not considered in the finite element modelling.

In order to establish the validity of the concrete material model used in NLV1, the finite element examples shown in figures 7.1 and 7.2 are executed using NLV2. In these NLV2 examples, concrete model 5 is replaced by model 8 (These models are discussed in Section 6.1).

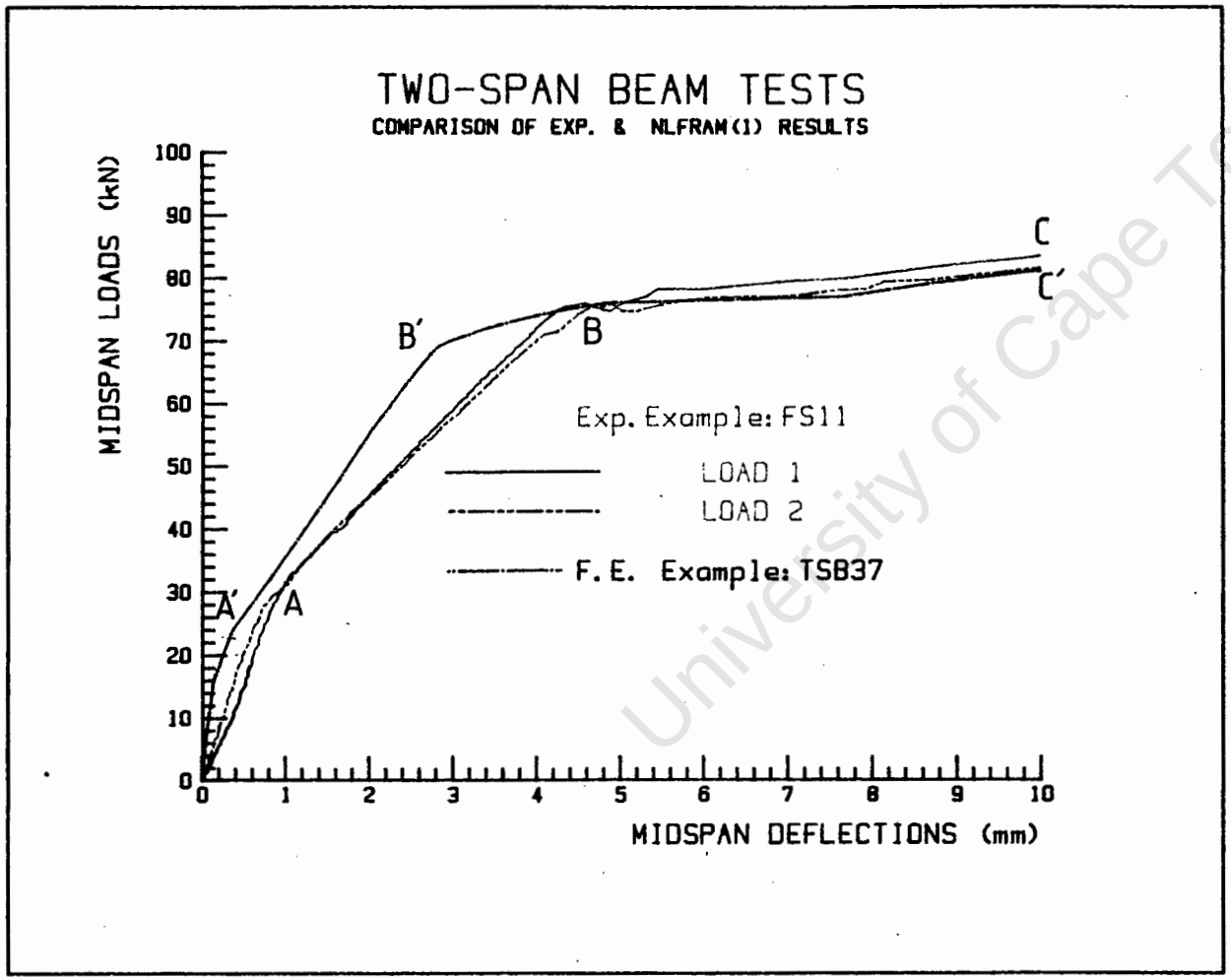

Figure 7.2: Comparison of Results of Beam FS11 (Set 1) and F.E. Example TSB37 (NLV1).

F.E. EXAMPLE : TSB37

MATERIAL PROPERTIES

STEEL-MODEL 3

E_S	=200 GPa
E_T	=110 GPa
E_H	= 5 GPa
f'_y	=410 MPa
f^2_y	=520 MPa

CONCRETE-MODEL 5

E_C	= 30 GPa
f_c	=-32 MPa
f'_{ct}	=1.5 MPa

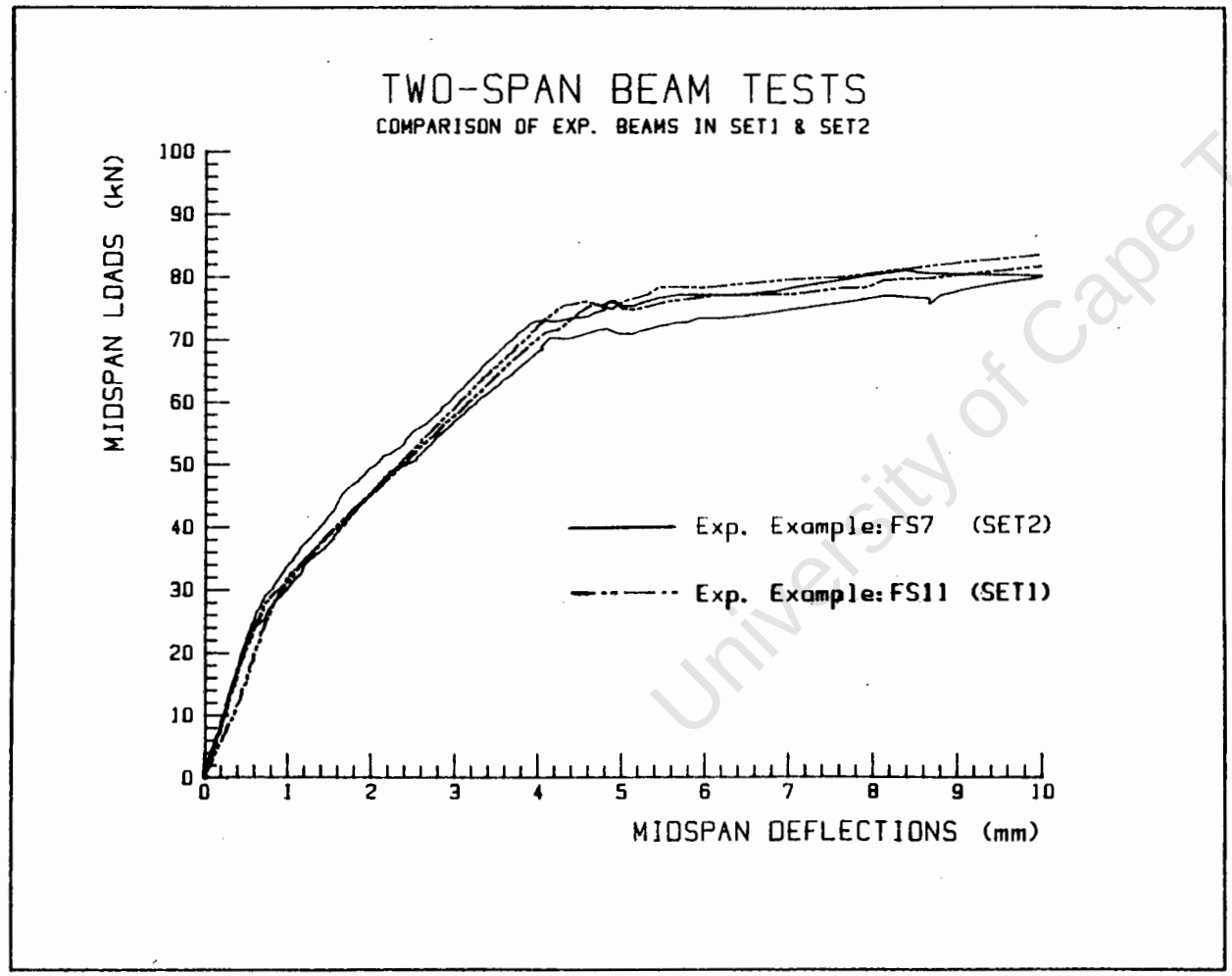

Figure 7.3: Comparison of the Results of the Experimental Beams FS7 and FS11.

The load-deflection results from these NLV2 examples are superimposed on the results of beam FS7 and FS11 in figures 7.4 and 7.5 respectively. Comparing the finite element results with the experimental results in these figures, it is observed that:

i) there is still a discrepancy between the actual and predicted displacements, especially in the elastic region and prior to the yielding of the steel.

ii) the initial cracking of the concrete for the NLV2 examples, occur when the loads have reached 16kN. These loads are only about 70% of the loads experienced by FS7 and FS11.

iii) the secondary elastic slope, as observed in the NLV1 examples is eliminated from the NLV2 results. This is more realistic since a secondary slope is also not observed experimentally.

From the observation in (ii) above, it is noted that the tensile strength of the NLV2 examples under-estimated the actual tensile strength of the experimental beams. Increasing this value from 1.5 to 2.2 MPa for the example simulating the behaviour of beam FS11 improves the predicted results to a certain extent (see figure 7.6). The initial cracking of the concrete is now predicted to occur when the loads reach 24kN. Although the initial cracking of the concrete for beam FS11 occurs when the loads reached 27kN, the predicted value is realistic. This is so because the initial concrete cracking loads varied between 23 and 28kN for the beams in Set1 (see figures 7.6, 7.7 and 7.8).

Although the displacements are still under-estimated the NLV2 example in figure 7.6 reproduced all the major effects of the two-span beams under monotonic loading. The concrete material model 8 in NLV2 thus appear to be better suited to model the concrete behaviour of these beams. Furthermore, it appears that model 5 in NLV1 does not adequately reflect the concrete behaviour in these beams. The difference between these two models is evident from the description of the concrete tensile stress-strain behaviour after the maximum tensile stress is reached (See Section 6.1). For model 5 this effect, called the tensile stiffening effect, lends itself to a stiffer result because of the delay in stress release after tensile cracking commenced (for Model 5, the stress remains constant until a limiting strain is reached before stress release occur). From the comparison of the results, it is clear that this does not occur experimentally. Although NLV2 improves the predicted results to some extent, the possibility that the experimental results were incorrectly measured or influenced by factors not accounted for in the finite element model cannot be excluded.

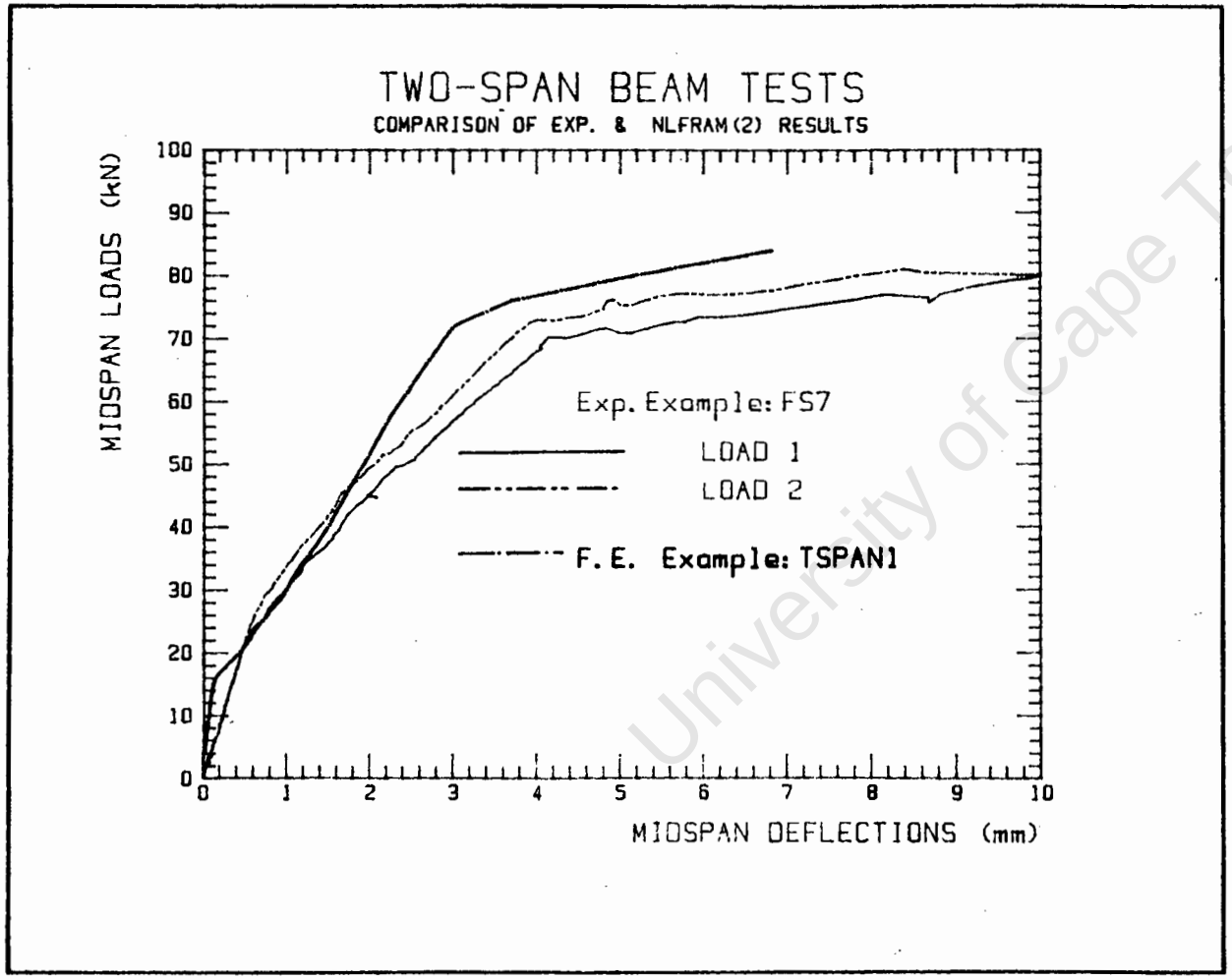

Figure 7.4: Comparison of the Results of Beam FS7 (Set 2) and F.E. Example TSPAN1 (NLV2)

F.E. EXAMPLE : TSPAN1

MATERIAL PROPERTIES

STEEL-MODEL 3

E_S =200 GPa
E_T =110 GPa
E_H = 5 GPa
f'_y =410 MPa
f'^2_y =520 MPa

CONCRETE-MODEL 8

E_C = 30 GPa
f_c =-40 MPa
f'_{ct} =1.5 MPa

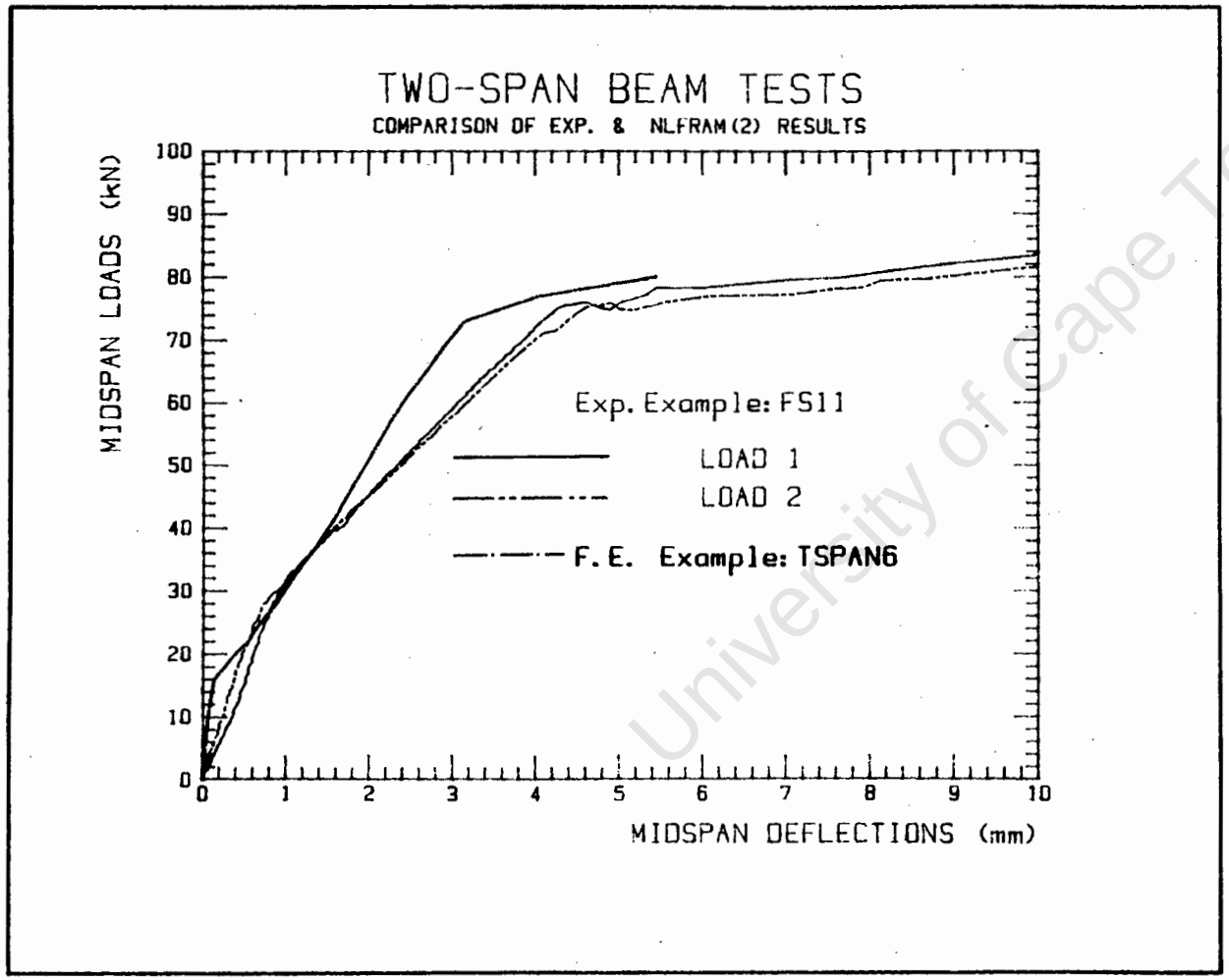

Figure 7.5: Comparison of the Results of Beam FS11 (Set 1) and F.E. Example TSPAN6 (NLV2).

F.E. EXAMPLE : TSPAN6

MATERIAL PROPERTIES

STEEL-MODEL 3

E_S =200 GPa
E_T =110 GPa
E_H = 5 GPa
f'_y =410 MPa
f^z_y =520 MPa

CONCRETE-MODEL 8

E_C = 28 GPa
f_c =-34 MPa
f'_{ct} =1.5 MPa

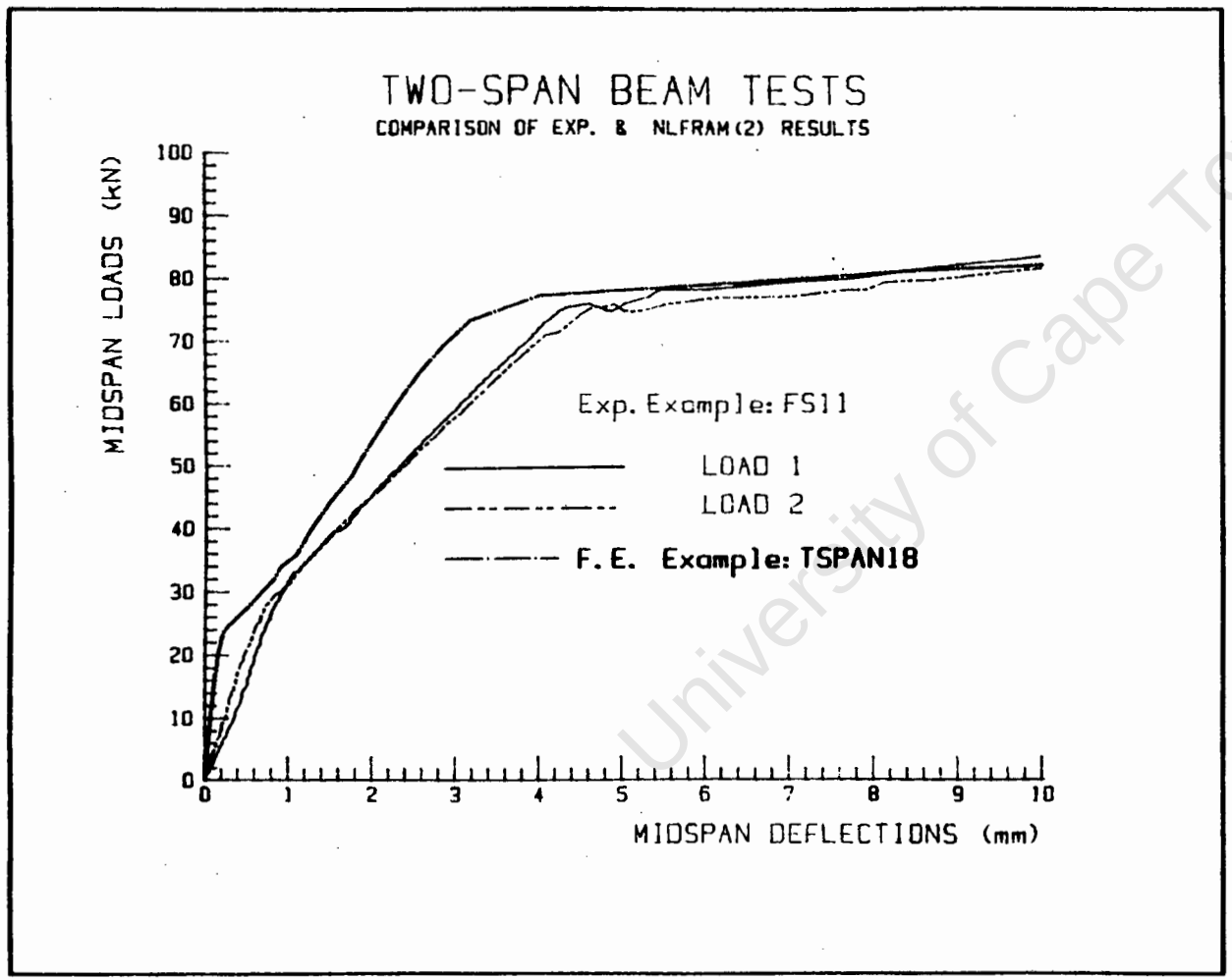

Figure 7.6: Comparison of the Results of Beam FS11 (Set 1) and F.E. Example TSPAN18 (NLV2).

F.E. EXAMPLE : TSPAN18

MATERIAL PROPERTIES

STEEL-MODEL 3

E_S =200 GPa
E_T = 70 GPa
E_H = 5 GPa
f'_y =410 MPa
f^2_y =520 MPa

CONCRETE-MODEL 8

E_C = 32 GPa
f_c =-36 MPa
f'_{ct} =2.2 MPa

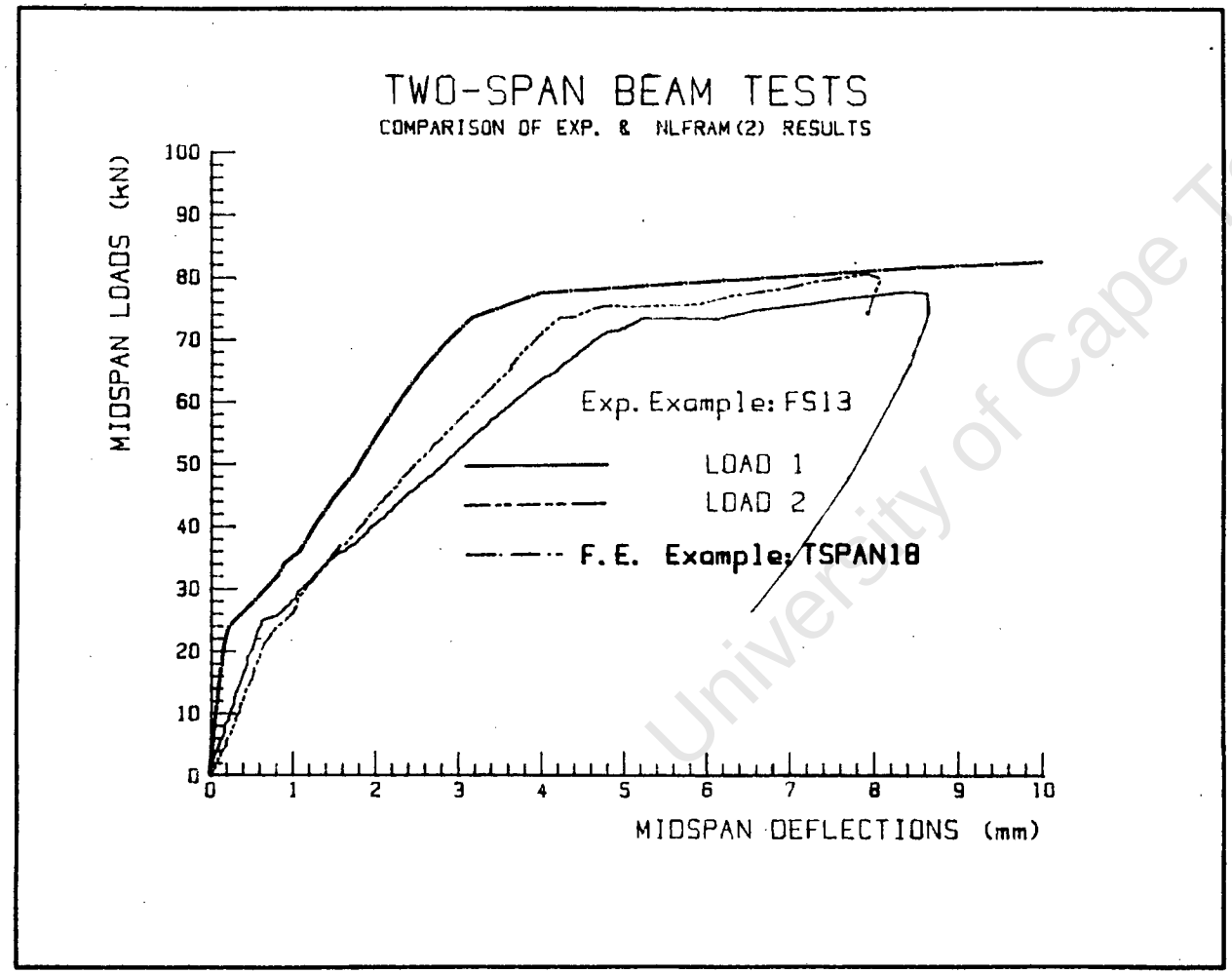

Figure 7.7: Comparison of the Results of Beam FS13 (Set 1) and F.E. Example TSPAN18 (NLV2).

F.E. EXAMPLE : TSPAN18

MATERIAL PROPERTIES

STEEL-MODEL 3

E_S =200 GPa
E_T = 70 GPa
E_H = 5 GPa
f'_y =410 MPa
f^2_y =520 MPa

CONCRETE-MODEL 8

E_C = 32 GPa
f_c =-36 MPa
f'_{ct} =2.2 MPa

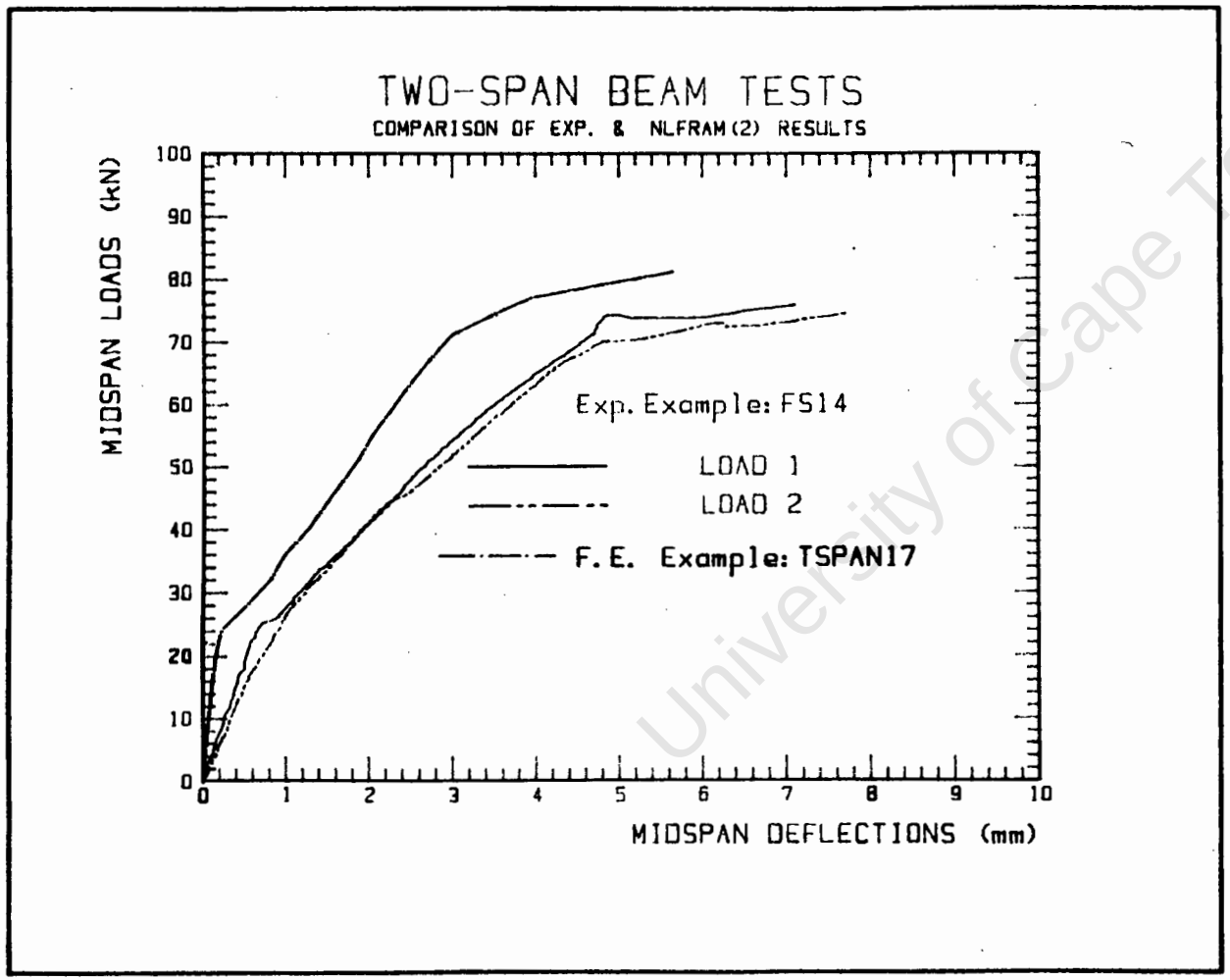

Figure 7.8: Comparison of the Results of Beam FS14 (Set 1) and F.E. Example TSPAN17 (NLV2).

F.E. EXAMPLE : TSPAN17

MATERIAL PROPERTIES

STEEL-MODEL 3

E_S =200 GPa
E_T = 70 GPa
E_H = 5 GPa
f_y' =410 MPa
f_y^2 =520 MPa

CONCRETE-MODEL 8

E_C = 30 GPa
f_c =-36 MPa
f_{ct} =2.2 MPa

The load-cells and displacement transducers were regularly calibrated throughout the experimental investigation (see Appendix A). These instruments proved to be sufficiently accurate to record the actual response. The possibility of incorrect measurement of the loads and displacements can thus be excluded.

However, examining the plots in figure 7.6 again, it is noted that the midspan displacement for the experimental beam is only about 4mm prior to the yielding of the steel (this occurs when the applied loads reaches about 70kN). Furthermore the difference in the predicted and actual displacement is about 0.3mm and 1.0mm when the applied loads reach 24kN and 70kN respectively. Although this represents a difference of about 100% and 25% at the respective loading positions, the difference is small in terms of actual measurement. The possibility of slippage of the longitudinal reinforcement with respect to the surrounding concrete is not accounted for in NLFRAM. Furthermore NLFRAM does not account for the presence of the stirrup reinforcement nor does it distinguish between the stiffness of the concrete confined by the stirrups and the unconfined concrete surrounding the stirrups. The inclusion of these effects into NLFRAM may have reduced the stiffness of the beam model, Model A and increased the overall predicted displacements of the beam. However, the influence of these factors is only apparent after the initial cracking of the concrete takes place. These factors would therefore not account for the lower predicted displacements in the elastic range. This observation emphasises the need to investigate the extent of external influences on the experimental set-up.

With this in mind, it is necessary to examine the support conditions for the two-span experimental beams. The beams were supported on three concrete blocks. Each block covered an area of 600 x 600mm and was 1000mm in height. A metal half cylinder, with a radius of about 35mm was placed on top of each concrete support. The beam was placed over the supports and the half cylinders were adjusted horizontally to ensure that the spans were equal (refer to figure 3.3). Final adjustments to the height of the supports were made by wedging in 0.5mm thick metal plates between the concrete block and the half cylinder to ensure that the beam was level (see Section 3.3).

These plates were not attached to one another nor to the concrete block or the half cylinder. Under increasing applied loads, these were able to compress against one another, thus allowing for some vertical movement to occur at the supports (figure 7.9). These added to the overall vertical displacement of the beam. Although this effect is not quantified experimentally, it is clear from figure 7.6 that a gradual contribution to the midspan deflection, accumulating to about 1mm just prior to the yielding of the steel, is sufficient to significantly influence the results.

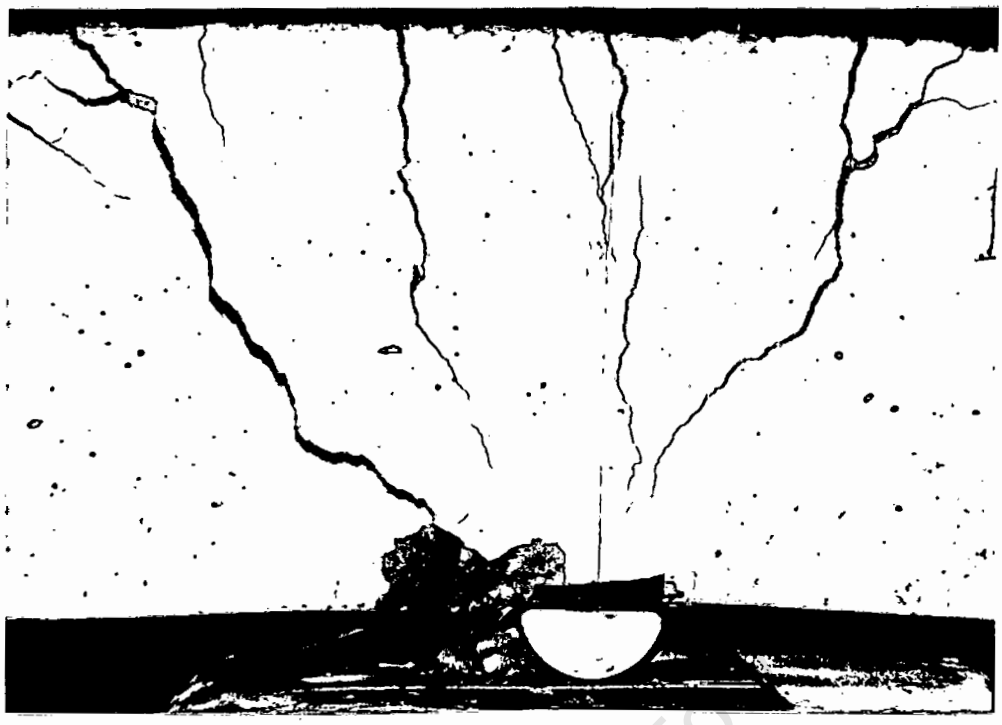

Figure 7.9 : 0,5mm thick metal plates between the concrete block and the half cylinder (interior support of beam FS5)

The effects of slippage of the reinforcement relative to the surrounding concrete, the presence of the stirrup reinforcement and the reduction of the beam stiffness due to the unconfined concrete (concrete not confined within the stirrups) losing its strength after concrete cracking commenced, is not modelled in NLFRAM. These effects are however insignificant prior to the cracking of the concrete [42], and can therefore not account for the discrepancy between the predicted and experimental results in this region. Because the beam models used in NLFRAM do not account for the vertical movements of the supports, it seems probable that the support movements are a significant cause of discrepancy between the finite element and experimental results.

Having compared the experimental results in Set 1 and Set 2 with the finite element results in NLV1 and NLV2 it is concluded that:

i) the beam model used in NLV2 reproduce all the major effects of the beams in Set1 and 2, with the exception that the displacements are under-estimated. This discrepancy can be ascribed to the fact that the supports are modelled as rigid in NLV2. The supports for the experimental beams are not completely rigid and thus contribute to the overall vertical displacements of the beams. This effect was shown to have significantly influenced the results. In future, precautions must be taken to ensure that the physical supports are rigid enough to exclude the effect of vertical support movements from the experimental beam behaviour.

ii) the combination of the concrete and steel models in NLV2 simulate the beams in Set 1 and Set 2, more realistically than the models used in NLV1. This was shown to be mainly due to the modelling of the concrete tensile behaviour. In NLV2, the maximum tensile stress specified was also shown to be experimentally and numerically justifiable. The models used in NLV2 eliminate the bilinear elastic load-deflection effect experienced using the models in NLV1.

iii) The finite element results in NLV1 and NLV2 are particularly sensitive to the maximum tensile stress specified. This value determines the load at which cracking of the concrete commence as well as the stiffness of the beam thereafter. It is therefore necessary that this parameter be determined fairly accurately for the concrete used in the manufacture of test beams.

7.3 Comparison of the simply supported beams in Set 3 and the finite element results in NLFRAM.

In this section, the load-deflection results of a typical simply supported experimental beam from Set 3 are compared with the finite element results of NLV1 and NLV2 obtained for the Model B, discussed in Section 6.3.

In figure 7.10 the load-deflection results obtained for a NLV1 example is superimposed on the curve for the Set 3 beam, FSS2. The material properties for this NLV1 example are also shown. Comparing the results in figure 7.10 it is noted that the two curves follow a similar load-deflection path. This indicates that the material models predict the material response in the correct fashion. In the elastic range, the two curves are virtually indistinguishable. After the loads have reached about 8kN, the NLV1 results gradually become stiffer with increasing load with the result that it under-estimates the displacements for beam FSS2. Although the difference in displacements is 1.6mm when the loads reach 40kN, this represents a difference of only 11%.

In figure 7.11, the load-deflection results from an NLV2 example is superimposed on the results for beam FSS2. This example differs from the previous NLV1 example only in that material Model 8, instead of Model 5 is used to describe the concrete stress-strain behaviour. The two curves remain virtually indistinguishable until the loads reach 20kN. Thereafter the NLV2 results again become stiffer with increasing load. The displacement for this example is also about 10% lower than for beam FSS2 when the loads reached 40kN.

From the parameter study for the simply supported beams, discussed in Section 6.3, it is noted that the stiffness of the beam may be reduced by specifying a lower initial modulus for the steel. In the NLV2 example shown in figure 7.12, the initial steel modulus is reduced from 230GPa to 220GPa. Also, the maximum tensile stress of the concrete is increased from 1.3MPa to 1.4MPa. Besides these parameter changes, this NLV2 example is the same as the example shown in figure 7.11. When these results are superimposed on those for beam FSS2, it is seen that the results remain indistinguishable until the loads reach about 26kN. Thereafter the NLV2 results become gradually stiffer as before but in this case, the difference in displacements is only about 6% when the loads reach 40kN. This discrepancy could possibly be due to the slippage of the reinforcement relative to the surrounding concrete. In general, these NLV2 results compare very well with the results for beam FSS2.

The above observations again indicate the superiority of the material models in NLV2 over NLV1 as far as reproducing the load-deflection effects on reinforced concrete beams under monotonic loading. Furthermore, they emphasise the earlier observations that the results of examples using NLV1 are inherently stiffer due to the modelling of the tensile stress release after the maximum tensile stress is reached in the concrete model, Model 5 (See Section 7.2).

Since the supports were completely rigid in these experimental beams, the effects of support movement are excluded. The good agreement between the predicted and measured results for these beams gives substance to the argument that the experimental results for the two-span beams were affected by the presence of the thin plates which were wedged in under the supports.

The NLV2 example in figure 7.12 thus reproduce the major effects on the beam, FSS2 under increasing monotonic loading. The elastic modulus of the steel and the maximum tensile stress of the concrete appear to be major parameters influencing the results. These material parameters affect the stiffness of the beam and thus determine the path of the load-deflection curve after the initial cracking of the concrete began. The results emphasise the importance of determining these parameters fairly accurately by experimental means for beams tested in the laboratory.

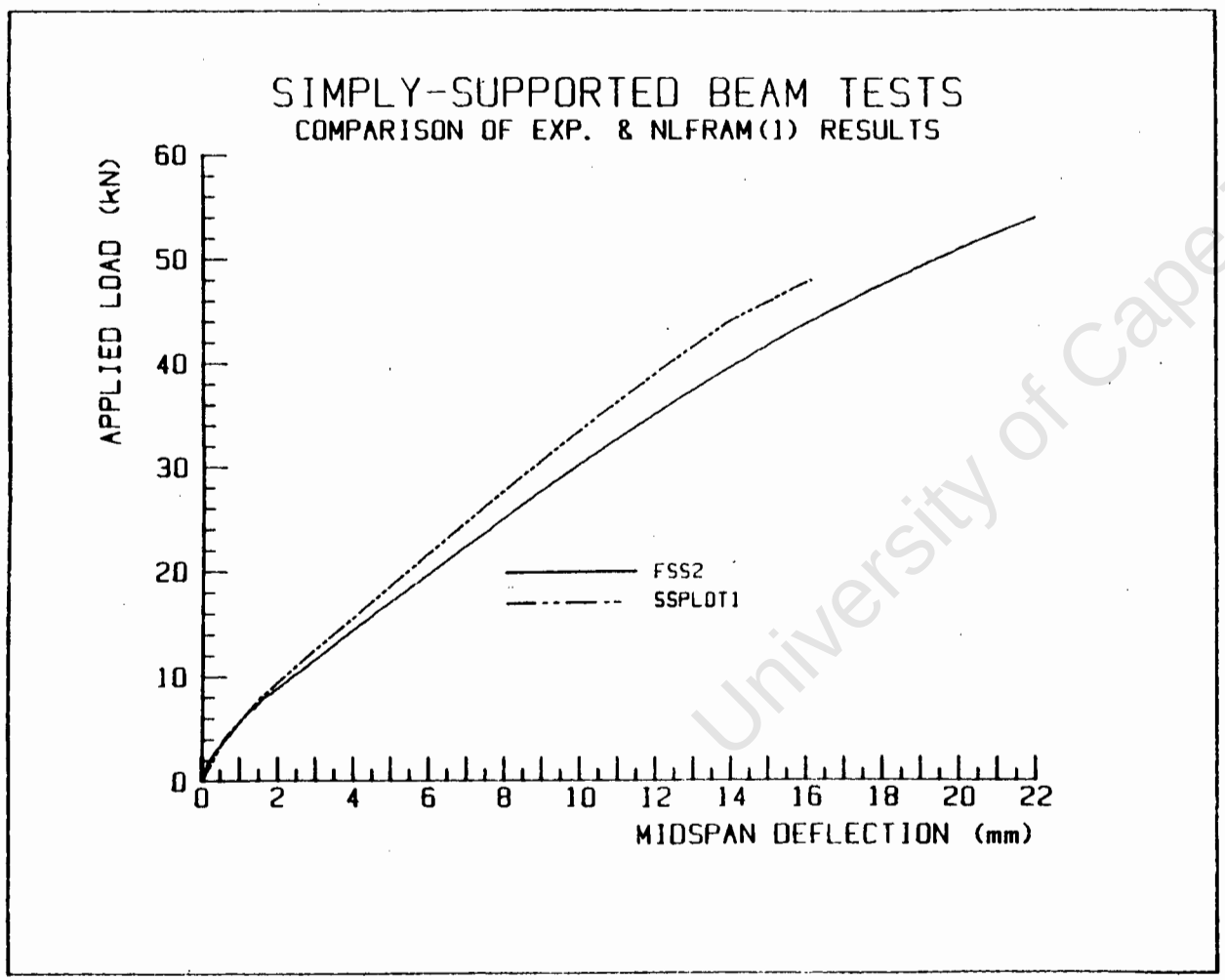

Figure 7.10 Comparison of the Results of Beam SS2 (Set 3) and F.E. Example SSPLOT1 (NLV1).

F.E. EXAMPLE : SSPLOT1

MATERIAL PROPERTIES

STEEL-MODEL 3

E_S =230 GPa
E_T =125 GPa
E_H =1.5 GPa
f_y' =420 MPa
f_y^2 =540 MPa

CONCRETE-MODEL 5

E_C = 28 GPa
f_c =-24 MPa
f_{ct}' =1.3 MPa

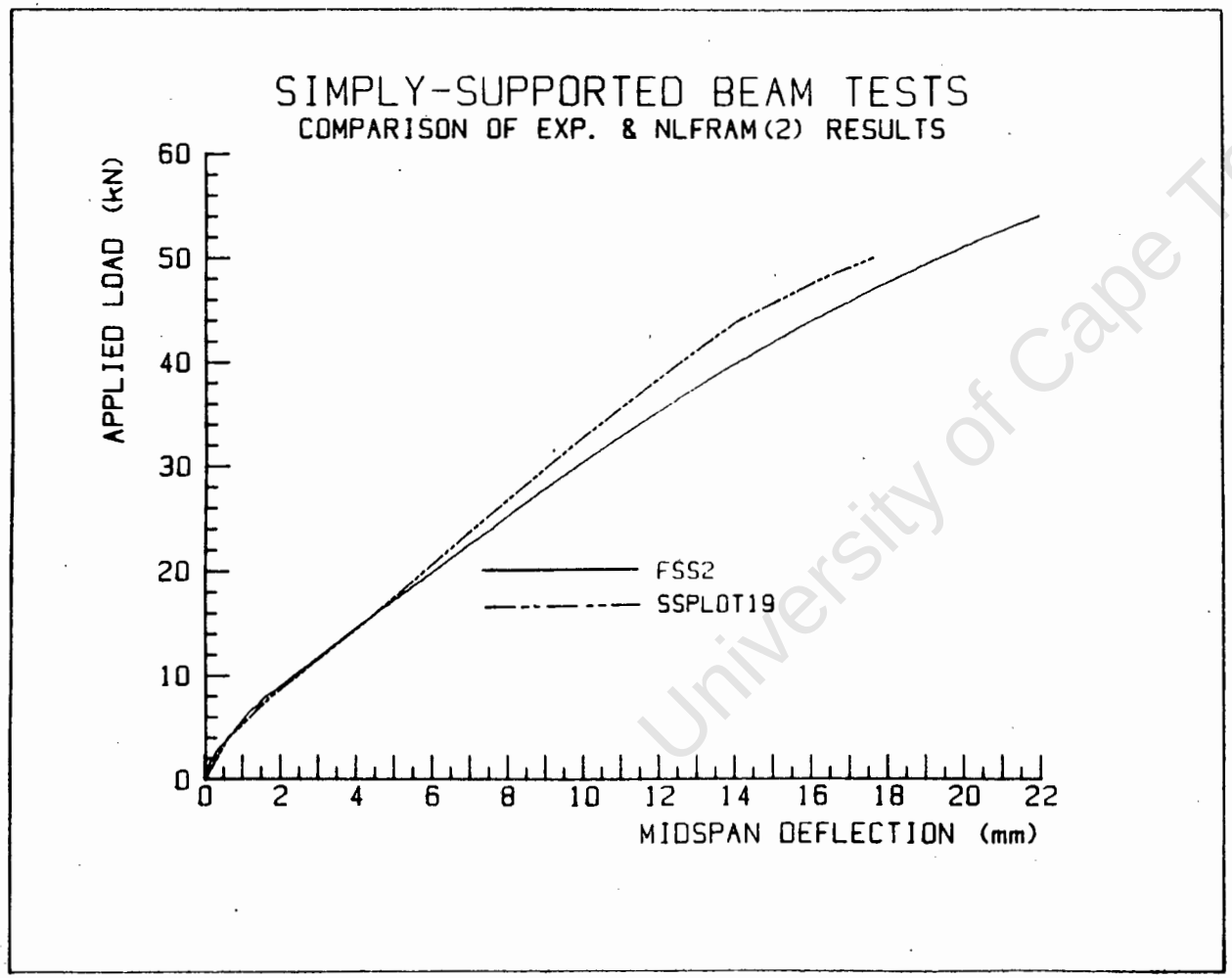

Figure 7.11 Comparison of the Results of Beam SS2 (Set 3) and F.E. Example SSPLOT 19 (NLV2).

F.E. EXAMPLE : SSPLOT19

MATERIAL PROPERTIES

STEEL-MODEL 3

E_S =230 GPa
E_T =125 GPa
E_H =1.5 GPa
f'_y =420 MPa
f^2_y =550 MPa

CONCRETE-MODEL 8

E_C = 28 GPa
f_c =-24 MPa
f_{ct} =1.3 MPa

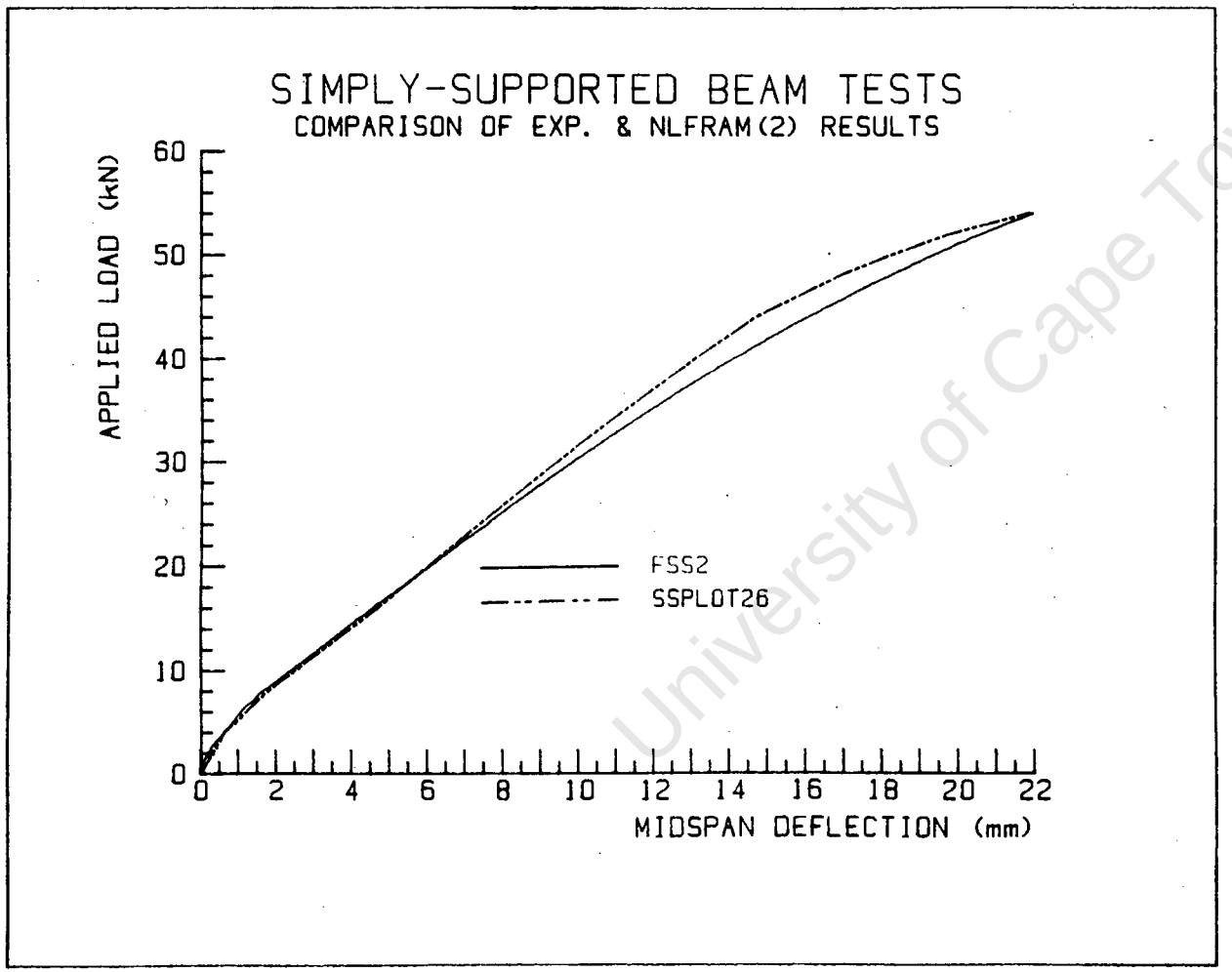

Figure 7.12 Comparison of the Results of Beam SS2 (Set 3) and F.E. example SSPLOT 2.6 (NLV2).

F.E. EXAMPLE : SSPLOT26

MATERIAL PROPERTIES

STEEL-MODEL 3

E_S =220 GPa
E_T =110 GPa
E_H =1,5 GPa
f'_y =420 MPa
f^z_y =550 MPa

CONCRETE-MODEL 8

E_C = 28 GPa
f_c =-24 MPa
f'_{ct} =1.4 MPa

CHAPTER 8

CONCLUSIONS

An experimental and analytical investigation into the material behaviour of reinforced concrete beams was undertaken. Firstly, the experimental investigation into the load-deflection behaviour of both under-reinforced two-span and slightly over-reinforced simply supported beams was performed under monotonic loading. Secondly, the behaviour of these beams was simulated using NLV1 and NLV2, the original and updated versions of the finite-element program, NLFRAM. The finite element models, Model A and Model B were used to model the two-span and simply supported beams respectively. A parametric study of the material behaviour was incorporated into the finite element analysis. The material parameters were systematically varied in NLV1 and NLV2 and changes in the rate of convergence of the equilibrium iterations and the load-deflection results were observed. The finite element load-deflection analysis were then compared with the instrumented tests on the experimental beams.

Results of the investigation support the following conclusions:

i) Finite element model, Model A, in NLV2 reproduced all the major characteristics of the experimental two-span beams with the exception that the actual displacements were under-estimated. This discrepancy is ascribed to the fact that in Model A the supports were defined as being completely rigid. The supports of the experimental beams were shown to have allowed for some vertical movement to occur. Under monotonic loading, the movement of the supports added to the overall vertical displacement of the beam. This effect was postulated as having significantly affected the experimental results.

ii) Finite element model, Model B, in NLV2 reproduced all the major characteristics on the simply-supported beams tested in the laboratory. The small discrepancy in the actual and predicted results in the region just prior to the ultimate load capacity of the beam may be due to slippage of the reinforcement relative to the surrounding concrete, an effect not accounted for in NLFRAM. The results of these comparisons give substance to the argument that the experimental two-span beams were affected by support movement.

iii) The combination of concrete and steel models in NLV2 proved to be more efficient in simulating the experimental results. This was mainly due to the difference in the modelling of the concrete tension-stiffening effect in Model 5 and Model 8. In Model 5, the tension stiffening model lead to stiffer load-deflection behaviour

ii) The material models in NLV2 need to be expanded to include multiaxial and material degradation effects in order to broaden the scope of application of the program.

iii) The data-base of experimental tests should be expanded. Additional two-span beam tests should be performed and the support system improved to exclude support movements.

REFERENCES

[1] Bathe, K.J. and Ramaswamy, S. "On three-dimensional Nonlinear Analysis of Concrete Structures", Nuclear Engineering and Design, 52, 1979, pp 385-409.

[2] Hawla, D.L., "NLFRAM - USER'S MANUAL, A Finite Element Program for the Static and Transient Dynamic Response Analysis of Geometrically and Materially Nonlinear Plane Frames", National Inst. for Aeronautics and Systems Technology, CSIR, March 1982.

[3] Hawla, D.L., **"NLFRAM - USER'S MANUAL, A Finite Element Program for the Static and Transient Dynamic Response Analysis of Geometrically and Materially Nonlinear Plane Frames", National Inst. for Aeronautics and Systems Technology, CSIR, May 1984.**

[4] Lloyd, A.R., "Reinforced Concrete Beam Tests - Series 2", Technical Report No 23, AMRU (formerly NSMRU), University of Cape Town, December 1982.

[5] Lloyd, A.R. and Hawla, D.L., "Nonlinear Analysis of Reinforced Concrete Beam", Technical Report No 30, AMRU (formerly NSMRU), University of Cape Town, January 1983.

[6] Hawla, D.L., "Analysis of Reinforced Concrete Using NLFRAM", National Inst of Aeronautics and Systems Technology, CSIR, No 117, 1983.

[7] Ngo, D. and Scordelis, A.C., "Finite Element Analysis of Reinforced Concrete Beams", Journal of the American Concrete Institute, Vol 64, No. 3, March 1967, pp152-163.

[8] Nilson, A.H., "Nonlinear Analysis of Reinforced Concrete by the Finite element Method", Journal of the American Concrete Institute, Vol 65, Sept 1968, pp 757-766.

[9] Valliappan, S. and Doolan, T.F., "Nonlinear Analysis of reinforced Concrete", Journal of the Structures Division, ASCE, Vol 98, No ST4, April 1972, pp 885-897.

[10] Phillips, D.V. and Zienkiewicg, O.C., "Finite Element Analysis of Concrete Structures", Proceedings of the Institute of Civil Eng., Vol 61, Part 2, March 1976, pp 59-88.

[11] Chen, W.F. and Saleeb, A.F., "Constitutive Equations for Engineering Materials", Vol 1, "Elasticity and Modelling, 1981, John Willey and Sons, New York.

[12] Kupfer, H.B. and Gerstle, K.H., "Behaviour of Concrete under Biaxial Stresses", Journal of the Eng. Mechanics Div., ASCE, Vol 99(4), 1973, pp 853-866.

[13] Cedolin, L., Crutzen, Y.R.J. and Deipoli, S., "Triaxial Stress Strain Relationship for Concrete", Journal of the Eng. Mechanics Division, ASCE, Vol 103(3), June 1977, pp 423-439.

[14] ASCE, "State of the Art Report on Finite Element Analysis of Reinforced Concrete", ASCE, 1982, New York.

[15] Chen, W.F., "Plasticity in Reinforced Concrete", 1982, McGraw - Hill, New York.

[16] Chen, W.F., and Ting, E.C., "Constitutive Models for Concrete Structures", Journal of the Eng. Mechanics Division, ASCE, Vol 106, No EM1, Feb 1980, pp 1-19.

[17] Suidan, M., Schnobrich, W.C., "Finite Element Analysis of Reinforced Concrete", Journal of the Structures Division, ASCE, Vol 99, No ST10, October 1973, pp 2109-2122.

[18] Owen, D.R.J, Figueiras, J.A., Damjanic, F., "Finite Element Analysis of Reinforced and Prestressed Concrete Structures including Thermel Loading", Computer Methods in Applied Mechanics and Eng., 41, 1983, pp 323-366.

[19] Chang, T.Y., Taniguchi, H. and Chen, W.F., "Nonlinear Finite Element Analysis of Reinforced Concrete Panels", Journal of Structural Engineering, ASCE, Vol 113, No 1, January 1987, pp 122-140.

[20] Han, D.J. and Chen, W.F., "Constitutive Modelling in Analysis of Concrete Structures", Journal of Engineering Mechanics, ASCE, Vol 113, No 4, April 1987, pp 577-593.

[21] Buyukoyturk, O., "Nonlinear Analysis of Reinforced Concrete Structures", Computers and Structures, Vol 7, 1977, pp149-156.

[22] Chen, W.F., and Suzuki, H., "Constitutive models for Concrete", Computers and Structures, Vol 12, ,1980, pp 23-32.

[23] Bazant, Z.P., and Shieh, C.L., "Endochronic Models for Nonlinear Triaxial Behaviour of Concrete", Nuclear Engineering and Design, Vol 47, 1978, pg 305-315.

[24] Bazant, Z.P. and Kim, S.S., "Plastic-Fracturing Theory for Concrete", Journal of the Eng. Mechanics Division, Proceedings, ASCE, Vol 105, June 1979, pp 407-428, with Errata in Vol 106.

[25] Bergan, P.G. and Holand, I., "Nonlinear Finite Element Analysis of Concrete Structures", Computer Methods in Applied Mechanics and Engineering, Vol 17/18, 1979 pp 443-467.

[26] Cedolin, L., Poli, S.D. and Iori, I., "Tensile Behaviour of Concrete", Journal of Engineering Mechanics, ASCE, Vol 113, No 3, March 1987, pp 431-449.

[27] Rashid, Y.R., "Analysis of Prestressed Pressure Vessels", Nucleur Eng. Design, Vol 7, No 4, April 1968, pp 334-344.

[28] Rahman, H.H.A., Hinton, E., and Huq, M.M., "Nonlinear Finite Element Analysis of Reinforced Concrete Slab and Slab-beam Structures", "Numerical Methods for Non-linear problems", Edited by C. Taylor, E. Hinton, and D.R.J. Owen, Dept. of Civil Engineering, University College, Swansea, U.K., Proceedings of the international College, Swansea, 2-5 September 1980.

[29] Bazant, Z.P., and Cedolin, L., "Fracture Mechanics of Reinforced Concrete", Journal of the Reinforced Engineering Mechanics Division, ASCE, Vol 106, No EM6, Dec 1980, pp 1287-1306.

[30] Bazant, Z.P., and Cedolin, L., "Finite Element Modelling of Crack Band Propagation", Journal of the Structural Division, ASCE, Vol 109 ST1, January, 1983, pp 69-92.

[31] Lin, C.S. and Scordelis, A.C. "Nonlinear analysis of Reinforced Concrete Shells of General Form", Journal of the Structures Division, ASCE, Vol 101, 1975, pp 523-538.

[32] Bazant, Z.P. and Oh, B.H., "Deformation of Progressively Cracking Reinforced Concrete Beams", ACI Journal, Title no 81-26, May-June 1984, pp 268-278.

[33] Gilbert, R.I. and Warner, R.F., "Tension Stiffening in Reinforced Concrete Slabs", Journal of the Structural Division, ASCE, Vol 104, No ST12, 1978, pp 1885-1900.

[34] Milford, R.V. and Schnobrich, W.C., "Nonlinear Behaviour of Reinforced Concrete Cooling Towers", Civil Engineering Studies, Structural Research series No 514, University of Illinois, May 1984.

[35] Fulton, F.S., "Concrete Technology - A South African Handbook", The Portland Cement Institute, Johannesburg, 1977.

[36] Lloyd, A.R., "Software for the HP3054 DL DATA LOGGER", Technical Report No 31, AMRU (formerly NSMRU), University of Cape Town, March 1983.

[37] Malvern, L.E., "An Introduction to the Mechanics of the Continuous Medium", Prentice Hall, 1969.

[38] Bathe, K.J., "Finite Element Procedures in Engineering Analysis, Prentice Hall, 1982.

[39] Becker, E.B., Carey, G.F. and Oden, J.T., "Finite Elements - An Introduction", Prentice Hall, 1981.

[40] Hawla, D.L. and Martin, J.B., "A Survey of Incremental Procedures in Nonlinear Mechanics", Technical Report No 12, AMRU (formerly NSMRU) University of Cape Town, December 1981.

[41] Stanton, J.F. and McNiven, H.D., "Towards an Optimum Model for the Response of Reinforced Concrete Beams to Cyclic Loading", Earthquake Engineering and Structural Dynamics, Vol 11, pp 200-312, 1983.

[42] Grootenboer, H.J., Leijten, S.F.C.H. and Blaauwendraad, J. "Numerical Models for Reinforced Concrete Structures in Plane Stress", Heron, Vol 26, No 1c, 1981.

APPENDIX A

MEASURING INSTRUMENTS

The calibration constants for the measuring instruments required for the program, FSTEST, were obtained from the manufacturer's specifications given in Figures A1 to A4.

For Load-Cell 1 (LC1) - BL-20TB

the calibration constant $CF = \frac{\text{load capacity}}{\text{sensitivity}}$

load capacity = 200kN

sensitivity = $1223\ ^{mV}/_{V}$

from Figure A1 $CF = \frac{200kN}{1223x10^{-6}}$

$CF = 163\ 532,3$

For Load-Cel 2 (LC2) - BT-20TB

from Figure A2 $CF = \frac{200kN}{1224x10^{-6}}$

$CF = 163\ 398,7$

For Displacement Transducer 1 (DT1) - DT-100A

from Figure A3 $CF = \frac{\text{measuring capacity}}{\text{sensitivity}}$

$CF = \frac{100mm}{1270x10^{-6}}$

$CF = 78740,16$

For Displacement Transducer 2 (DT2)

from Figure A4 $CF = \frac{100mm}{1262x10^{-6}}$

$CF = 79239,3$

LOAD CELL 1 (LC1)

検 査 成 績 表

CALIBRATION SHEET

土 木 用 変 換 器

TRANSDUCERS FOR CIVIL ENGINEERING

型式名 Model	BL-20TB	容 量 Capacity	20tf	製造番号 Serial No.	BJ 6945
検査年月日 Inspected date	1992.12.24	温 度 Temperature	20 ℃	湿 度 Humidity	60. %

1．出力電圧感度 Sensitivity
1223 μV/V
(2446 ×10⁻⁶)

2．初期不平衡 Initial bridge unbalance
+ 249 μV/V
(+ 498 ×10⁻⁶)

3．較正係数 Calibration constant
0.0164 tf /1 μV/V
(0.00818 tf /1.0×10⁻⁶)

4．入出力抵抗 Input & output resistance
入力 Input 347.6 Ω
出力 Output 347.6 Ω

5．絶縁抵抗 Insulation resistance
1000 MΩ (50VDC)

注 Note 1 μV/V = 2 ×10⁻⁶ 等価ひずみ (G.F.=2.00) Equivalent strain

株式会社 共和電業
KYOWA
ELECTRONIC INSTRUMENTS CO.,LTD.

検査者 Inspector

責任者 Supervisor

FIGURE A1

LOAD CELL 2 (LC 2)

検 査 成 績 表

CALIBRATION SHEET

土 木 用 変 換 器

TRANSDUCERS FOR CIVIL ENGINEERING

型式名 Model	BL-20TB	容 量 Capacity	20 tf	製造番号 Serial No.	BJ 6943
検査年月日 Inspected date	1982.12.24	温 度 Temperature	20 ℃	湿 度 Humidity	60 %

1. 出力電圧感度 Sensitivity: 1224 μV/V (2448 ×10⁻⁶)

2. 初期不平衡 Initial bridge unbalance: + 239 μV/V (+ 478 ×10⁻⁶)

3. 較正係数 Calibration constant: 0.0163 tf /1 μV/V (0.00817 tf /1.0 ×10⁻⁶)

4. 入出力抵抗 Input & output resistance: 入力 Input 351.7 Ω; 出力 Output 351.8 Ω

5. 絶縁抵抗 Insulation resistance: 1000 MΩ (50VDC)

注 Note: 1 μV/V = 2 ×10⁻⁶ 等価ひずみ (G.F.=2.00) Equivalent strain

株式会社 共和電業
KYOWA ELECTRONIC INSTRUMENTS CO.,LTD.

検査者 Inspector

責任者 Supervisor

FIGURE A2

DISPLACEMENT TRANSDUCER 1 (DT1)

検 査 成 績 表
CALIBRATION SHEET

型式 Model	DT-100A	容量 Capacity	mm 0~100	製造番号 Serial No.	YM8605
検査年月日 Inspected date	1983.1.14	温度 Temp.	23 ℃	湿度 Humid.	67 %

1. 出力電圧感度 Sensitivity: 1270 μV/V (2540 ×10⁻⁶)
2. 非直線性 Non linearity: 0.12 %F.S.
3. ヒステリシス Hysteresis: 0.01 %F.S.
4. 較正係数 Calibration constant: 0.07874 mm/1μV/V (0.07874 mm/1.0×10⁻⁶)
5. 零点の温度影響 Thermal zero shift: — %F.S./℃
6. 出力の温度影響 Thermal effect on sensitivity: — %/℃
7. 入出力抵抗 Input & output resistance: 入力 Input 122.3 Ω; 出力 Output 122.3 Ω

株式会社 共和電業
KYOWA ELECTRONIC INSTRUMENTS CO., LTD.
TOKYO, JAPAN

検査者 Inspector

責任者 Supervisor

FIGURE A3

DISPLACEMENT TRANSDUCER 2 (DT2)

検査成績表
CALIBRATION SHEET

MAX ALLOWABLE INPUT VOLTAGE = 5 V

型式 Model	DT-100A	容量 Capacity	0~100 mm	製造番号 Serial No.	YM2899
検査年月日 Inspected date	1982.8.28	温度 Temp.	25 ℃	湿度 Humid.	68 %

1. 出力電圧感度 Sensitivity: 1262 μV/V (2524 ×10⁻⁶)
2. 非直線性 Non linearity: 0.08 %F.S.
3. ヒステリシス Hysteresis: 0.08 %F.S.
4. 較正係数 Calibration constant: 0.07924 mm/1μV/V (0.6392 mm/1.0×10⁻⁶)
5. 零点の温度影響 Thermal zero shift: — %F.S./℃
6. 出力の温度影響 Thermal effect on sensitivity: — %/℃
7. 入出力抵抗 Input & output resistance: 入力 Input 121.8 Ω; 出力 Output 121.9 Ω

株式会社 共和電業
KYOWA ELECTRONIC INSTRUMENTS CO., LTD.
TOKYO, JAPAN

検査者 Inspector

責任者 Supervisor

FIGURE A4

APPENDIX B

DATA LOGGER SOFTWARE

Two programs, FSTEST and FSPLOT, have been written to perform data logging and plotting of experimental results for static load tests on reinforced concrete beams. These programs are modified versions of BTEST and BPLOT, written by Lloyd [35] for his under-reinforced simply-supported beam tests. There is a fair degree of generality in the programs, so that they may also be used for other purposes, e.g. a load deflection test on any other test piece.

The data logging equipment is an HP 3054 DL data logger which comprises an HP87 micro-computer with dual disc drives, seperate printer and plotter, and a 3497A Data acquisition control unit.

A description of the two programs FSTEST and FSPLOT follows:

A. Program FSTEST

FSTEST has been written to perform data logging during a static load test on a typical reinforced concrete beam. The program monitors the two load cells (LC1 and LC2) and the two displacement transducers (DT1 and DT2).

The program consists of a main program into which the following Level 3 System Subprograms have been incorporated:

Init	Warn	Dcv	Shunt
Brmeas	Strain	Plot	

The program has been written to perform a maximum of 400 scanning loops. During each scan a burst of readings is taken, the results are printed, and the data is written to a data file previously created on a data disc by the user. The scans will continue until the programmmable key K1 is pressed. The program then exits from the scanning loop, and produces plots on the HP87 screen as follows:

i) Load vs deflection (LC1 vs DT1 and LC2 vs DT2)

Paper plots may be obtained using the program FSPLOT which is described later.

To perform an experiment using FSTEST

1. Place the program disc in DRIVE 0 and a data disc in DRIVE 1.

2. Type:
   MASS STORAGE IS ":D701"
   CREATE "DATA 1", 50 (creates a data file DATA1 of size 50 records).
   MASS STORAGE IS ":D700"
   LOAD "FSTEST"
   RUN

3. The program will then perform various checks on the devices connected to the HP87, and print its findings.

4. Enter the data in response to questions that appear on the screen. Note that the beam title requested by the program should be identical to the name of the data file created on the data disc (DATA1 in this example).

5. Zero readings are then performed, and scanning is commenced. Results from each scan are printed on the printer.

   NB At least one scan should be completed before any loads are applied. This ensures that the zero readings have been completed.

6. Continue with the test (up to a maximum of 400 scans). To terminate the scanning, press programmable key K1.

7. Wait for all the plots to be displayed on the HP87 screen. On completion, "END PROGRAM EXECUTION" will appear on the printer.

8. Remove the data disc, and plot the results using program FSPLOT if desired.

Notes

i) The data file name (DATA1 above) may have a maximum of 6 characters, including blanks.

ii) The program assumes devices connected to the following channel numbers on the data logger:

0	:	power source
6	:	load cell 1 (LC1)
7	:	displacement transducer 1 (DT1)
8	:	load cell 2 (LC2)
9	:	displacement transducer 2 (DT2)

iii) One power supply is used for all devices and the supply voltage is set at approximately 5 volts. (See page 3-1 in the Operating Manual of the HP6214A Power Supply, for instructions on setting the supply at a constant voltage). Note that the power source is also connected to channel 0 (zero) on the 20-channel multi-plexer relay card, and the supply voltage is monitored and printed as a check at the start of the scanning loop.

iv) Before running the logging program, it is good practice to manually close each channel and check the voltage reading, to ascertain whether the lead wire connections are all intact. This is performed via the data logger front panel as follows:

(Analog Close Channel) (6) (Execute)

where each bracket indicates one button being pressed. This closes channel 6 which monitors the load cell. The front panel display should indicate the bridge output voltage, and this should fluctuate as load is applied to the load cell.

Checks on the other channels (7,8,9) may be carried out in the same way.

B. Program FSPLOT

FSPLOT has been written to read back the data stored by FSTEST, and to produce A4 plots on a pen plotter. Plots are as follows:

i) Load vs deflection (LC1 vs DT1 and LC2 vs DT2)

ii) Load vs scan number

To execute FSPLOT, proceed as follows

1. Place the program disc in DRIVE 0.

2. Type MASS STORAGE IS "D700"
   LOAD "FSPLOT"
   RUN

3. Enter the data in response to the questions that appear on the screen. Note that the beam title requested by the program should be identical to the name of the data file used during the experiment.

4. The program will request that the data disc be placed in DRIVE 1. After doing this, press CONT to continue.

5. The first plot will then be produced. Before each subsequent plot is commenced, the program requests the user to insert a new sheet of paper in the plotter. Having done so, press CONT to continue.

6. When all the plots are completed, "END PROGRAM EXECUTION" will appear on the screen.

APPENDIX C

THE FOLLOWING COURSES WERE COMPLETED IN PARTIAL FULFILLMENT OF THE M.Sc. (ENG) DEGREE AT THE UNIVERSITY OF CAPE TOWN

Course		Date Credited	Credit Value
CE441A	FRAME ANALYSIS	1983	2
CE551B	PLATES AND SHELLS	1983	2
CE552A	INTRODUCTION TO THE FINITE ELEMENT METHOD	1983	2
CE552B	FINITE ELEMENT ANALYSIS	1983	3
CE556	CONTRACT LAW	1983	3
AM343	NUMERICAL METHODS	1983	4
AM344	ADVANCED NUMERICAL ANALYSIS	1984	4
CE5B7	INTRODUCTION TO THE THEORY OF ELASTICITY	1984	2
		TOTAL	22

Course Credits: 22
Thesis Credits: 20
Total: 42

Total credit requirements for the M.Sc. (Eng) Degree: 40.

A brief description of the courses are given as follows:-

CE551A - FRAME ANALYSIS

The application of the force method of analysis to framed structures of straight and curved memebers. The stability of equilibrium of framed structures.

CE-551C - PLATES AND SHELLS

An introduction to the elastic theory of plates and shells. Generalised stresses, generalised strains, elastic constitution relations, co-ordinate systems, Analytical solutions of simple problems. Variational methods using Energy Principles.

CE-552A - INTRODUCTION TO THE FINITE ELEMENT METHOD

Generalised displacement method of analysis for framed structures. Elastic energy theorems. Basic procedures of the finite element method illustrated for framed structures.

CE552B - FINITE ELEMENT ANALYSIS

Plane stress and plane strain elements, plate bending elements, shell elements, three-dimensional elements. Programming of the finite element displacement methods. Techniques for equation solving.

CE556 - CONTRACT LAW

General law of contract, partnerships, company law and case-studies.

CE5B7 - INTRODUCTION TO THE THEORY OF ELASTICITY

Stress, strain, equilibrium, strain displacement relationships. Elastic constants. Solutions of simple boundary value problems in plane stress and plane strain.

AM343 - NUMERICAL METHODS

The theory and practice of numerical methods - approximate solutions of nonlinear equations, interpolation numerical integration, numerical solution of ordinary differential equations.

AM344 - ADVANCED NUMERICAL METHODS

Solving of partial differential equations using the Galerkin Method with Finite Element Approximations.